Doctoral theses at NTNU, 2021:162

Savin Viswanathan

Multiphysical Simulation of Ocean Engineering Systems

— Modelica Ocean Engineering Library
— Cosimulation for Drilling Riser Analysis

Doctoral thesis

NTNU
Norwegian University of Science and Technology
Thesis for the Degree of
Philosophiae Doctor
Faculty of Engineering
Department of Mechanical and Industrial Engineering

NTNU
Norwegian University of
Science and Technology

Savin Viswanathan

Multiphysical Simulation of Ocean Engineering Systems

— Modelica Ocean Engineering Library
— Cosimulation for Drilling Riser Analysis

Thesis for the Degree of Philosophiae Doctor

Trondheim, May 2021

Norwegian University of Science and Technology
Faculty of Engineering
Department of Mechanical and Industrial Engineering

NTNU
Norwegian University of
Science and Technology

NTNU
Norwegian University of Science and Technology

Thesis for the Degree of Philosophiae Doctor

Faculty of Engineering
Department of Mechanical and Industrial Engineering

ISBN 978-82-326-6112-1 (printed ver.)
ISBN 978-82-326-6218-0 (electronic ver.)
ISSN 1503-8181 (printed ver.)
ISSN 2703-8084 (online ver.)

Doctoral theses at NTNU, 2021:162

Printed by NTNU Grafisk senter

To life! The best teacher, and the worst student...

Preface

This thesis is submitted in partial fulfilment of the requirements for the degree of philosophiae doctor (Ph.D.) at the Norwegian University of Science and Technology (NTNU).

The work presented in this thesis is the result of the doctoral research funded by the the Research Council of Norway, under work package 4.1 of the Center for Research Based Innovation (SFI) Offshore Mechatronics (OM) Project, which was carried out at the Department of Mechanical and Industrial Engineering (MTP), NTNU, from December 2017 to December 2020.

The research was carried out under the guidance of Assoc. Prof. Christian Holden (MTP, NTNU), as the principal supervisor, along with Prof. Olav Egeland (MTP, NTNU), and Sr. Er. Dr. Ronny Sten (National Oilwell Varco), as co-supervisors.

Acknowledgements

I would like to thank Dr. Raghavan Ramankutty, of Dathathreya Ayurveda, for the numerous ways in which he has influenced my life. Without his presence, I doubt if I would have had the sense, health or determination to pursue academics after my bachelors.

I would like to express my gratitude to Assoc. Prof. Christian Holden for giving me the opportunity to pursue this research, for his trust, and guidance.

I would like to thank Prof. Olav Egeland for his invaluable inputs, and for finding time, in-spite of his busy schedule, to go through the research outputs.

I would like to thank Dr. Ronny Sten for his enthusiasm, for his inputs that kept me from viewing the research from an entirely academic point of view, and for his efforts in making available field measurements, which was no mean a task.

I would like to thank professors Carl M. Larsen, Svein Sævik, Lars E. Holmedal, Marilena Greco, and Trygve Kristiansen, at the department of marine technology, for the efforts they take in disseminating knowledge through the PhD courses they teach.

I would like to thank my colleagues Mishiga Vallabhan, Njål Tengesdal, and Jan Sramota for the interesting conversations while I shared office space with them.

I would like to thank all my friends at the Robotics and Automation group at MTP, for the lighter moments of PhD life, the pay day beers, and the cabin trips.

I would like to thank Mukhlas Sabara, at the department of marine technology and Marcelo Jaculli, State university of Campinas, for the wonderful group study sessions on hydrodynamics.

I would like to thank Mæl Moreau, at the department of marine technology, and Stefan Wiechert, at the department of energy and process engineering, for the interesting discussions on ocean waves.

I would like to thank my mother Suja for kindling the inquisitive spirit in me by inspiring me to read and to open up my toys as a child.

I would like to thank my father Viswanathan for ensuring that the toys and books kept coming, even under difficult circumstances.

I would like to thank my sister Neena for being an example of perseverance and focus.

I would like to thank my wife Aswathy for believing in me, inspiring me and affording me the freedom to follow my dreams.

I would like to thank my son Madhav for hopefully forgiving my physical absence during his early years, and for the baby smiles over video calls that would instantly take away all my worries.

Summary

The advancements in computing has made it possible to carry out integrated simulation of complex multiphysical systems, to better evaluate system performance and safety. The discipline of multiphysical simulation, though well established in many domains, is not used as extensively in the analysis of ocean engineering systems, which even in their simplest applications, is highly multiphysical and interdisciplinary.

One factor that limits the of use of multiphysical simulation techniques in the analysis of offshore systems is the lack of mutiphysics capabilities in hydrodynamics simulation software, and vice versa.

This thesis presents the efforts and results in the direction of implementing such a multiphysical approach in the ocean engineering domain, and thereby encompasses facets such as the development of Modelica component models to constitute an Ocean Engineering Library for *OpenModelica*, a popular open-source multiphysics software; and the formulation of a co-simulation interface between *Simulation X*, a commonly used commercial multiphysics software, and *OrcaFlex*, a popular commercial ocean engineering software.

Being an article based thesis, the project scope is divided into parts, and each part is dealt with in an article along with the relevant theory. The first chapter introduces the project, and details the arrangement of the thesis.

In the first article, preliminary results from the multiphysical simulation of a representative ocean engineering system in *OpenModelica* is compared with those obtained using *OrcaFlex*, as an indicator of the possibilities of implementing such a multiphysical approach. A detailed description of the theory behind the development of component models to simulate regular and irregular waves, and depth-varying current is presented in the second article, while the response of non-diffracting floating objects, and mooring response based on the quasi-static approach, is presented in the third article. The third article also brings out the limitations of the quasi-static approach in the simulation of mooring forces.

The fourth article describes the lumped-mass approach to simulation of mooring line dynamics, while the fifth article deals with the development of *Modelica* component-models for subsea cable dynamics based on the lumped-mass approach.

The sixth article lays the foundation for the future development of *Modelica* component-

models for simulating the hydrodynamics of larger objects, where wave diffraction and radiation effects are significant, by presenting a *Python* code for the evaluation of the frequency dependent hydrodynamic coefficients.

The seventh article is concerned with the development of a co-simulation methodology for riser analysis and presents a co-simulation interface between *SimulationX* and *OrcaFlex*.

The last and eighth article compares the results of a multiphysical simulation, based on the above co-simulation methodology, of a planned riser disconnect procedure with field measurements, and demonstrates the possibilities that open up.

The conclusion section sums up the contributions of the present work and suggests avenues for future research in the domain.

Contents

List of figures

List of tables

Chapter 1

Introduction

The Research Council of Norway is a national strategic body for research. It manages research funding from all of the Norwegian ministries, and allocates funds to basic and applied research and innovation within all fields and disciplines.

The Research Council of Norway provides long-term funding to the Centre for Research-based Innovation (SFI). The scheme promotes innovation through close cooperation between R&D intensive companies and prominent research institutions. The Center for Offshore Mechatronics (SFI-OM), (sfi.mechatronics.no), is a third generation SFI center established with the aim of developing advanced offshore mechatronic systems for autonomous operation and condition monitoring of offshore equipment and systems.

Work Package 4 (WP4) of the SFI-OM project is concerned with modelling and simulation, and Prof. Olav Egeland, from the department of Mechanical and Industrial Engineering (MTP), NTNU, was designated the work-package leader. Sub-package WP4.1 is concerned with the simulation of multiphysical systems in offshore operations, and Assoc. Prof. Christian Holden, from MTP, NTNU, was assigned the responsibility of guiding the PhD candidate in research. Dr. Ronny Sten, senior simulation engineer from National Oilwell Varco, the industrial partner in WP4.1., was assigned as a co-supervisor to the PhD candidate. Subsequently the call for application for the PhD position was issued [Appendix A], and the author was selected to fill the position.

1.1 Background and motivation

Ocean-engineering systems, even in their simplest applications, are highly multiphysical and interdisciplinary.

The hydrodynamic response of the ocean platform has a considerable influence on the performance of on-board systems, which are in all cases multiphysical. Most, if not all, commercial and open-source hydrodynamic software do not have multiphysics capabilities, or interfacing capabilities that allow for the simulation of the whole system in

an integrated fashion. Similarly, most, if not all, multiphysics simulation software do not have hydrodynamics capabilities that allow for the simulation of the ocean engineering system in its entirety. At present, either the hydrodynamic component, or the multiphysics component, is simplified and included as a sub-component to carry out integrated simulations. This simplification, however, has a bearing on the simulation results.

The development of capabilities that allow for fully integrated simulations are relevant from the aspects of both the newly emerging domains of offshore wind, open-ocean based aquaculture, wave energy conversion, and ocean mining, and the conventional offshore oil and gas industry.

1.2 Identification of research potential

In this section, we discuss the identification of the broader scope of the project.

1.2.1 Development of OpenModelica component-models

In the case of the emerging domains such as wave energy conversion, ocean mining, etc., it is the high cost associated with experimental analysis of ocean engineering systems, the low rate of return on investments compared to conventional oil and gas, and heavy dependence of system design synthesis to system response, that necessitates the development of integrated simulation capabilities, especially in the open-source format.

Modelica is an object-oriented, declarative, multi-domain modelling language for component-oriented modeling of complex systems. It is developed by the non-profit Modelica Association, which also develops the free-to-use Modelica Standard Library.

The commercial implementations of Modelica include *Dymola* from Dassault Systemes, *Simulation-X* from ESI ITI Gmbh, *MapleSim* from Maplesoft, *JModelica* from Modelon AB, and *Wolfram SystemModeler* from Wolfram Research.

The only open-source Modelica-based modelling and simulation environment intended for industrial and academic usage is *OpenModelica*. The non-profit organization, Open Source Modelica Consortium (OSMC), supports its long-term development, and *OMEdit* is an open-source graphical user interface (GUI) that functions as the front end for the OpenModelica environment.

The *Modelica Standard Library* contains about 1600 model components and 1350 functions from the electric, electrical, mechanical, fluid, and control engineering domains. Both the commercial and open-source *Modelica* simulation environments have been extensively used by the industry, especially in the automotive sector, to carry out complex multiphysical system simulations.

Inspite of the many advantages that *Modelica* has to offer, its utilization in the offshore domain has been minimal. One of the reasons behind this could be the lack of *Modelica* component-models to simulate waves, currents, hydrodynamic loads, mooring loads, etc.

It was suggested that the development of component-models to constitute an *Ocean Engineering Library* for *OpenModelica* would be beneficial to both academia, and the rapidly emerging non-conventional offshore industry.

1.2.2 Development of co-simulation interfaces between domain-specific commercial software

With the current outlook in the oil and gas industry pointing to brent crude-oil prices of around USD 109 per barrel in 2040 [17] when the cheap reserves of oil are expected to run out, the main focus of offshore field development in the foreseeable future would be to lower capex and opex costs. The pre-2014 trend of over-design is being stripped away from offshore projects and the industry is now witnessing a trend where operators are making deep-water projects more competitive to be economically feasible at crude oil prices of around USD 50 per barrel [22].

The large degree of conservatism incorporated into conventional analysis methods result in a smaller operability envelope, thus driving up offshore project costs. Hence, better methods of analysis that aid in maximizing the operability envelope, with minimal increase in risk, is the need of the hour. Under the prevailing requirement to maximize operability, there is an increased possibility of drift-offs of the dynamically positioned (DP) vessel under harsher environmental conditions necessitating more frequent and quicker Emergency Disconnect Sequences (EDS).

Contemporary coupled riser analysis does not consider the multiphysical model for the hydro-pneumatic riser tensioner system. Instead, linear or non-linear springs are used to model the response of the tensioner cylinders. Riser tensioner systems are a part of the product portfolio of NOV, and it was suggested that the development of co-simulation methodologies to enable the multiphysical simulation of the platform, riser, and riser-tensioner system by interfacing the commercial riser analysis software, *OrcaFlex*, and the commercial multiphysics software *SimulationX*, would be of interest to the industry, in addition to providing benefits to academia.

1.3 The arrangement of this thesis

The remainder of this work is arranged as follows:

Chapter 2 deals with the basics, for the benefit of those unfamiliar with marine hydrodynamics and/or multiphysical modelling. Knowledge of the contents in this chapter is also required to better comprehend the details in the project description and the theory sections of the articles in the subsequent chapters.

Chapter 3 describes the aims of the project, in the light of the information given in the earlier chapter. It also describes correlations between the different articles that constitute this thesis, and the project objectives.

Chapter 4 presents articles dealing with the concept of developing a dedicated *Ocean engineering* standard library for *OpenModelica*. In particular, it deals with the development of component models for simulating waves, currents, the hydrodynamic response of small floaters, and for quasi-static catenary moorings.

Chapter 5 presents articles dealing with the implementation of the lumped-mass method in the *Modelica* environment to simulate the dynamics of sub-sea cable structures.

Chapter 6 presents an article dealing with the implementation of the boundary-element method to determine frequency dependent hydrodynamic parameters associated with larger floating objects, where wave diffraction and radiation effects are significant.

Chapter 7 presents articles dealing with the implementation of the *co-simulation* methodology to link *OrcaFlex* and *SimulationX*, to carry out the multiphysical simulation of the riser–riser-tensioner–platform system.

Chapter 8 draws up conclusions based on the work presented by the articles in the preceding chapters, presents the scientific and academic contributions realized by the current research, and gives an outline for further research in this direction.

Chapter 2

Background Theory

The two classical theories dealing with the hydrodynamic response of floating objects are:

Maneuvering theory which deals with the study of a ship moving in calm water, and,

Seakeeping theory which deals with the motion of ships, at zero or constant speed and heading, interacting with waves.

In conventional offshore operations, we are mostly concerned with seakeeping problems, formulated using the *seakeeping axes*. For more information, see [11, pp. 8–12].

2.1 The co-ordinate systems

The different coordinate systems used in seakeeping analysis are explained in Figure 2.1.

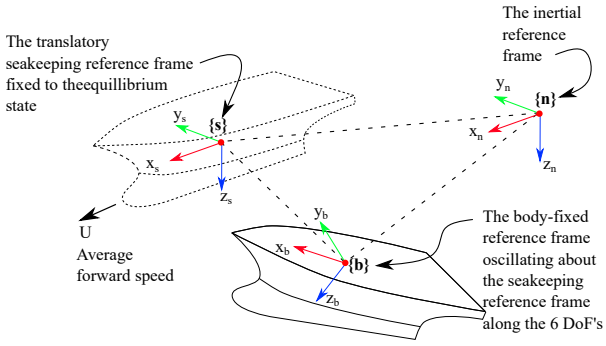

Figure 2.1: Coordinate systems used in seakeeping analysis. Adapted from [11, Figure 1.6].

2.2 The seakeeping problem

The general problem to be solved is the equation of motion for a floating object with six degrees of freedom (DoF), in the presence of environmental and operational loads, as shown in Figure 2.2.

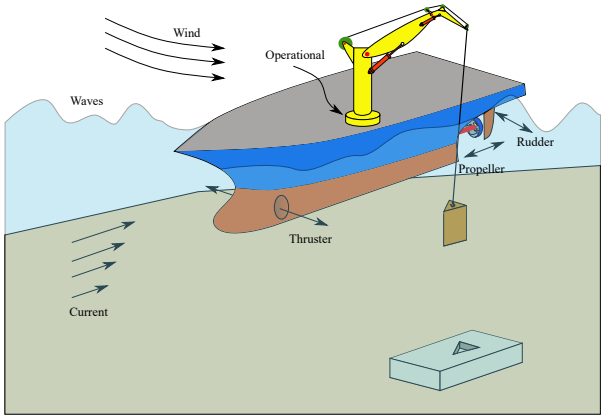

Figure 2.2: Loads on a floating object

The environmental loads are the loads due to wind, waves, current, and other external loads, while operational loads are loads arising due to the operations being carried out, e.g., thruster loads from the dynamic positioning (DP) system, the crane load, etc. Though not exactly correct, for the ease of comprehension, the equations of motion for a 6 DoF object, formulated in the Newton–Eularian from, may be expressed by the pseudo-differential equation [11, p. 12]

$$[M_{RB} + A(\omega)]\ddot{x} + [B_v + B(\omega)]\dot{x} + Cx = F_w(\omega, \beta) + F_c + F_a + F_o, \tag{2.1}$$

where M is the mass/moment of inertia matrix, $A(\omega)$ is the frequency dependent added-mass matrix, B_v is the viscous damping matrix, $B(\omega)$ is the potential damping matrix, C is the stiffness matrix, and x is the displacement vector with respect to the seakeeping frame. Further, $F_w(\omega, \beta)$ is the wave load where β is the angle of incidence, F_c is the current load, F_a is the wind load, and F_o represents the operational loads.

The frequency dependence of added-mass and potential damping terms are associated with the fact that the added-mass arises due to the inertia of the fluid mass that is set in motion due to the movement of the body, while the damping is caused due to dissipation of energy from the system by the radiation waves generated by the motion of the body in the fluid. A more detailed description of the frequency dependence of these terms can be found in Sec. 2.3 and 2.6.

The current loads and the aerodynamic loads may be approximated as drag and applied as point loads on the centroid of the drag area, while operational loads may be applied as point or distributed loads obtained from the dynamic analysis of the subsystem modelling the operation, e.g., the thruster force being applied as a point load based on a model for the thruster.

The determination of wave loads is not so straight straightforward, and for a better understanding we need to look at the wave-body interaction problem.

2.3 The wave-body interaction problem

The description of the wave-body interaction problem given below is based on the subject matter of [19, Sec. 6.15] and [9, p. 39].

Consider an object floating on the surface of a semi-infinite body of water bounded only by the free surface. In calm water, the buoyancy, which is the *hydrostatic* pressure integrated over the wetted surface of the body, keeps the body afloat.

If we now consider a progressive monochromatic wave traversing the free surface and interacting with a floating object, we observe that the object begins to respond to the wave. The response of the object is brought about by the fluctuation of the fluid pressures on the wetted surface due to the motion of the fluid, and this pressure component is referred to as the *hydrodynamic* pressure. After the initial transients die out, these responses attain a steady state, and the object begins to oscillate in its 6 DoFs with a response frequency equal to the incident wave frequency.

The presence of the object scatters the incident waves, and this phenomena causes the *diffraction* of the incident wave. The motion of the object in the fluid also generates surface waves, called *radiation waves* that originate at the interface between the body and fluid surface, and propagate away from the body. Both the scattered and the radiated waves exhibit amplitude decay, and die out at a distance away from the object.

Figure 2.3 represents the behaviour of the free surface and the object, frozen in time.

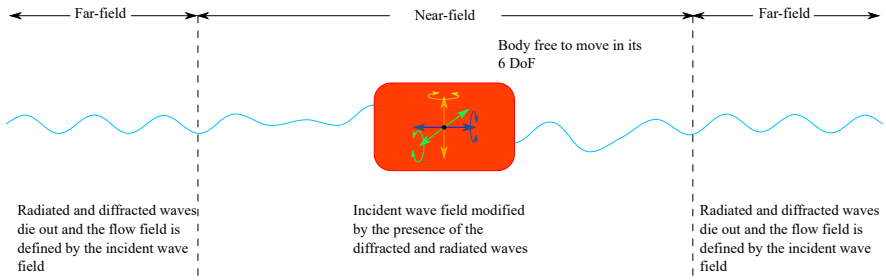

Figure 2.3: Wave–Body Interaction

The hydrodynamic pressure originates due to the flow of the fluid, and hence we progress to discussions on fluid flows.

2.4 Fluid flows

The subject matter discussed in this section may be found in any basic fluid mechanics book, e.g., [3].

The two methods of describing fluid motion are [3, Ch. 5]:

Lagrangian Method A single fluid particle is followed as it traverses the flow domain, and its velocity, acceleration, pressure, density, etc. are described.

Eulerian Method The properties of a fluid are described at a point in the flow domain.

The Eulerian method is commonly used in fluid mechanics problems.

2.4.1 Types of flows

Fluid flows may be classified as [3, Ch. 5]:

Steady flow Fluid characteristics like velocity $\vec{u}$, pressure p, density ρ, etc., at any point $\vec{x} = x\hat{i} + y\hat{j} + z\hat{k}$, do not change with time, i.e.,

$$\left.\frac{\partial \vec{u}}{\partial t}\right|_{\vec{x}} = 0, \left.\frac{\partial p}{\partial t}\right|_{\vec{x}} = 0, \left.\frac{\partial \rho}{\partial t}\right|_{\vec{x}} = 0$$

Unsteady flow The fluid characteristics at any $\vec{x}$ change with time, i.e.,

$$\left.\frac{\partial \vec{u}}{\partial t}\right|_{\vec{x}} \neq 0, \left.\frac{\partial p}{\partial t}\right|_{\vec{x}} \neq 0, \left.\frac{\partial \rho}{\partial t}\right|_{\vec{x}} \neq 0$$

Uniform flow The instantaneous fluid velocity do not change in magnitude or direction when evaluated at any point in the fluid domain, i.e.,

$$\left.\frac{\partial \vec{u}}{\partial \vec{x}}\right|_{t=t_1} = 0$$

Non-uniform flow The instantaneous fluid velocity changes either in magnitude or direction when evaluated at any point in the fluid domain, i.e.,

$$\left.\frac{\partial \vec{u}}{\partial \vec{x}}\right|_{t=t_1} \neq 0$$

Rotational flow The fluid particles rotate about their centres of mass as they traverse the domain.

Irrotational flow The fluid particles do not rotate about their centre of mass as they traverse the domain.

The xyz rotation components $\omega_x, \omega_y, \omega_z$, for a flow with velocity $\vec{u} = u\hat{\imath}+v\hat{\jmath}+w\hat{k}$, is given as

$$\omega_x = \frac{1}{2}\left(\frac{\partial w}{\partial y} - \frac{\partial v}{\partial z}\right), \omega_y = \frac{1}{2}\left(\frac{\partial u}{\partial z} - \frac{\partial w}{\partial x}\right), \omega_z = \frac{1}{2}\left(\frac{\partial v}{\partial x} - \frac{\partial u}{\partial y}\right) \tag{2.2}$$

The flow is irrotational if $\omega_x = \omega_y = \omega_z = 0$.

Laminar flow Fluid particles move in parallel paths in layers, such that the path of individual particles do not cross.

Turbulent flow Fluid particles move in a random manner and cross each other's paths resulting in rapid and continuous mixing of the fluid, leading to momentum transfer between the particles.

2.4.2 Forces on fluids and the equation of motion

The forces acting on a fluid in motion are [3, Ch. 6]:

- Gravity force (F_g) due to the weight of the fluid
- Pressure force (F_p) due to the pressure gradient within the fluid domain
- Viscous force (F_v) due to viscosity
- Turbulent force (F_t) due to turbulence
- Surface tension force (F_s) due to surface tension
- Compressibility force (F_e) due to the elastic property of the fluid

Considering mass M of fluid in motion moving with an acceleration a, the equation of motion can be formulated based on Newton's second law as

$$Ma = F_g + F_p + F_v + F_t + F_s + F_e.$$

When the effects due to some of the above forces are negligible, we get:

Reynolds' EoM When the effects of surface tension and compressibility are negligible; $Ma = F_g + F_p + F_v + F_t$.

Navier–Stokes EoM When the effect of turbulence is also negligible; $Ma = F_g + F_p + F_v$.

Euler's EoM When the effect of viscosity is also negligible; $Ma = F_g + F_p$.

2.5 The assumptions in ocean wave mechanics and the existence of the velocity potential

Ocean waves generated by homogeneous wind fields are described by plane waves, in which surfaces of constant phase are planes. Hence, the waves are assumed to be propagating in one direction, say the x direction, and no-flow conditions are assumed appropriate for velocities in the y direction [6, p. 51]. Hence, the incident waves are considered to be plane waves.

Influence from surface tension is only relevant for wave lengths much smaller than those considered in the sense of ocean waves [24, p. 43], and hence surface tension effects can be neglected in the case of ocean waves.

Compressibility of water is a negligible 4.6×10^{-10} Pa^{-1}, and hence compressibility effects can be neglected in the case of surface gravity waves on water [1, p. 35].

The Reynolds number $R_e = \frac{UL}{\nu}$, where U [m/s] is velocity of flow, L [m] is the wave length, and ν [m^2/s] is the kinematic viscosity, is the ratio of inertial to viscous forces. The kinematic viscosity of water at typical ocean temperature is 1^{-6} m^2/s, while the velocities encountered are the order of 10 m/s, with flow structures on the scale of meters or more. Hence, the Reynolds number is very large and viscous forces may be neglected. This means that $\vec{\omega}$ is zero, and hence the flow may be assumed to be irrotational [1, p. 37].

The impact of these assumptions is that the motion of the fluid is now governed by the Euler's equation of motion, with the assumption of irrotationality implying the existence of the scalar velocity potential [13, p. 40] Φ such that

$$\vec{u} = \nabla\Phi. \tag{2.3}$$

Here, the vector differential operator $\nabla = \hat{\imath}\frac{\partial}{\partial x} + \hat{\jmath}\frac{\partial}{\partial y} + \hat{k}\frac{\partial}{\partial z}$.

2.6 The diffraction-radiation problem

Picking up on our discussions on the wave-body interaction problem in Sec. 2.3, if we assume that the displacements of the floating body with respect to the seakeeping coordinate system is small, and that the wave loads are linearized, then the whole effect of the wave interacting with the floating object can be expressed as the sum of the *diffraction* effects and the *radiation* effects [9, p. 39], as shown pictorially in Figure 2.4.

Each wave, viz. the incident wave, the scattered wave, and the six radiation waves, causes respective variation of fluid pressures on the submerged surface of the body. The loads exerted by each wave can be determined by integrating the respective hydrodynamic pressure along the wetted surface of the body. Thus, we define:

Froude–Kriloff Loads The hydrodynamic loads associated with the undisturbed incident wave on the body which is held fixed at its equillibrium position, assuming that the presence of the body does not change the incident wave field.

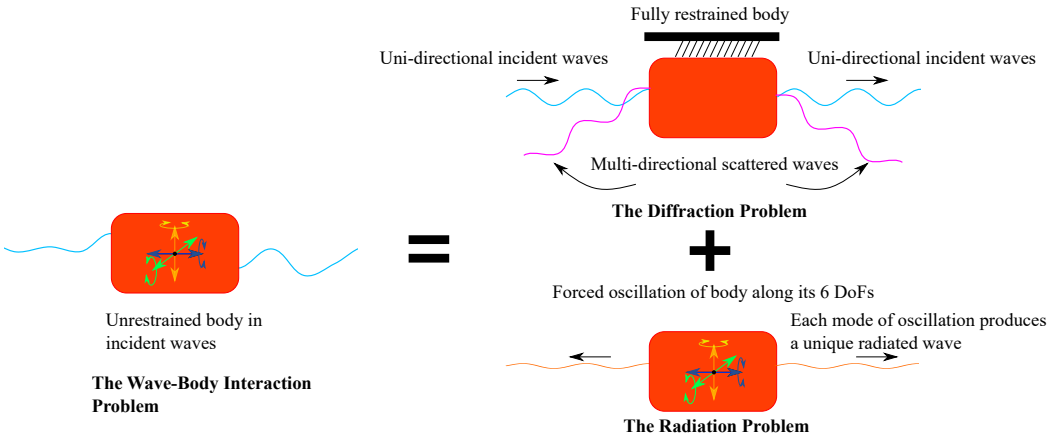

Figure 2.4: The Diffraction–Radiation Problem. Adapted from [9, Fig. 3.1]

The Diffraction Loads The hydrodynamic loads associated with the scattered wave on the body held fixed at its equillibrim position.

Added-mass Loads The part of the hydrodynamic loads associated with the radiation waves that is proportional to the acceleration of the body.

The Damping Loads The part of the hydrodynamic loads associated with the radiation waves that is proportional to the velocity of the body.

The Froude–Kriloff and Diffraction loads together constitute the wave excitation loads $F_w(\omega, \beta)$, while the added-mass and damping loads give the $A(\omega)$ and $B(\omega)$ matrices. These terms may then be plugged into the equation of motion (2.1), to determine the body response.

The hydrodynamic pressures associated with the incident, scattered, and radiated waves, can be determined from the respective velocity potentials by the use of the Bernoulli equation (2.11), which relates the fluid pressures and velocity potentials.

2.7 The boundary value problem for the velocity potential

The velocity potential associated with the incident, scattered, and radiated waves can be determined by solving the governing equation subject to the associated boundary conditions.

2.7.1 The governing equation

The two starting principles for the derivation of the equations of fluid mechanics are the conservation of mass and the conservation of momentum.

Balancing the mass influx of an incompressible fluid, through the bounding surfaces of a fixed control volume, with the internal change of mass associated with the volume, and taking the infinitesimal limits of this control volume, leads to the equation for conservation of mass for an incompressible fluid [6, pp. 7–10],

$$\nabla \cdot \vec{v} = 0 \text{ in } \Omega, \tag{2.4}$$

where, Ω is the fluid domain.

If we consider the definition of the velocity potential given by (2.3) in the above equation, we get

$$\nabla^2 \Phi = 0 \text{ in } \Omega, \tag{2.5}$$

which is the well known Laplace Equation.

The principle of superposition is valid for solutions of the Laplace Equation [16, p. 60], and hence the total potential $\Phi(\vec{x}, t)$ may be expressed as [10, Eq. (11)]

$$\Phi = \Phi_0 + \Phi_7 + \sum_{j=1}^{6} \Phi_j, \tag{2.6}$$

where Φ_0 is the incident wave potential, Φ_7 is the scattered wave potential, and $\Phi_j, j \in \{1, 2 \dots 6\}$ are the radiation potentials.

The task at hand, therefore, is to select solutions for the velocity potential Φ that satisfy certain conditions at the domain boundaries, as depicted in Figure 2.5.

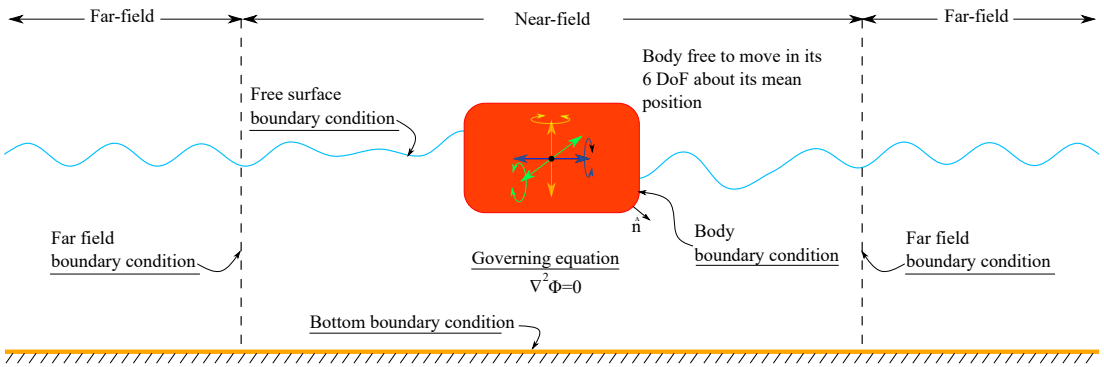

Figure 2.5: The BVP for the total velocity-potential

The formulation the boundary conditions follow.

2.7.2 The boundary conditions

The principle of conservation of momentum implies that, in a control volume moving with the fluid flow, the change in momentum equals the total force acting on the control

volume. Since we ignore forces due to surface tension, compressibility, and viscosity, from Euler's equation of motion given in Sec. 2.4.2, we get, for an infinitesimal volume,

$$\frac{\mathrm{D}(\rho\vec{u})}{\mathrm{D}t} = \vec{F}_g + \vec{F}_p, \tag{2.7}$$

where $\frac{\mathrm{D}}{\mathrm{D}t} = \dfrac{\partial}{\partial t} + \vec{u}\cdot\nabla$ denotes the material derivative with respect to fluid velocity.

Since the fluid is incompressible, (2.7) gives

$$\rho\frac{\mathrm{d}\vec{u}}{\mathrm{d}t} = -(\nabla p) + \rho\vec{g}. \tag{2.8}$$

Here $\vec{g} = [0, 0, -g]^{\mathrm{T}}$, is the gravitational acceleration vector. For details, see [6, Sec. 2.2.3].

Considering (2.3) in (2.8) gives

$$\frac{\partial\nabla\Phi}{\partial t} + (\nabla\Phi.\nabla)\nabla\Phi + \frac{1}{\rho}\nabla p - \vec{g} = 0, \tag{2.9}$$

which can be simplified to

$$\nabla\left(\frac{\partial\Phi}{\partial t} + \frac{1}{2}|\nabla\Phi|^2 + \frac{p}{\rho} + gz\right) = 0. \tag{2.10}$$

Integrating (2.10) gives the Bernoulli equation

$$\frac{\partial\Phi}{\partial t} + \frac{1}{2}|\nabla\Phi|^2 + \frac{p}{\rho} + gz = f(t), \tag{2.11}$$

from which the integration constant $f(t)$ can be eliminated by redefining Φ. For details, see [6, Sec. 2.5].

Free surface flow is usually considered as a limiting case of two-phase flow in which the dynamics of one phase are greatly simplified or ignored. In the case of ocean waves, the velocity field of air is considered zero and a constant atmospheric pressure is assumed at the air-water interface [24, Sec. 2.1.2], referred to as the *free surface*.

For the maintaining the equillibrium of the free surface, there should be continuity of normal stresses over the water-air interface, i.e., the pressure at the free surface equals the atmospheric pressure. Hence, at the free surface defined by $z = \eta(x, t)$, (2.11) gives

$$\frac{\partial\Phi}{\partial t} + \frac{1}{2}|\nabla\Phi|^2 + \frac{p_{atm}}{\rho} + g\eta = f(t), \tag{2.12}$$

which is called as the *dynamic free-surface boundary-condition* (DFSC) [6, p. 48]. Here p_{atm} denotes the atmospheric pressure.

At any physical boundary, either fixed or dynamic, there should not be any flow across the boundary. This means that the fluid particle at the boundary moves with the

boundary, or in other words, the component of the fluid velocity along the normal to the surface at any point on the boundary should be equal to the normal velocity of the boundary at that point.

At the free surface defined by

$$F(\vec{x}, t) = z - \eta(x, y, t) = 0, \tag{2.13}$$

the unit vector normal to the surface is $\hat{n} = \nabla F / |\nabla F|$.

If the surface varies with time, then the total derivative of the surface with respect to time would be zero on the surface. In other words, if we move with the surface, then the surface does not change [6, p. 45].

$$\frac{\mathrm{D}F}{\mathrm{D}t} = 0 \implies \frac{\partial F}{\partial t} + \vec{q} \cdot \nabla F = 0. \tag{2.14}$$

where $\vec{q}$ is the velocity vector associated with a point on the surface.

Since the fluid particle at a point on the boundary stays there at all times, $\vec{u} = \vec{q}$ on the surface. Now, (2.14) gives

$$\frac{\partial F}{\partial t} + \vec{u} \cdot \nabla F = 0. \tag{2.15}$$

If we consider the free-surface given by (2.13), the above equation gives

$$\frac{\partial \eta}{\partial t} + \frac{\partial \Phi}{\partial x} \cdot \frac{\partial \eta}{\partial x} + \frac{\partial \Phi}{\partial y} \cdot \frac{\partial \eta}{\partial y} = \left. \frac{\partial \Phi}{\partial z} \right|_{z=\eta}. \tag{2.16}$$

(2.16) is called the *kinematic free-surface boundary-condition* (KFSC) [6, pp. 47–48].

If we consider the fixed bottom boundary defined by $F(x, y) = z + h(x, y)$, (2.14) gives

$$\frac{\partial \Phi}{\partial x} \cdot \frac{\partial h}{\partial x} + \frac{\partial \Phi}{\partial y} \cdot \frac{\partial h}{\partial y} + \left. \frac{\partial \Phi}{\partial z} \right|_{z=-h} = 0. \tag{2.17}$$

(2.17) is called the *bottom boundary condition* (BBC).

At any point on the body surface, the velocity of the fluid equals the velocity of the body surface, and hence

$$\frac{\partial \Phi}{\partial n} = \frac{\partial \vec{\delta}}{\partial t} \cdot \hat{n}, \tag{2.18}$$

where $\vec{\delta}$ is the position vector of the point on the body surface and $\hat{n}$ is the unit normal vector at the body surface, pointing into the fluid domain. (2.18) is called the *body surface boundary condtion* (BSC). For details, see [6, Sec. 3.2.2].

For waves that are periodic in space and time, the following periodicity conditions apply [6, p. 52]

$$\Phi(x,t) = \Phi(x+L,t), \tag{2.19}$$
$$\Phi(x,t) = \Phi(x,t+T). \tag{2.20}$$

Here L is the wave length and T is the wave period.

(2.19) and (2.20) are not mathematically rigorous. The understanding is that the velocity potential at two points separated by a distance equal to the wave length, along the direction of propagation of the wave, are the same. Also, the velocity potentials at any point in the flow domain evaluated at time instants separated by a wave period are also the same.

The velocity potential of the *scattered* and *radiated* waves should, in addition to the above conditions, satisfy the *far-field boundary conditions*

$$\Phi_7 = 0, \text{ as } r \to \infty, \tag{2.21}$$
$$\Phi_i = 0, \text{ as } r \to \infty, \text{ where } i \in \{1, 2 \dots 6\}. \tag{2.22}$$

Here, r is the distance of the field point from the body surface, or in other words, the norm of $\vec{x}$. The *scattered* and *radiated* waves should also be outgoing, and satisfy proper amplitude behaviour. Details can be found in [15] and [23].

Thus, the BVP to be solved is the governing equation (2.5) subject to the DFSC given by (2.12), the KFSC given by (2.16), the BBC given by (2.17), the BSC given by (2.18), and the LPBCs given by (2.19) and (2.20), and the *far-field* conditions given by (2.21) and (2.22).

Unfortunately, seeking a solution to the above BVP is not an easy task due to the following factors:

i. The DFSC, KFSC, BBC, and BSC contain nonlinear terms, and the presence of nonlinear terms greatly reduces the chances of finding closed analytical solutions.

ii. The DFSC and KFSC are to be applied at the free surface, whose position is a part of the solution, and thus unknown.

For these reasons, a number of additional assumptions are introduced, mainly to obtain a *linear* system of equations with surface boundary conditions imposed at a fixed *mean* position.

2.8 The incident wave velocity potential

The assumption of linearity implies the validity of the superposition principle, and hence, the irregular sea-surface elevation may be represented as the sum of elevations due to

N constituent regular waves with different frequencies, headings, amplitudes, and with random phases. In the case of *long-crested* waves [9, p. 23]

$$\eta(x,t) = \sum_{i=1}^{N} \zeta_{0i} \cos(k_i x - \omega_i t - \epsilon_i), \tag{2.23}$$

where η is the sea surface elevation at a point x along the wave propagation direction at time t, ω_i is the wave frequency, k_i is the wave number, and ϵ_i is the phase of the i^{th} component wave. This extends to all other properties of the wave, viz. the velocity potential, the wave-induced water particle kinematics, and dynamic pressures.

For a regular wave with amplitude a, with wave length L, in water depth h, it is shown that the essential assumptions for the linearization are [7, p. 41]

$$a \ll h, \quad a \ll L, \tag{2.24}$$

Further, the assumption of a horizontal bottom simplifies the solution.

Thus, the BVP for plane, linear, progressive surface gravity waves propagating over a flat sea bed is simplified to seeking the solution for

$$\nabla^2 \Phi_0 = 0, \text{ in } \Omega$$

subject to

i. the linearized DFSC given by

$$\frac{\partial \Phi_0}{\partial t} + \frac{p_{atm}}{\rho} + g\eta = 0, \text{ at } z = \eta(x,t)$$

ii. the linearized KFSC given by

$$\frac{\partial \eta}{\partial t} = \frac{\partial \Phi_0}{\partial z}, \text{ at } z = \eta(x,t)$$

iii. the linearized BBC given by

$$\frac{\partial \Phi_0}{\partial z} = 0, \text{ at } z = -h$$

iv. and the LPBCs given by

$$\Phi_0(x,t) = \phi_0(x+L,t)$$
$$\Phi_0(x,t) = \phi_0(x,t+T)$$

The solution for the above, along with the procedure for computer simulation of regular and irregular waves is discussed in detail in Sec. 4.2.

2.9 The scattering and radiation potentials

We make use of the Green's second identity to arrive at the boundary integral equations (BIE) for the scattering and radiation potentials, as detailed below.

2.9.1 Sources, Sinks, and Dipoles

With reference to (2.3), the velocity potential of a uniform flow with velocity $\vec{u} = u\hat{\imath} + v\hat{\jmath} + w\hat{k}$ [m/s], is $\phi = ux + vy + wz$.

This flow field will be disturbed if a body is introduced into the flow domain, or if the boundary of the fluid domain changes configuration. From a mathematical view point, such a change in the flow field can be effected by the consideration of a point which generates or annihilates fluid mass. Since such points generate or annihilate mass, they violate the continuity condition, and hence the Laplace Equation, at the points where they are located, and they are referred to as *singularities*. Therefore, their presence is permissible only within the body, or at most on the boundary surfaces, and is not allowed within the interior of the fluid [19, pp.116–120].

The singularities that generate fluid are called *sources*, and those that annihilate fluid are called *sinks*.

The velocity potential at point $P(x, y, z)$ due to a source of strength m [m^3/s], located at (ξ, η, ζ) is

$$\phi = \frac{-m}{4\pi r}, \text{ where } r = [(x-\xi)^2 + (y-\eta)^2 + (z-\zeta)^2]^{1/2}. \tag{2.25}$$

If m is negative, the flux direction is negative, and the singularity is called a *sink*.

We note that, in the earlier section, we had used η to represent the sea surface elevation. We use it here again to represent the co-ordinate of the *source* point to maintain uniformity with reference texts.

If we introduce a source and a sink of equal strength in a uniform flow U [m/s] along the positive x direction, with the sink placed downstream, then we observe that the flow field behaves as if it is flowing past an ovoid, called the *Rankine ovoid*, as shown in Figure 2.6.

The pressure distribution on the body represented by the Rankine ovoid may now be determined using the Bernoulli equation, and the hydrodynamic pressure force calculated.

A combination of two equal and opposite sources of strengths $\pm m$, placed at a distance $2a$ apart, where in the limit, $2a$ is taken to be infinitely small, and m infinitely great, such that the product $2ma$ is finite and equal to μ, is called a *dipole* of strength μ. The lines segment considered as drawn in the direction from $-m$ to $+m$ is called its axis.

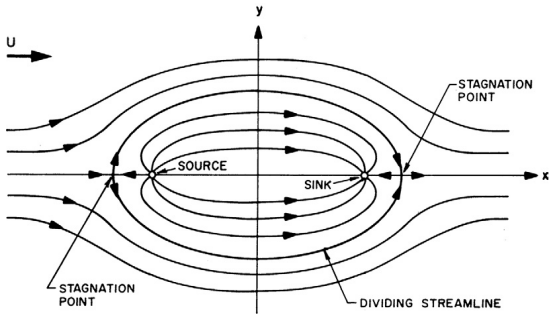

Figure 2.6: Streaming flow past a Rankine ovoid. Sourced from [19, Figure 4.2]

The velocity potential at point $P(x, y, z)$ due to a dipole of strength μ [m^3/s], located at (ξ, η, ζ), and having axis along n' with direction cosines (l, m, n) may be expressed as

$$\phi = \frac{\mu}{4\pi} \frac{\partial}{\partial n'} \left(\frac{1}{r} \right), \text{ where } r = [(x-\xi)^2 + (y-\eta)^2 + (z-\zeta)^2]^{1/2}. \tag{2.26}$$

When the dipole is placed in a uniform flow, the flow field behaves as if the flow was deflected by a sphere of radius $r = (\mu/2\pi U)^{1/3}$ [19, p. 120].

This gives us the intuition that the effects of the presence of bodies of arbitrary shape, in a fluid domain, may be approximated by a proper distribution of singularities.

2.9.2 Green's second identity

In vector calculus, Green's identities relate the bulk with the boundary of a region on which the differential operators act. The derivation of Green's second identity from the divergence theorem follows.

2.9.2.1 The Divergence theorem

Let V be a region in $\mathbb{R}^3$ and let S be the surface of V, oriented with inwards pointing normal $\hat{n}$. Gauss Divergence theorem states that for a C^1 vector field $\vec{F}$,

$$\oiint_{\mathrm{S}} (\vec{F} \cdot \hat{n}) \, \mathrm{dS} = - \iiint_{\mathrm{V}} (\nabla \cdot \vec{F}) \, \mathrm{dV}. \tag{2.27}$$

If $\vec{F}$ is the flow velocity vector, then this equation states that the fluid flux through the closed boundary of the control surface is equal to the rate of convergence of fluid inside the control volume.

2.9.2.2 Green's Identity

If we assign $\vec{F} = (\phi\nabla\psi - \psi\nabla\phi)$ in (2.27), where ϕ and ψ are two single valued scalar functions of position, then we get

$$\oiint_{\mathrm{S}}(\phi\nabla\psi - \psi\nabla\phi)\cdot\hat{n}\ \mathrm{dS} = -\iiint_{\mathrm{V}}(\phi\nabla^2\psi - \psi\nabla^2\phi)\ \mathrm{dV}, \tag{2.28}$$

which is known as Green's second identity.

2.9.3 Boundary integral method for the velocity potential

The theory presented in this section is based on the subject matter in [18, Ch 3], [19, Ch. 4], and [8].

Consider a 3D fluid domain bounded by surface S_0, represented in 2D by Figure 2.7. Let $\mathrm{P}_1(\vec{r_1})$ be a point in the fluid domain, with position vector $\vec{r_1} = (x_1, y_1, z_1)$. Let $\mathrm{P_f}(\vec{r_f})$, with position vector $\vec{r_f} = (x_f, y_f, z_f)$, be any arbitrary field point within the domain. Let ψ and ϕ be two single-valued functions such that $\nabla^2\psi = 0$, and $\nabla^2\phi = 0$. Let $\psi(\vec{r_f}, \vec{r_1}) = 1/r$, where $r = |\vec{r}|$, for $\vec{r} = \vec{r_f} - \vec{r_1}$. Let ϕ represent the velocity potential at any arbitrary field point.

Since ψ becomes singular as $r \to 0$, we need to exclude P_1 from the fluid domain, in order to apply Green's identity. Hence, we consider a spherical surface S_ϵ enclosing P_1, thereby excluding it from the fluid domain.

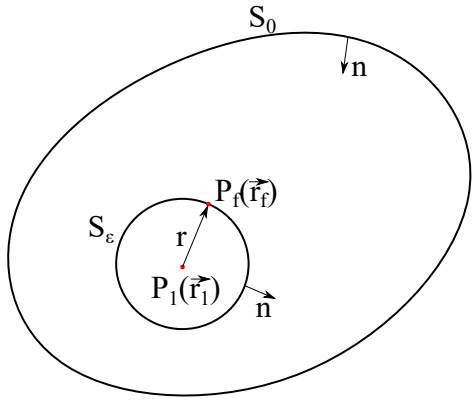

Figure 2.7: Boundary integral representation of field point velocity potential

Now, applying (2.28) gives

$$\iint_{\mathrm{S}_0+\mathrm{S}_\epsilon}\left[\phi\frac{\partial\psi}{\partial n} - \psi\frac{\partial\phi}{\partial n}\right]\ \mathrm{dS} = 0 \tag{2.29}$$

$$\iint_{\mathrm{S}_0}\phi\frac{\partial\psi}{\partial n}\ \mathrm{dS} + \iint_{\mathrm{S}_\epsilon}\phi\frac{\partial\psi}{\partial n}\ \mathrm{dS} = \iint_{\mathrm{S}_0}\psi\frac{\partial\phi}{\partial n}\ \mathrm{dS} + \iint_{\mathrm{S}_\epsilon}\psi\frac{\partial\phi}{\partial n}\ \mathrm{dS}. \tag{2.30}$$

For the spherical surface S_ϵ, the elemental area $dS{=}r^2 \cos\theta d\theta d\beta$ as evident from Figure. 2.8.

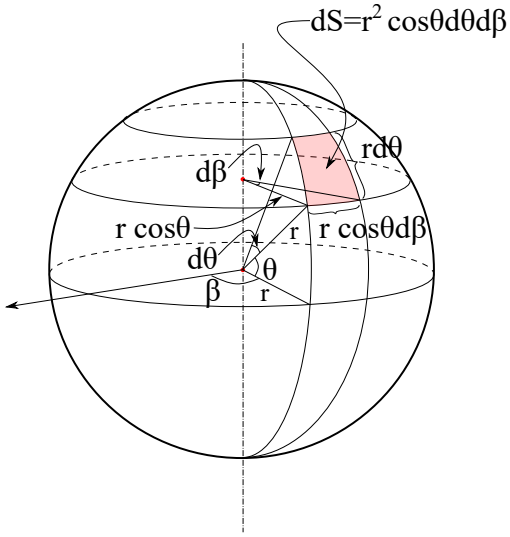

Figure 2.8: Expression of the elemental area dS of a sphere

Here, as $r \to 0$, the spherical surface S_ϵ converges to $P_1(\vec{r_1})$, and the velocity potential may now be considered to be constant inside the small region bounded by S_ϵ. The constant potential $\phi(\vec{r_1})$ may now be taken out of the integral sign. Also, the normal to the surface S_ϵ points in the direction of $\vec{r}$, and hence $\frac{\partial}{\partial n} = \frac{\partial}{\partial r}$. Also, $\iint_{S_\epsilon} dS = 4\pi r^2$.

Considering the second term of the L.H.S.,

$$\lim_{r\to 0} \iint_{S_\epsilon} \phi \frac{\partial \psi}{\partial n}\, dS = \phi(\vec{r_1}) \lim_{r\to 0} \iint_{S_\epsilon} \frac{\partial}{\partial r}\left(\frac{1}{r}\right)\, dS = -4\pi\phi(\vec{r_1}). \tag{2.31}$$

Similarly, considering the second term of the R.H.S.,

$$\lim_{r\to 0} \iint_{S_\epsilon} \psi \frac{\partial \phi}{\partial n}\, dS = \lim_{r\to 0} \int_0^{2\pi} \int_{-\pi/2}^{\pi/2} \left(\frac{1}{r}\right)\left(\frac{\partial \phi}{\partial n}\right) r^2 \cos\theta\, d\theta\, d\beta = 0. \tag{2.32}$$

Therefore, from (2.30), we get

$$\phi(\vec{r_1}) = \frac{-1}{4\pi} \iint_{S_0} \left[\psi \frac{\partial \phi}{\partial n} - \phi \frac{\partial \psi}{\partial n}\right]\, dS. \tag{2.33}$$

Thus, (2.33) represents the velocity potential at point $P_1(\vec{r_1})$ as the sum effect of a distribution of sources with density $\partial\phi/\partial n$ and a distribution of dipoles with dipole density $-\phi$. The distributions are over S_0, and the dipoles are oriented along the normal to S_0.

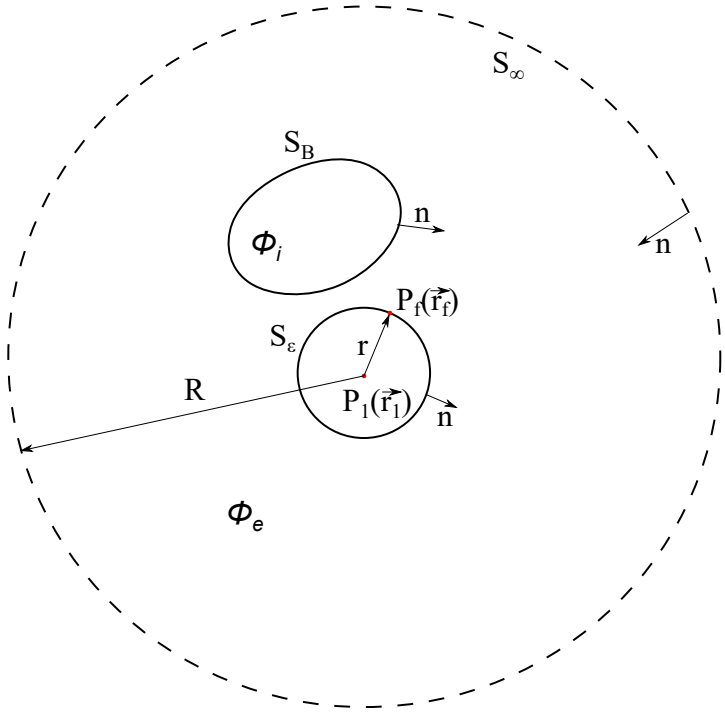

Figure 2.9: Body in infinite fluid

2.9.3.1 Body in infinite fluid domain

Let $P_1(\vec{r_1})$, be a point in the fluid domain, with position vector $\vec{r_1} = (x_1, y_1, z_1)$. Let $P_f(\vec{r_f})$, with position vector $\vec{r_f} = (x_f, y_f, z_f)$, be any arbitrary field point within the domain, as shown in Figure 2.9.

Let $\psi(\vec{r_f}, \vec{r_1}) = 1/r$, where $r = |\vec{r}|$, for $\vec{r} = \vec{r_f} - \vec{r_1}$.

Let S_B represent the body surface and S_∞ represent the imaginary surface bounding the fluid domain at a large distance R from $P_1(\vec{r_1})$.

Let ϕ_e represent the velocity potential in the region interior to S_∞ and exterior to S_B. Let ϕ_i represent the velocity potential inside S_B.

Our aim is to find the potential at a point $P_1(\vec{r_1})$ in the flow domain exterior to the body bounded by the surface S_B, and interior to the flow domain bounded by the surface S_∞.

For fluid flow in the region exterior to S_B and interior to S_∞, we need to consider the potential ϕ_e. Also, in this flow domain, ψ becomes singular at $x_f = x_1, y_f = y_1, z_f = z_1$. Hence, to apply Green's second identity and arrive at the boundary integral representation for the field point velocity potential at $x_f = x_1, y_f = y_1, z_f = z_1$, we employ the limiting procedure described in the earlier section, and arrive at

$$\phi_e(\vec{r_1}) = \frac{-1}{4\pi} \iint_{S_B+S_\infty} \left[\psi \frac{\partial \phi_e}{\partial n} - \phi_e \frac{\partial \psi}{\partial n} \right] \, dS. \tag{2.34}$$

Since S_∞ lies at a large distance from $P_1(\vec{r_1})$, the contribution of the source and dipole distributions on S_∞ to the velocity potential at $P_1(\vec{r_1})$ may be neglected, and hence,

$$\phi_e(\vec{r_1}) = \frac{1}{4\pi} \iint_{S_B} \left[\phi_e \frac{\partial \psi}{\partial n} - \psi \frac{\partial \phi_e}{\partial n} \right] \, dS. \tag{2.35}$$

Since $P_1(\vec{r_1})$ lies outside the region of flow with velocity potential ϕ_i, ψ is never singular inside S_B, and hence, direct application of the Green's second identity inside S_B gives

$$0 = -\frac{1}{4\pi} \iint_{S_B} \left[\phi_i \frac{\partial \psi}{\partial n} - \psi \frac{\partial \phi_i}{\partial n} \right] \, dS. \tag{2.36}$$

Here, we note that the normal to S_B points outside the domain bounded by S_B.

Adding (2.35) and (2.36) gives

$$\phi_e(\vec{r_1}) = \frac{1}{4\pi} \iint_{S_B} \left[(\phi_e - \phi_i) \frac{\partial \psi}{\partial n} - \psi \left(\frac{\partial \phi_e}{\partial n} - \frac{\partial \phi_i}{\partial n} \right) \right] \, dS. \tag{2.37}$$

Setting $(\phi_e - \phi_i) = -\mu$, and $\left(\frac{\partial \phi_e}{\partial n} - \frac{\partial \phi_i}{\partial n} \right) = -\sigma$ in the above yields

$$\phi_e(\vec{r_1}) = \underbrace{\frac{-1}{4\pi} \iint_{S_B} \sigma \psi \, dS}_{\text{Source distribution}} + \underbrace{\frac{1}{4\pi} \iint_{S_B} \mu \frac{\partial \psi}{\partial n} \, dS}_{\text{Dipole distribution}} \tag{2.38}$$

Thus, the velocity potential at any point in an infinite domain may be expressed as the effect of source distributions of strength σ and dipole distributions of strength μ over the body surface.

Determination of the strength of the source and dipole distributions enable the calculation of the velocity potential at any point in the flow domain. Since (2.38) does not specify a unique combination of sources and dipoles for a particular problem, depending on the physics of the problem, we may require:

- $\phi = \phi_i$ on S_B, whereby the dipole term vanishes, and the flow is then caused by the presence of a source distribution on the body surface. The tangential velocities on the two sides of the boundary are then continuous, while the normal velocities are discontinuous.
- $\frac{\partial \phi}{\partial n} = \frac{\partial \phi_i}{\partial n}$ on S_B, whereby the source term vanishes, and the flow is then caused by the presence of a dipole distribution on the body surface. The normal velocity across the boundary is then continuous, while the tangential velocities are discontinuous.

The Green function

In formulating (2.38), we had specified the function $\psi = \frac{1}{r}$, which is defined at all points except at the point when $r = 0$. Such functions are referred to as *Green functions*, and also as *source potentials* since the velocity potential at a point due to a point source located at a distance r, is proportional to $1/r$.

In problems where the body moves in a domain bounded by other boundaries, such as the fluid free surface, the sea bottom, or canal walls, additional boundary conditions are imposed on the problem, and there is often a computational advantage if the associated Green function is modified to satisfy the same boundary conditions as the velocity potential ϕ. Unfortunately such Green functions are not readily known, except for some simple body geometries.

However, once such a Green function is known, an explicit solution for the velocity potential in terms of the prescribed normal velocity on the boundaries may be formulated [19, pp. 137–138], as will be detailed in the following discussions.

2.9.4 The Hess and Smith panel method

From Sec. 2.9.1, we get the intuition that the effect of the presence of a body, in a fluid domain, may be approximated mathematically by a proper distribution of singularities on the body surface [19, p. 133].

From our discussions on (2.38), we notice that requiring $\phi_e = \phi_i$ enables the specification of the field point velocity potential, in the case of a body placed in infinite fluid, to be prescribed by simple sources distributed on the body. Thus

$$\phi(x, y, z) = \iint_{S_B} \sigma(\xi, \eta, \zeta) G(x, y, z; \xi, \eta, \zeta) \, \mathrm{dS}, \text{ where } G = -\frac{1}{4\pi r}. \tag{2.39}$$

Here, (x, y, z) are the co-ordinates of the field point where the potential is to be determined, while (ξ, η, ζ) are the co-ordinates of the source point on the body surface defined by $S_B(\xi, \eta, \zeta) = 0$.

Determination of the source strength $\sigma(\xi, \eta, \zeta)$ at all points on the body surface would enable the evaluation of the required velocity potential.

Considering the problem of a submerged body in infinite fluid, with a uniform incident flow for simplicity, we may express the fluid velocity at any point in the flow domain as the gradient of a resultant velocity potential $\phi = \phi_d + \phi_\infty$, where ϕ_∞ is the undisturbed velocity potential defining the incident flow, while ϕ_d is the disturbance potential caused due the presence of the body in the flow domain. This disturbance potential is induced by the source distribution on the body surface.

The resultant velocity potential should satisfy:

i. The Laplace equation $\nabla^2 \phi = 0$ at all points in the fluid domain

ii. The impenetrability condition on the body surface $\left.\frac{\partial \phi}{\partial n}\right|_S = \left.\hat{n} \cdot \nabla \phi\right|_S = 0$

iii. The far field condition $\phi \to \phi_\infty \implies \phi_d \to 0$ as $r \to \infty$

The impenetrability condition states that, at the rigid surface boundary, the normal component of the fluid velocity should be zero. To effect this mathematically, it is required that the normal component of the velocity specified by the disturbance potential should oppose the normal component of the incident velocity potential, i.e., $\partial\phi_d/\partial n = -\partial\phi_\infty/\partial n$, at all points on the body surface.

Thus, in applying the impenetrability condition at the body surface, one is required to determine the normal component of the induced velocity at a point on the body surface, due to source distributions on the body surface.

The normal component of the disturbance potential ϕ_d at p, expressed as $\partial\phi_d(p)/\partial n(p)$, due to sources of strength $\sigma(q)$ at q on the body surface, is expressed as

$$\frac{\partial \phi_d(p)}{\partial n(p)} = \frac{\partial}{\partial n(p)} \left[\iint_{S_B} \sigma(q) G(p,q) \, \mathrm{dS} \right]. \tag{2.40}$$

Here, $G(p,q)$ is the Green function defined in (2.39). At $p = q$, $r = 0$, and $G(p,q)$ becomes singular. Hence, the contribution of the local source density to the local normal velocity is to be determined in the Cauchy principal-value sense, while the contribution of the remainder of the surface to the local normal velocity is given by equations of the form of (2.40) [14, p. 19].

It is seen that the self-induced normal velocity on the positive side of the body surface at p is $\sigma(p)/2$.

Application of the impenetrability condition gives

$$\frac{\sigma(p)}{2} + \iint_{S_B} \frac{\partial}{\partial n(p)} \{\sigma(q) G(p,q)\} \, \mathrm{dS} = -\hat{n}(p) \cdot \nabla \phi_\infty \tag{2.41}$$

Once this equation is solved for σ, for all points on the body surface, the velocity components at any point of the flow are obtained by differentiating equations of the form (2.39) in the co-ordinate directions and adding the components of the incident flow.

Hess and Smith [14] presents a method for the numerical solution of (2.41), where the body surface is approximated by flat quadrilateral panels, over each of which the source density is assumed constant, thereby replacing the integral equation by a set of linear algebraic equations.

They also present analytical expressions for the velocity potential and component velocities induced by a plane source quadrilateral in terms of the panel co-ordinates and their distance from the point where the potential is to be evaluated.

The normal velocity at the centroid of the i^{th} quadrilateral due to a unit source density distribution on the j^{th} quadrilateral can be expressed as

$$A_{ij} = \hat{n}_i \cdot \vec{V}_{ij}, \tag{2.42}$$

where $\vec{V}_{ij}$ is the induced velocity at the centroid of the i^{th} quadrilateral due to a unit source density distribution on the j^{th} quadrilateral.

The normal velocity at the centroid of the i^{th} quadrilateral due to source density distributions over the entire body surface approximated by N quadrilaterals is thus

$$\sum_{j=1}^{N} A_{ij}\sigma_j. \tag{2.43}$$

The algebraic equivalent of the integral equation (2.41) is thus

$$\sum_{j=1}^{N} A_{ij}\sigma_j = -\hat{n}_i \cdot \nabla\phi_\infty, \quad i = 1, 2 \ldots N \tag{2.44}$$

Once the values of the source densities are obtained, the resultant velocity potential and fluid velocities at the null point may be determined, from which the hydrodynamic pressures exerted at the panel null point may be obtained by using the Bernoulli equation. Once the hydrodynamic pressures associated with each panel are known, the loads are calculated by simple multiplication with the respective panel area.

The Hess and Smith method may be extended to determine the wave excitation and radiation loads by the use of the appropriate boundary conditions and Green function.

Ch. 6 deals comprehensively with the subject matter.

2.10 Simplifications for a non-diffracting object

The relative dimension D of the object, with respect to the wave length λ and the wave height H, determines the significance of forces to be considered in a wave-body interaction problem. See Figure 2.10.

When the structure is relatively small compared to the wave length ($L > 5D$), the diffraction forces are negligible [9, p. 61]. The wave loads in such cases can be determined based on the significance of the inertia and drag forces [4, p. 169].

2.10.1 The Froude–Kryloff force

When the drag force is small, and the inertia force predominates, the wave loads can be approximated based on the Froude–Krylov theory [4, p. 169]. The force acting on the object, in this case, can be expressed as [9, p. 61]

$$F_i = -\iint_{S_{0B}} pn_i \mathrm{dS} + A_{i1}a_1 + A_{i2}a_2 + A_{i3}a_3, i \in \{1, 2, 3\}. \tag{2.45}$$

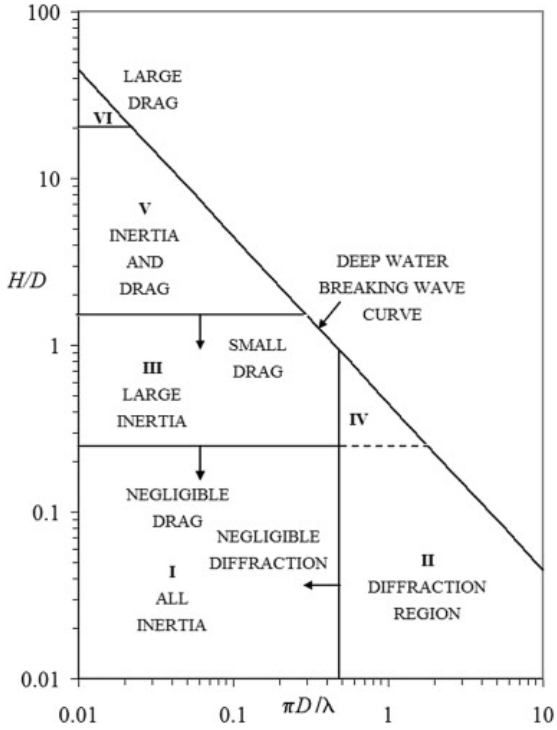

Figure 2.10: Force Regimes [excerpt from DNV-RP-C205]

Here, p is the pressure in the undisturbed wave field, $\hat{n} = (n_1, n_2, n_3)$ is the unit normal vector to the body surface, defined to be positive into the fluid. The integration is over the average wetted surface of the body S_{0B}, and a_1, a_2, a_3 are the acceleration components along the x, y, z axes of the undisturbed wave field evaluated at the geometrical mass centre of the body. A_{i1}, A_{i2}, and A_{i3} are the added masses along the i^{th} direction due to fluid flow along the three co-ordinate axes.

The first term in the R.H.S. of (2.10.1) is the Froude-Kryloff force.

2.10.2 The Morison equation

When the drag forces are not negligible, then the wave loads can be approximated using the Morison equation. The Morison equation assumes the force to be composed of inertia and drag forces linearly added together. For unit length of a vertical cylinder extending from the sea-bed to the still water level (SWL), the Morison loads may be expressed as

[4, pp. 170–171]

$$f = \underbrace{C_M \rho \frac{\pi}{4} D^2 \dot{u}}_{\text{Inertia term}} + \underbrace{C_D \frac{1}{2} \rho D u |u|}_{\text{Drag term}} . \tag{2.46}$$

The components involve an inertia coefficient C_M and a drag coefficient C_D, which must be determined experimentally. ρ [kg/m^3] is the water density, D [m] is the diameter of the cylinder, and u [m/s] is the horizontal water particle velocity evaluated at the centre-line of the cylinder.

The Morison equation may be extended to the case of inclined and/or oscillating cylinders in the presence of waves and current [4, p. 189].

The articles presented in Ch. 4 are based on the application of Froude–Kryloff and Morison loading to develop *Modelica* component models.

2.11 Mooring systems

Mooring systems are required to limit excursions of the floating platform from its station due to environmental and operational loads. A mooring system is made up of a number of cables, attached to the floating structure at different points, with the lower end of the cables attached to the sea bed. The configuration of this arrangement, and the materials used in the fabrication of the mooring cable, is dictated by several factors like the type of floater, system concept, water-depth, offshore site, environmental conditions, etc. For details, see [5, Ch. 8].

Irrespective of the mooring system viz. spread, taut, single point, turret etc, the line itself may be either slack or taut, as shown in Figure 2.11. In carrying out dynamic analysis of a mooring line, it is usual to establish a static configuration, and then develop nonlinear time domain solutions about this initial shape [5, Sec. 8.5.3]. The initial configuration, in case of a slack mooring, is based on catenary theory, while for a taut mooring, it may be established based on the anchor and floater positions.

2.11.1 Catenary theory

When one end of a chain or rope lying on a horizontal surface is raised to a height, the curve of the line follows a half catenary. The derivation of the intrinsic equation of the catenary, the catenary equation in rectangular co-ordinates, and other simple relations are given in [21], while [9, Ch. 8] describes solutions of the inelastic cable line (catenary) equations.

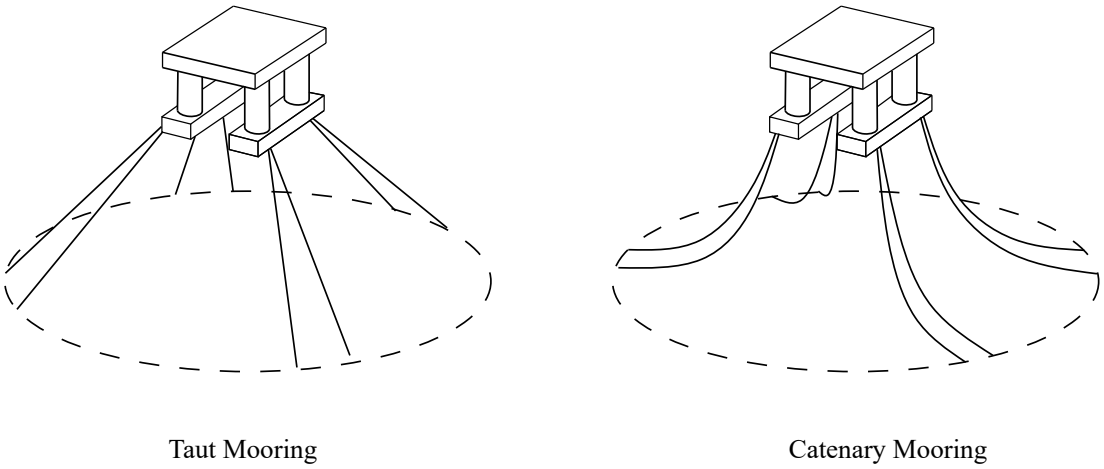

Figure 2.11: Taut and catenary mooring spread

2.11.2 Lumped-mass method

Mooring simulations predominantly use the lumped-mass, finite-element or finite-difference schemes to model small segments of each line whose shape is altered from the static catenary profile by the water resistance.

The basic concept of the lumped-mass method is that a cable may be represented as a series of segments joined at points called nodes. In one variation of this method, all forces and masses along each segment are assumed to be shared equally by the two nodes associated with the segment. Inextensible cable segments are considered to be straight lines without mass, and sections of extensible cable are considered to be straight springs without mass. In another type of the method, the segments are imagined to be straight rigid cylinders with massless universal joints at the junctions.

Equations governing the motion of the elements can now be determined directly from Newton's laws of motion, or indirectly from Langrange's equations or Hamilton's principle.

Articles presented in Ch. 4 are based on the quasi-static catenary theory, while the article presented in Ch. 5 is based on the lumped-mass approach.

2.12 Risers and riser tensioner systems

A riser is a unique common element to many offshore structures and is basically a conduit that connects the platform to the subsea infrastructure component, which in most cases is a well head. Drilling risers are used to contain fluids for well control, while production risers are used to convey hydrocarbons from the seabed to the platform. While production risers remain connected much of the time, drilling risers undergo repeated deployment

and retrieval operations during their lives. Details can be found in [2, Part IV] and [5, Ch. 9].

With reference to Figure 2.12, we understand that it is required to isolate the riser from the motions of the platform in order to prevent buckling of the riser pipe. In the case of drilling risers, it is also required to prevent excessive deformation of the riser due to current loads, which hinders the drilling operation. Further, it is also required to ensure a clean lift-off of the LMRP from the BOP, in case the riser needs to be disconnected.

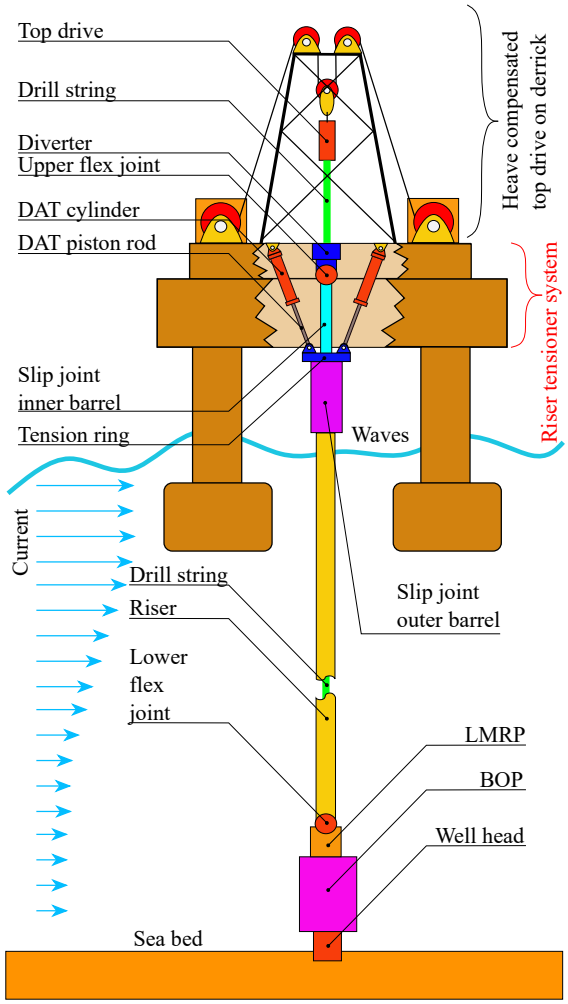

Figure 2.12: MODU with drilling riser attached to well head

The above requirements are met by the provision of a means to keep the riser pipe always in tension. For a production riser, this may be achieved by the provision of buoyancy

tanks, while for drilling risers, as shown in Figure 2.12, it is usually a hydro-pneumatic arrangement, commonly referred to as the riser tensioner, that provides this tension.

The two widely used arrangements for the riser tensioner system are the wire-line tensioner (WRT), and the direct-acting tensioner (DAT). The principle of operation is the same for both systems, with the difference lying in the way in which the tensioner cylinder force is applied to the top end of the riser, as illustrated in Figure 2.13.

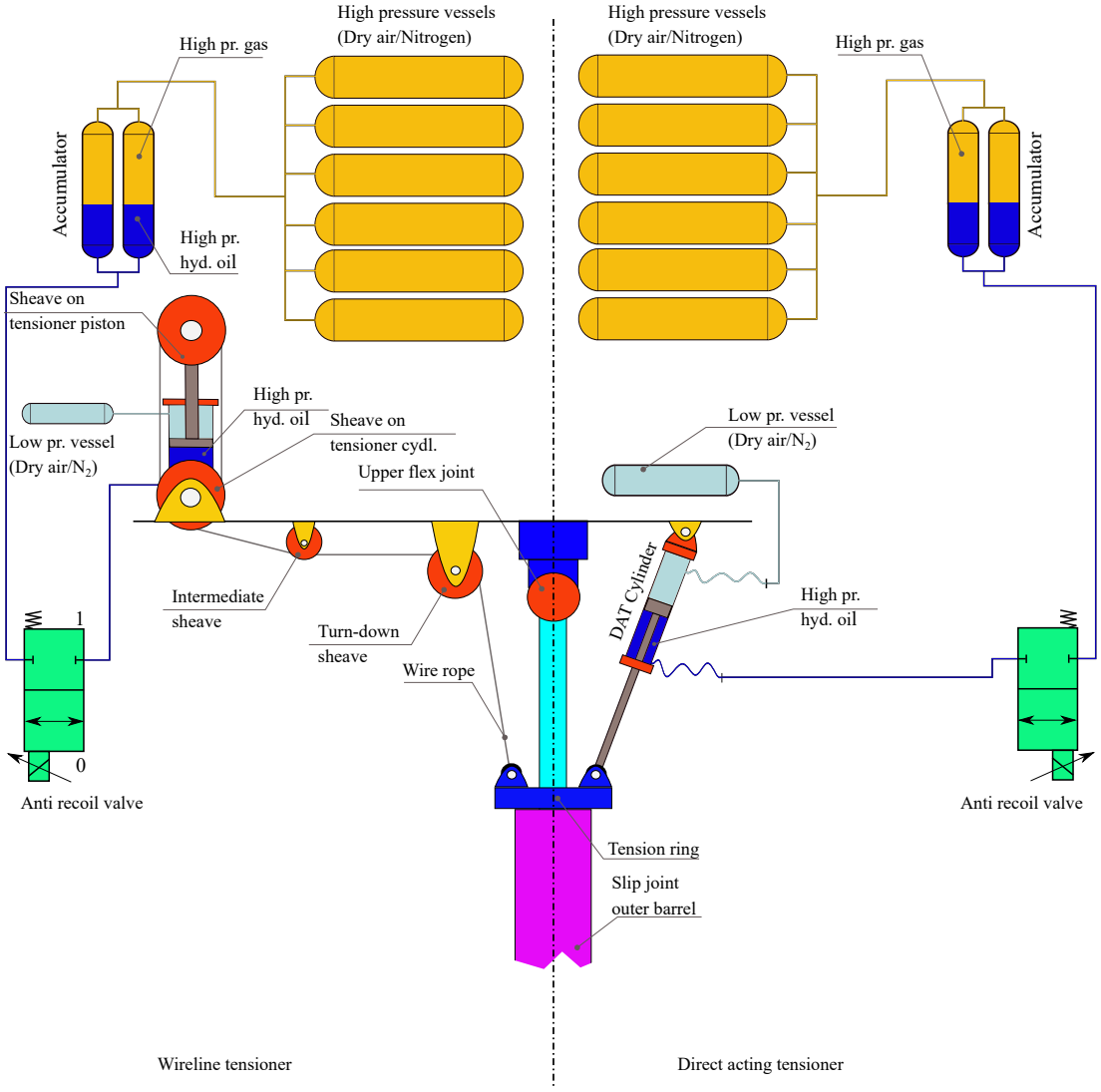

Figure 2.13: Riser-tensioner types

The volume of the high-pressure vessels being much larger than the stroke of the

tensioner cylinder, the force on the high pressure side of the hydro-pneumatic cylinder remains fairly constant as the tensioner cylinders extend and contract to compensate for the heave motion of the platform, thus ensuring that the riser is kept in a near constant tension at all times.

The articles presented in Ch. 7 deal with multiphysical simulations of a drilling riser.

2.13 Contemporary practices in simulation of offshore systems

The prevailing practice when it comes to simulation of offshore systems may be summarized briefly as below:

1. Determine the force regime depending on the relative size of the object.
2. For non-diffracting objects, time domain simulation software like *OrcaFlex* can determine the wave loads directly. For diffracting objects, a frequency domain hydrodynamic analysis has to be carried out using software like *WAMIT* or *Ansys-Aqwa*, which use the panel method, to determine the frequency dependent hydrodynamic parameters. These hydro-dynamic parameters are then passed on to time-domain software like *OrcaFlex* for subsequent use in time domain simulation.
3. Slender structures like moorings, risers etc. can be modelled directly in software like *OrcaFlex*, and attached to the floating platform, for coupled simulations.
4. Application programming interfaces allow for specification of thruster loads, winch wire tensions, winch wire pay-out rates etc.

As an example, we list the steps for simulating the response of a subsea load suspended from a crane mounted on an offshore support vessel.

1. Since the vessel is a diffracting object, we need to determine the hydrodynamic coefficients. The steps for carrying out a frequency domain hydrodynamic analysis using *Ansys-Aqwa* are listed below:
   a) Develop the surface model of the vessel hull, and split it at the waterline using *Spaceclaim*, the built-in surface modeler in *Ansys-Aqwa*, as illustrated in Figure 2.14a.
   b) Mesh the surface, and specify the wave directions and frequencies for which the hydrodynamic parameters are to be determined, as illustrated in Figure 2.14b.
   c) Run the frequency domain analysis to determine the hydrodynamic parameters, as illustrated in Figure 2.14c.
2. Import the hydrodynamic parameters into time domain software *OrcaFlex*, attach slender non-diffracting objects like mooring lines, winch wires, loads etc, specify the environmental parameters like wave heights, wave periods, current profiles etc., and

run the time domain analysis to determine the required dynamics, as illustrated in Figure 2.14d.

In the above example, one may use the application programming interface capabilities of *OrcaFlex* to control the pay-out rate of the crane winch, based on a controller coded in *Python*, as described in the demonstration example from *Orcina* [20].

However, to simulate the dynamic response of the actual electro-hydraulic crane, one needs to either:

1. Devise novel methods to link the electro-hydraulic model of the crane, modelled in a multiphysics software, to the load component in the ocean engineering software, where the hydrodynamics are simulated, and then run both software in a *co-simulation* approach.

(OR)

2. Develop component models to simulate the hydrodynamic response of diffracting as well as non-diffracting objects in the multiphysics software where the electro-hydraulic crane is modelled, and simulate the response in an *integrated* simulation approach.

Multiphysical simulations are usually carried out using software based on the *Modelica* modelling language, as discussed in the following section.

The articles presented in Ch. 7 deals with the *co-simulation* approach, while those presented in Ch. 4–6 are geared towards development of component models for carrying out *integrated* simulations.

2.14 Dynamic simulation using Modelica

Modelica is a non-proprietary, object oriented, declarative, multi-domain modelling language for dynamic simulation. It follows the *acausal* modelling philosophy, and is used extensively in the automotive and aerospace sectors. Hilding Elmqvist is the key architect of *Modelica*, but many others have contributed to its development. The non-profit *Modelica Association* manages the continually developing Modelica language and the *free* Modelica Standard Library. At present, the standard library has over 1600 *component-models* and 1350 *functions* from the electric, electronic, mechanical, fluid, and control engineering domains. However, lack of hydrodynamics, mooring, and other relevant component models currently limit the use of Modelica in the simulation of ocean engineering systems.

Modelica has many commercial implementations like *Dymola*, *SimulationX*, *MapleSim*, and *JModelica*, to name a few. *OpenModelica* is currently the only open-source implementation of *Modelica*, and *OMEdit* is its graphical user interface.

For more technical details, see [12].

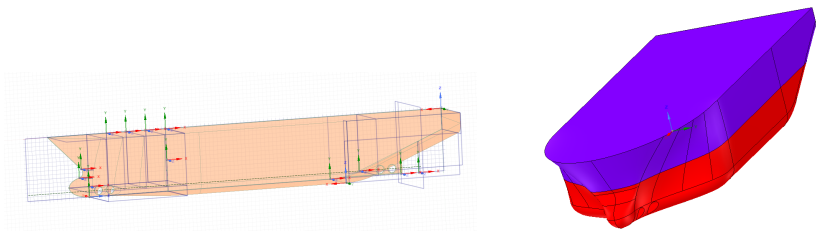

(a) Develop the surface model, split at the waterline

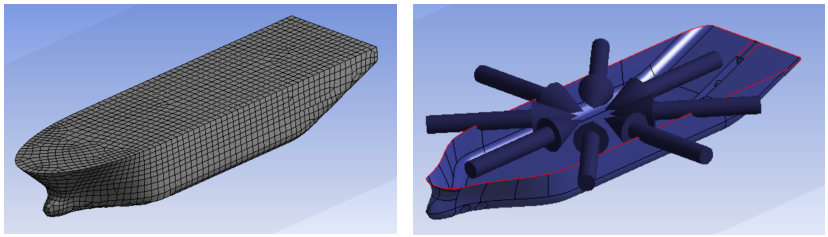

(b) Mesh the surface and specify wave directions and frequencies

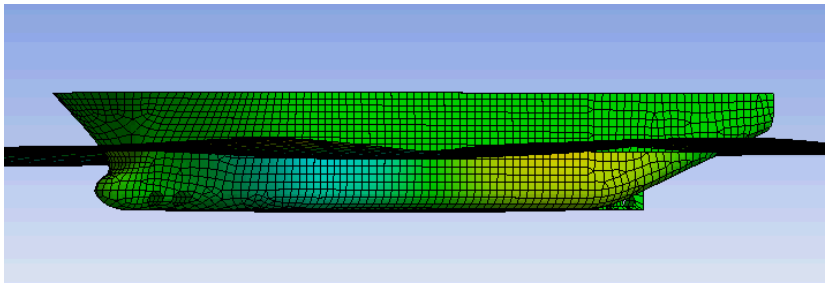

(c) Run the frequency domain analysis to get the hydrodynamic parameters

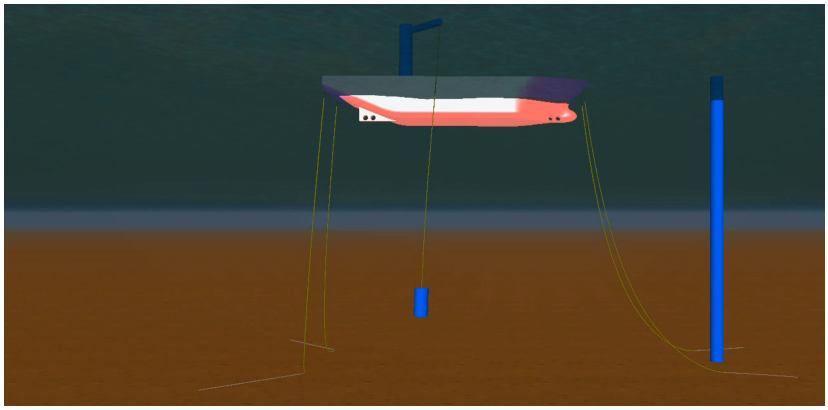

(d) Import the hydrodynamic parameters from the frequency domain analysis, attach non-diffracting objects like moorings, subsea loads, etc., and carry out time domain analysis

Figure 2.14: Steps in contemporary simulation of offshore operations

Chapter 3

The current research

3.1 The project description

The detailed project description is given in Appendix B. For a quick reference, we list out the main objectives, followed by a description of the correlation between the articles presented in the following chapters and the project objectives.

3.2 Objectives

The main objectives of the research, as stated in the project description, are:

1. Develop component models to constitute a *Standard Library* for ocean-engineering in the open-source *OpenModelica* environment, through the performance of three sub-tasks:
    a) Modelling of a simple wave energy conversion system involving the implementation of *Modelica* components to simulate regular and irregular waves, heave and surge responses of a cylindrical floating object, and the response of a catenary mooring system.
    b) Simulate the response of a simple geometry semi-submersible by the implementation of a Modelica component that solves the diffraction-radiation problem, to determine the frequency dependent hydrodynamic parameters.
    c) Simulate the response of a flexible slender structure, like the marine riser, in the *Modelica* environment.
2. Develop a multiphysics model using industry accepted commercial software (*Ansys-Aqwa, SimulationX* and *OrcaFlex*), to simulate the fully coupled response of a drilling riser in recoil, effectively capturing the influences from the platform, the riser hydrodynamics, and the response of the hydro-mechanical riser-tensioner system to:

a) Formulate a method to improve fatigue performance of the riser by controlling the response of the anti-recoil valve of the riser tensioner system.

b) Compare the performance of the multiphysics model with real world operational data (not necessarily recoil only), sourced through the industrial partners.

3.3 The articles

The research to be conducted under the project was planned in a away so as to be presented as articles in peer-reviewed conferences and journals. The article-based approach adopted in this thesis is a natural extension of such a research pattern. Each article presented is correlated to the objectives of the project as detailed in the introduction section of the chapter in which the article is included. A brief overview is shown below for easy reference:

S.No	Article Name	Article Type	Objective Correlation	Status
1.	Towards the Development of an Ocean Engineering Library for OpenModelica	Conference paper	1(a)	Published
2.	Modelica Component Models for Oceanic Surface-Waves and Depth-Varying Current	Conference paper	1(a)	Published
3.	Modelica Component Models for Non-Diffracting Floating Objects and Quasi-Static Catenary Moorings	Conference paper	1(a)	Published
5.	Dynamic Simulation of a Mooring Catenary Based on the Lumped-Mass Approach: OpenModelica and Python Implementations	Conference paper	1(c)	Published
4.	Simulating the Dynamics of a Chain Suspended Sub-Sea Load Using Components from the Modelica MultiBody Library	Conference paper	1(c)	Published

S.No	Article Name	Article Type	Objective Correlation	Status
6.	An Open-Source Python-Based Boundary-Element Method Code for the Three-Dimensional, Zero-Froude, Infinite-Depth, Water-Wave, Diffraction-Radiation Problem	Journal paper	1(b)	Submitted
7.	Co-Simulation of the Hydro-Pneumatic Riser-Tensioner System I – Methodology Synthesis	Journal paper	2(b)	Submitted
8.	Co-Simulation of the Hydro-Pneumatic Riser-Tensioner System II – Field Verification and Advanced Simulations	Journal paper	2(b)	Submitted

Table 3.1: The articles presented in this work, and their correlation to the objectives of the research project.

Thus, we see that articles produced in the course of the research demonstrate attainment of the two broader objectives of the project. Though specific project objectives 1(b), 1(c) and 2(b) of the project have not been met in full, from the articles in the following chapters, one can observe that a strong foundation for research towards the attainment of the above objectives have been laid.

The articles listed in Table 3.1 are grouped together, inside chapters, based on their theoretical basis and their relevance to the project objectives. An overview is given in the table below:

Chapter	Article Number(s)
Chapter 4	Articles 1, 2, and 3
Chapter 5	Articles 4 and 5
Chapter 6	Articles 6
Chapter 7	Articles 7 and 8

Table 3.2: The grouping of articles into chapters.

Chapter 4

An ocean engineering library for OpenModelica

In Sec. 2.8, we discuss the formulation of the BVP for the incident wave velocity potential. In Sec. 2.10, we describe how the Froude–Kriloff and Morison equation can be used to determine wave and current loads on relatively small structures. In Sec. 2.11.1, we introduce the catenary theory.

In the articles presented in this chapter, we build upon the theoretical basis, and develop component models to simulate regular and irregular waves, depth-varying current, hydrodynamic response of non-diffracting floating objects, and response of moorings based on the quasi-static catenary approach. The component models so developed are grouped together to constitute the preliminary OceanEngineering library for *OpenModelica*, and the associated files are made available for public access at locations specified inside the articles.

In the first article, presented in Sec. 4.1, we introduce the concept of the *Modelica Ocean Engineering Library*, through the example of trying to model a catenary moored wave-energy converter.

In the second article, presented in Sec. 4.2, we go into the details of the general requirements to be kept in mind while developing a *Modelica* library for ocean engineering applications. We also describe in detail the development of component models to simulate regular as well as irregular waves, and depth varying current.

In the third article, presented in Sec. 4.3, we go into the details of the development of component models to simulate the hydrodynamic response of non-diffracting floating objects, and catenary moorings based on the quasi-static catenary theory.

Thus, the articles presented here have direct correlation with general project objective 1, and specific project objective 1(a), as given in Sec. 3.2.

4.1 Towards the development of an ocean engineering library for OpenModelica

The citation of the published article is given below:

S. Viswanathan and C. Holden. *Towards the Development of an Ocean Engineering Library for OpenModelica*. Proceedings of the ASME 2019 38th International Conference on Ocean, Offshore and Arctic Engineering. Volume 7B: Ocean Engineering. Glasgow, Scotland, UK. June 9–14, 2019. V07BT06A025. ASME. https://doi.org/10.1115/OMAE2019-95054

The postprint version of the paper follows.

TOWARDS THE DEVELOPMENT OF AN OCEAN ENGINEERING LIBRARY FOR OPENMODELICA

Savin Viswanathan*
Department of Mechanical and Industrial Engineering
Norwegian University of Science and Technology
NTNU
NO-7491, Trondheim, Norway.
Email: savin.viswanathan@ntnu.no

Christian Holden
Department of Mechanical and Industrial Engineering
Norwegian University of Science and Technology
NTNU
NO-7491, Trondheim, Norway.
Email: christian.holden@ntnu.no

ABSTRACT

The development of component models to populate a proposed *OpenModelica* standard library for the ocean engineering domain is described through the process of modelling the response of catenary-moored wave-energy converters in the 'free-to-use' *OpenModelica* simulation environment and its associated *OMEdit* graphical user interface. A wave energy conversion concept is presented, followed by the implementation of *Modelica* component models and functions to simulate wave, current, and mooring loads on a cylindrical floating object. The irregular sea surface is specified using the Pierson-Moskowitz spectrum and the heave force on the buoy is determined based on the Froude-Krylov formulation. Mooring load formulation is based on the catenary theory. Combined wave and current loads on the buoy and on the mooring chain are arrived at using the Morison equation. The results are verified with the commercial software *Orcaflex*, and the preliminary *OceanEngineering* library is made available for download. The integrated simulation of the multiphysical wave energy buoy system is then carried out to determine the energy harvest potential, and results discussed. An alternative design is then suggested and simulated to demonstrate the advantages of using the component-based approach.

Keywords: *Modelica* ocean engineering library, Multiphysical simulation of offshore systems, *Modelica* component models for ocean waves, non-diffracting objects, and catenary mooring.

*Corresponding author.

INTRODUCTION

Modelica is a non-proprietary, object-oriented, equation-based programming language to mathematically model complex multiphysical systems for the purpose of dynamic simulation. Since it is based on equations instead of assignment statements, the causality is unspecified and becomes fixed only when the corresponding equation systems are solved (acausal modelling). The main advantage with acausal modelling is that the solution direction of the equations will adapt to the data flow context in which the solution is computed, and this makes *Modelica* component models more reusable than traditional classes containing assignment statements where the input-output causality is fixed [1].

The *Modelica Standard Library* contains about 1600 model components and 1350 functions from the electric, electronic, mechanical, fluid, and control engineering domains. Commercial as well as free-of-charge *Modelica* simulation environments are available, and have been used by industry, especially in the automotive sector, to simulate and analyze product performance [2].

In spite of the many advantages that *Modelica* has to offer, its utilization in the offshore domain, which, even in its simplest engineering applications, is highly multiphysical and interdisciplinary, has been minimal. One of the reasons behind this could be the lack of *Modelica* component models relating to offshore engineering, especially those dealing with simulation of irregular ocean surface waves, hydrodynamics, mooring, etc.

The present work is directed towards the development of a *Modelica* standard library for the ocean engineering domain pop-

ulated with domain-specific component models and functions. The work is carried out in the free-to-use *OpenModelica* simulation environment and its *OMEdit* graphical user interface. An online search for literature revealed that very little has been published on the subject, the most relevant being Brommundt *et al.* on the experiences of modeling a floating support structure for offshore wind turbines [3].

As a first step, the modelling and simulation of a simple wave energy converter buoy is described, involving the development of *Modelica* component models for the ocean engineering domain. The widely used commercial software, *Orcaflex* is used to verify the satisfactory performance of the hydrodynamics and mooring characteristics. The components and functions are then packaged to constitute the *OceanEngineering* library, which is available for public download at `https://github.com/Savin-Viswanathan/OELib_OMAE2019`. The integrated model of the multiphysical system is then built up using these components and simulated. Following the discussion of the simulation results, an alternative design is proposed and simulated to showcase the benefits of component-based modelling.

Keeping in line with the intent of this work, which is *only* to showcase the advantages of developing an *Ocean Engineering* library for *Modelica*, and *not* the detailed modelling of wave energy conversion devices, modelling is described only to the extent required to simulate the motion of the permanent-magnet core inside the coil of the linear electric generator, as a measure of electrical energy output potential, in both cases.

THE WAVE BUOY CONCEPT

A free-floating point-absorber wave buoy with an internal spring-suspended permanent-magnet core which is free to oscillate inside an induction coil will produce some electrical power when subjected to wave action [4].

Let us consider, for the purpose of developing a *Modelica* model, that we would like to simulate the performance of a system working on the concept of the *DC3* buoy described in [4], but, with some design changes, and the inclusion of a mooring catenary to constrain buoy drift. The present system concept is shown in Fig. 1, and the internal detail of the buoy is depicted in Fig. 2. The power output will be a function of the wave load, the hydrodynamic response of the buoy in the heave direction, and the mooring force. The mooring system response is in turn a function of the hydrodynamic response of the buoy in the surge direction, which is dependent on the wave as well as the current force on both the buoy and on the mooring line itself.

The objective at this stage is to develop an integrated *Modelica* component model to simulate the multiphysics of the whole system so as to determine the motion response of the suspended core, as a measure of power output potential in various sea states.

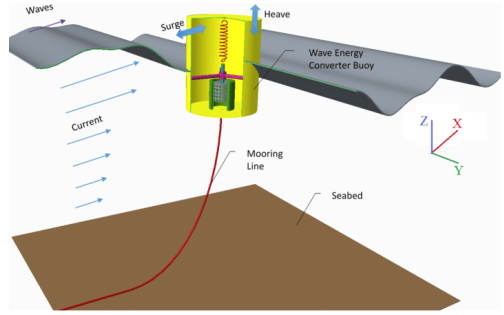

FIGURE 1. CONCEPT OF THE WAVE ENERGY CONVERTER BUOY.

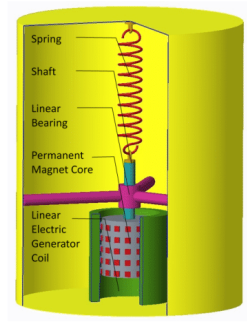

FIGURE 2. INTERNAL ARRANGEMENT OF THE WAVE ENERGY CONVERTER BUOY.

SIMULATING THE OCEAN SURFACE

Considering the Fourier series representation of the irregular sea surface, and the concept of the wave spectrum [5, pp. 87–90, and p. 101], one may represent the sea surface elevation, $\eta(t)$ [m] at a required horizontal coordinate x [m] at time t [s] as [5, p. 123, 124]:

$$\eta(t) = \sum_{i=1}^{N} \eta_{0i} \cos(k_i x - \omega_i t - \varepsilon_i), \tag{1}$$

$$\eta_{0i} = \sqrt{2 S_\eta(\omega_i) \Delta\omega}. \tag{2}$$

Here, N is the total number of wave components (frequency bands), η_0 [m] is the component wave amplitude, ω [rad/s] is

the wave angular frequency, and ε [rad] is the phase. Subscript i refers to the number of the component wave under consideration. The wave number k [rad/m] is to be determined from the dispersion relation $\omega^2 = gk\tanh kd$ by iteration. g [m/s^2] is the acceleration of gravity and d [m] is the water depth. $S_\eta(\omega_i)$ [m^{2}s] is the energy spectral density and $\Delta\omega$ [rad/s] is the width of the frequency bands dividing the total wave spectrum.

If the component frequencies are evenly distributed, $\eta(t)$ will be periodic, which is undesirable. Selecting frequency components randomly (uniformly distributed) within each frequency band will avoid this problem and give a quasiperiodic signal [6, p. 209].

The generation of wave records in this work is based on the Pierson-Moskowitz spectrum which may be expressed in terms of its significant wave height H_s [m], as [5, pp. 105–107]:

$$S_\eta(\omega_i) = \frac{5\pi^4 H_s^2}{T_p^4 \omega_i^5} \exp\left(\frac{-20\pi^4}{T_p^4 \omega_i}\right). \tag{3}$$

Here, T_p [s] is the peak period of the spectrum, and is related to H_s through the relations $T_p = \frac{2\pi}{\omega_p}$, and $\omega_p^2 = \frac{0.161g}{H_s}$. Here, ω_p [rad/s] is the peak angular frequency.

A *Modelica* component **IRW_PM_RDFCWI** which calls functions **spectrumGenerator_PM**, **randomNumberGenerator**, **frequencySelector**, and **waveNumberIterator** was implemented to perform the above calculations for specified H_s.

Figure 3 shows the generated sea surface elevation based on a Pierson–Moskowitz spectrum with $H_s = 1$ m, and $d = 50$ m. Sinusoidal ramping of the wave amplitude was implemented to prevent impulse loads at the start of simulation.

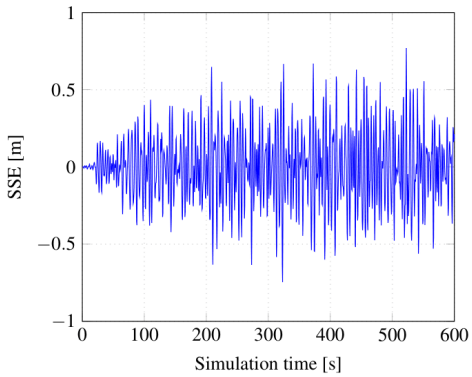

FIGURE 3. SEA SURFACE ELEVATION

To facilitate regular-wave analysis, a *Modelica* component **RegularAiryWave**, which computes the wave elevation $\eta(t) = \eta_0 \cos(kx - \omega t)$, was implemented. Here, η_0 [m] is the specified wave amplitude and $\omega = 2\pi/T$, where T [s] is the specified wave period.

THE CURRENT PROFILE

The current profile is specified as an array of depths z_{cg} and current velocities U_{cg}, at a specified number of points, enabling the interpolation of the current velocity at any depth. A *Modelica* component **CurrentProfile_4pt** was coded to perform this task.

SIMULATING THE HYDRODYNAMICS OF A NON-DIFFRACTING FLOATING OBJECT

Of the 6 degrees of freedom of the cylindrical buoy, it is heave that has the most significant effect on the power generated, and surge that has the most significant effect on the mooring forces. Hence, the present work considers only the uncoupled heave and surge response of the cylindrical floating object. Further, it may be safely assumed in this case that heave and pitch are uncoupled.

Considering the heave motion of a floating object in still waters, the single degree of freedom equation of motion for damped oscillations,

$$M\ddot{z} + C\dot{z} + Kz = F(t), \tag{4}$$

is applicable. Here, $M = m(1 + C_{ma})$, $C = \zeta C_c$, $C_c = 2M\omega_n$, $\omega_n = \sqrt{\frac{K}{M}}$, and $K = A_{wp}\rho g$.

In the above, m [kg] is the mass of the body, C_{ma} [-] is the added mass coefficient, C [Ns/m] is the damping coefficient, K [N/m] is the stiffness, z [m] is the body displacement (from its mean position), $F(t)$ [N] is the time dependent external force acting on the body, ζ [-] is the damping coefficient, C_c [Ns/m] is the critical damping, ω_n [rad/s] is the natural frequency, A_{wp} [m^2] is the water-plane area, ρ [kg/m^3] is the density of water, and g [m/s^2] is the acceleration of gravity. For small structures, C_{ma} and C are obtained from experimental data [5, pp. 331–338]. These may also be determined from a frequency domain analysis using software like WAMIT or ANSYS AQWA. In this example, we are assuming $C_{ma} = 1$ and $\zeta = 0.5$ for heave. Motion in surge direction is considered un-damped and the added mass is taken to be equal to the instantaneous displacement mass.

The external forces constituted by wave, current, and mooring loads are to be specified on the RHS of Eqn. (4) to simulate the forced damped oscillations of a floating object. The wave loading in the heave direction is determined using the Froude-Krylov force formulation which may be applied in cases of small (with respect to wave length) structures if the flow is assumed

irrotational and the diffraction effect small [5, p. 233], as is the case here. The Froude-Krylov force is given by $F_z^{\mathrm{FK}} \approx \rho g A_{\mathrm{wp}} \eta$. [7]. The horizontal wave and current loads are determined using the equation for the Morison force on a cylindrical object free to move in presence of waves and current, given as [5, p. 189]

$$\begin{aligned} M_{\mathrm{F}} =& C_{\mathrm{M}} \rho \frac{\pi}{4} D^2 \dot{u} - C_{\mathrm{A}} \rho \frac{\pi}{4} D^2 \ddot{x} \\ &+ C_{\mathrm{D}} \frac{1}{2} \rho D \mid u \pm U - \dot{x} \mid (u \pm U - \dot{x}). \end{aligned} \tag{5}$$

Here, M_{F} [N] is the Morison force (per unit length, in this case), C_{M} [-] is the inertia coefficient, ρ [kg/m^3] is water density, D [m] is the body diameter, $\dot{u}$ [m/s^2] is the wave induced water particle acceleration along x, C_{A} [-] is the added mass coefficient , $\ddot{x}$ [m/s^2] is the body acceleration along x, C_{D} [-] is the drag coefficient, u [m/s] is the wave induced water particle velocity along x, U [m/s] is the current velocity along x, and $\dot{x}$ [m/s] is the body velocity along x. C_{M} and C_{D} are available from numerous field and laboratory tests, which allows the designer to choose appropriate values [5, p. 172]. Also, $C_{\mathrm{M}} = 1 + C_{\mathrm{A}}$ [5, p. 178]. The wave kinematics are given by [5, pp. 48–52]:

$$u = \frac{\pi H}{T} \frac{\cosh\, k(z+d)}{\sinh\, kd} \cos(kx - \omega t), \tag{6}$$

$$\dot{u} = \frac{2\pi^2 H}{T^2} \frac{\cosh\, k(z+d)}{\sinh\, kd} \sin(kx - \omega t). \tag{7}$$

Here, H [m] is the wave height, T [s] is the wave period, k [rad/m] is the wave number, z [m] is the vertical coordinate of the point at which the wave kinematics are to be calculated, d [m] is the water depth, x [m] is the horizontal coordinate of the point at which the wave kinematics are to be calculated, and ω [rad/s] is the angular frequency of the wave.

A *Modelica* model **CylindricalBuoy** which utilizes the above equations to determine the heave and surge forces was implemented to determine the hydrodynamic response. The *Modelica* function **morisonForceCydlBuoy** calculates the Morison loading on the buoy. The velocity and acceleration profiles for the wave and current are moved with the instantaneous sea surface [8, sec. B1.4.5.5]. Fig. 4 shows the comparison of the heave response between *Modelica* and *Orcaflex* (modelled as a spar buoy of same the dimensions) models, and Fig. 5, the surge response in various situations of waves and current. The buoy is of diameter 1.2 m, height 2 m, and mass 850 kg, while the wave has a height of 1 m and a period of 7 s. The slight phase difference between the model responses is due to the different wave start times between *Orcaflex* and *Modelica*. The minor variation in heave response could be due to the simplified approach adopted in this work as compared to the method used by *Orcaflex*, and is to be investigated. All other responses are found to be a close fit.

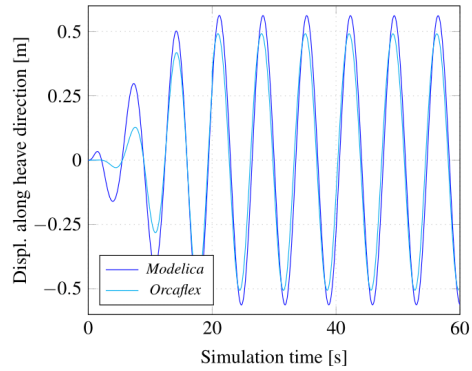

FIGURE 4. HEAVE RESPONSE OF A FREE-FLOATING CYLINDRICAL BUOY.

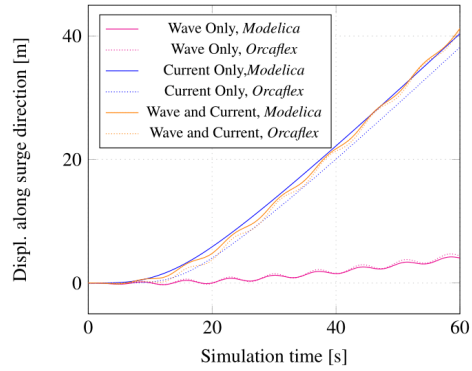

FIGURE 5. FLOATING CYLINDER IN WAVES AND CURRENT.

Since the buoy drifts in the presence of waves and current, it has to be moored. To transfer the mooring loads, a **Fairlead** connector of type *Modelica.Mechanics.Translational.Interfaces.Flange_a*, available in the *Modelica* standard library for mechanical interfaces, is specified at the centre of the bottom surface of the buoy. The **Fairlead** connector is composed of two flanges, one each for transfer of horizontal and vertical components of the mooring load. In addition, another flange connector named **Tophook** was defined at the centre of the top surface of the buoy to suspend the spring-mass system representing the core of the linear electric generator.

SIMULATION OF CATENARY FORCES

When a chain is laid on the ground, and one of its ends is raised to a height, it assumes a half-catenary shape between the ground and the point of suspension. At the point of suspension, the suspended chain weight has a horizontal and a vertical component, the magnitudes of which depend on angle ψ, as indicated in Fig. 6. If the chain is attached to a floating object, this horizontal force component acts to restrain the drifting of the object from its equillibrium, and this constitutes the principle of the catenary mooring system. The equation of a catenary in cartesian

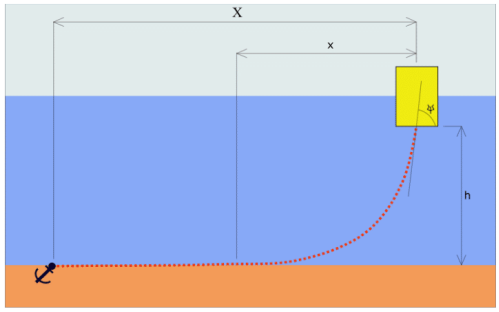

FIGURE 6. THE MOORING HALF-CATENARY.

co-ordinates is given by $z = a\cosh(\frac{x}{a})$ [9]. Here x [m] and z [m] are the catenary coordinates and a [m] is the catenary parameter.

Considering the relations $a = \frac{T_H}{w}$, $z = a\sec(\psi) = a+h$ and $z^2 = l_s^2 + a^2$, one may arrive at the following relations [10]:

$$T_H = \frac{xw}{\cosh^{-1}\left(1+\frac{wh}{T_H}\right)}, \tag{8}$$

$$l_s = h\sqrt{\left(1+\frac{2T_H}{wh}\right)}. \tag{9}$$

Here, T_H [N] is the horizontal tension, w [N/m] is the submerged specific weight of the catenary, ψ [rad] is the angle of the catenary w.r.t. x-axis at the point of suspension, h [m] is the vertical distance of the point of suspension of the catenary from the sea floor, and l_s is the length of the catenary from the point of suspension on the buoy to the touchdown point on the sea floor.

Now, considering that while X varies from $X_{\min} = (l_c - d)$ to $X_{\max} = \sqrt{l_c^2 - d^2}$, x varies from $x_{\min} = 0$ to $x_{\max} = X_{\max}$, where l_c [m] is the total length of the mooring chain and d [m] is the water depth (ref. Fig 6), Eqn. (8) can be iterated to get values for T_H for $x = \{0, 0.1, 0.2 \ldots, x_{\max}\}$. l_s may then be calculated using Eqn. (9) and X can be calculated using the relation

$$X = l_c - l_s + x\,. \tag{10}$$

We can thus arrive at a table of values of T_H for specified X. The mooring load at any time step can then be linearly interpolated for the required x coordinate of the body's centre of gravity.

A *Modelica* model **CatenaryMooring**, calling on functions **catXIterator** and **catThIterator**, was implemented to simulate the mooring loads.

The mooring is attached to the fairlead fixed at the centre of the bottom surface of the buoy, the connection being effected through a **Shackle** connector complementary to the **Fairlead** connector.

The mooring catenary will also be acted upon by waves and currents, and this force will be transferred to the buoy through the mooring chain. The assumption made in calculating the Morison loading of the mooring catenary is that the instantaneous catenary shape remains unaltered due to Morison loads on the chain, and that the net effect of the Morison loads is a modification of the vertical and horizontal components of the mooring load. The chain length is discretized into a number of segments, and combined wave and current kinematics calculated at the segment centres are used to determine the Morison loads on the chain based on the hydraulic diameter and drag coefficients. The water particle kinematics are determined using Eqns. (6), (7) and [5, pp. 48–52]:

$$w = \frac{\pi H}{T}\,\frac{\sinh\, k(z+d)}{\sinh\, kd}\,\sin(kx - \omega t), \tag{11}$$

$$\dot{w} = \frac{-2\pi^2 H}{T^2}\,\frac{\sinh\, k(z+d)}{\sinh\, kd}\,\cos(kx - \omega t). \tag{12}$$

Here, w [m/s] is the wave-induced water-particle velocity and $\dot{w}$ [m/s^2] is the wave-induced water-particle acceleration in the z direction.

Figure 7 and Fig. 8 shows the effect of the mooring line on the excursion of a buoy of the same dimensions as earlier, but with a mass of 1100 kg, moored with chain of specific mass 16 kg/m, when subjected to a uniform current of 1 m/s acting over a depth of 10 m and tapering to 0 m/s at a depth of 25 m, in a water depth of 50 m. Fig. 9 shows the corresponding catenary shape of the mooring chain at various simulation time steps. *Orcaflex* approximates the chain as a series of rigid interconnected mass-spring-dampers, while the *Modelica* component uses a catenary approximation approach for the mooring line model, and this results in a minor variation in the mooring load as shown in Fig. 10. The buoys float at the same initial draught of 1.535 m in both models, and this implies that the x coordinate of the mooring line top end should have been positioned at $(50+1.535)$ m. However

it is observed that *Orcaflex* places it at 51.95 m. The exact reason for this shift is yet to be ascertained.

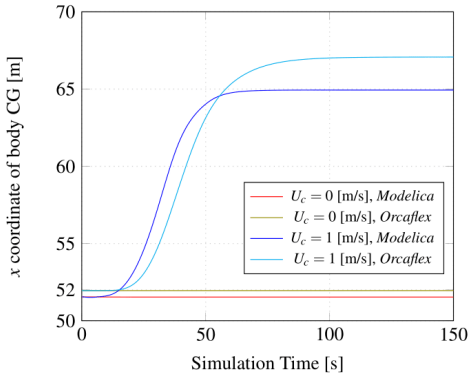

FIGURE 7. SURGE RESPONSE OF MOORED BUOY IN CURRENT.

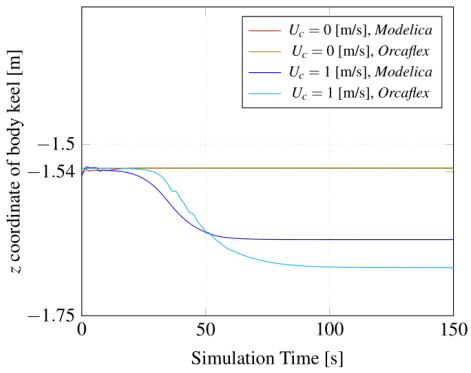

FIGURE 8. HEAVE RESPONSE OF MOORED BUOY IN CURRENT.

Figure 11 compares the surge response of the same buoy in the presence of a regular wave of height 1 m, period 7 s, and a current of 0.5 m/s (profile as discussed earlier), with and without considering mooring chain Morison forces, while Fig. 12 compares the heave response for the same cases by plotting the buoy

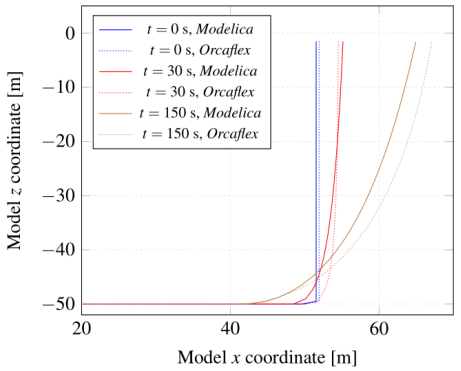

FIGURE 9. EVOLUTION OF THE MOORING CATENARY.

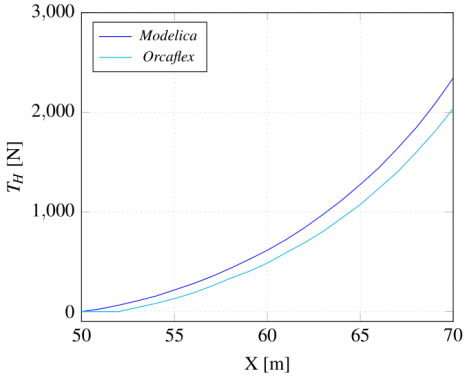

FIGURE 10. COMPARISON OF T_H.

keel position. Note the negligible effect of mooring chain Morison loads on the heave response. The higher surge response of the *Orcaflex* model seen in Figure 11 is due to the lower mooring T_H, as can be inferred from Fig. 10.

The following mooring components have been defined:

CatenaryMooring_Mf0 which does not consider current or wave loads on the mooring line.

CatenaryMooring_MfC which considers only current and wave velocity loads on the mooring line.

CatenaryMooring_MfCW which considers both current and wave velocity as well as acceleration loads on the mooring line.

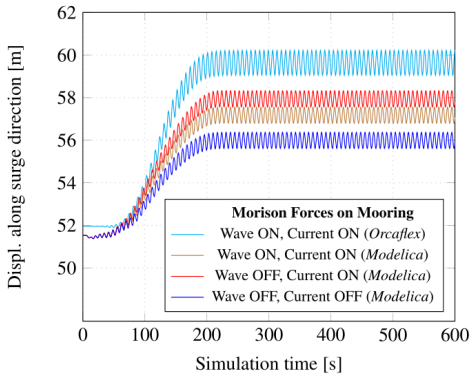

FIGURE 11. EFFECT OF MOORING CHAIN MORISON LOADS ON SURGE RESPONSE OF BUOY IN WAVES AND CURRENT.

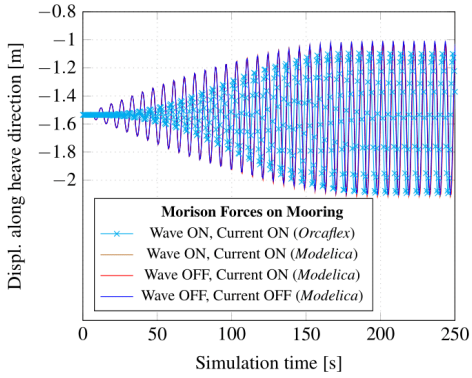

FIGURE 12. HEAVE RESPONSE OF BUOY WITH AND WITHOUT MORISON LOADING OF MOORING.

It has been noticed that the model becomes sluggish when using the **CatenaryMooring_MfCW component**. However, noting the negligible impact of the mooring-line wave Morison loading on the buoy's response, we henceforth consider only current loads on the mooring line.

SIMULATING THE SPRING-MASS SYSTEM

The spring-mass system is modelled using standard components already available in the *Modelica* Mechanics library. A **SpringDamper** component and a **Mass** component are coupled to represent the spring-suspended core of the linear electric generator, as shown in Fig. 15, under the System Integration section.

Figure 13 shows the effect of the oscillations of the spring-suspended mass of 50 kg on a floating buoy of mass 350 kg, in still water. The mass is released from different initial positions and the vertical motions of the mass' centre of gravity and buoy keel are plotted. Note the coupling between the mass and buoy response. Thus, the dynamics of the buoy and the spring-suspend mass are coupled through the **TopHook** connector.

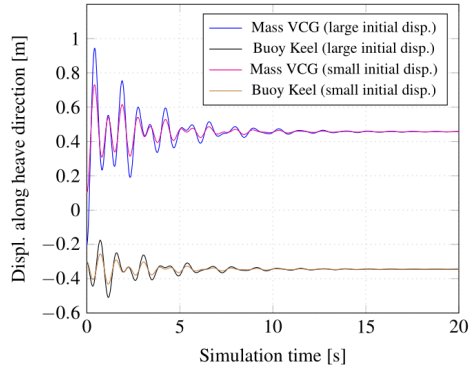

FIGURE 13. COUPLING OF SPRING MASS AND BUOY HEAVE RESPONSE.

THE MODELICA OCEAN ENGINEERING LIBRARY

Having verified the satisfactory simulation of hydrodynamic and mooring loads, we now proceed to build up a preliminary library for the ocean engineering domain.

All the components discussed earlier are packaged to constitute the **OceanEngineeringLibrary** as shown in Fig. 14. The custom-developed models for waves, current profile, floaters, and moorings are grouped together as **Components**, while the modified *SpringDamper* and *Mass* models from the already available mechanics library are grouped under **MiscellaneousComponents**. All the custom-developed functions are grouped as **Functions**, while the custom-developed connectors are grouped as **Connectors**. All the simulations discussed in this paper are grouped under **SampleSimulations**, and are ready for simulation. The library is available for free public download at `https://github.com/Savin-Viswanathan/OELib_OMAE2019`. To use the library, one must download the

files to a computer in which the free-to-use *OMEdit* is installed and double click **OceanEngineering.mo**.

The *Orcaflex* simulation files are also accessible through the download link.

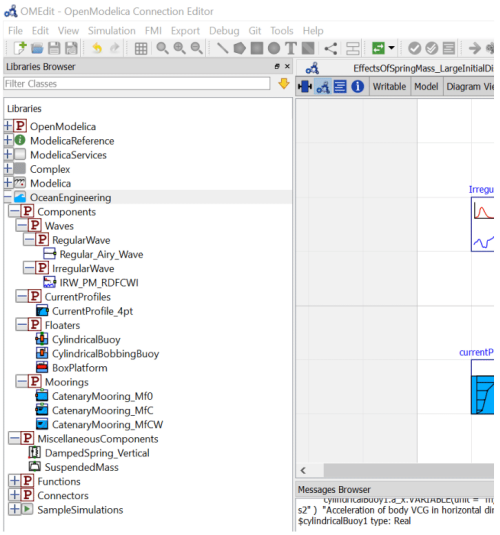

FIGURE 14. SCREENSHOT OF THE OCEAN ENGINEERING LIBRARY.

4. *Modelica* connector **CurrentDataConnector** links this information to the *Modelica* expandable connector **EnvironmentBus**.
5. *Modelica* connector **EnvironmentMooringDataConnector** links the required information from the **EnvironmentBus** to the *Modelica* Model **CatenaryMooring** while *Modelica* connector **EnvironmentBuoyDataConnector** links the required information to the *Modelica* model **CylindricalBuoy**.
6. *Modelica* flange connector **Shackle** of **CatenaryMooring** is connected to flange connector **Fairlead** of **CylindricalBuoy** while the flange connector **TopHook** of **CylindricalBuoy** is connected to the top flange of the **DampedSpring**, and the bottom flange of the **DampedSpring** is connected to the top flange of the **Mass** component.

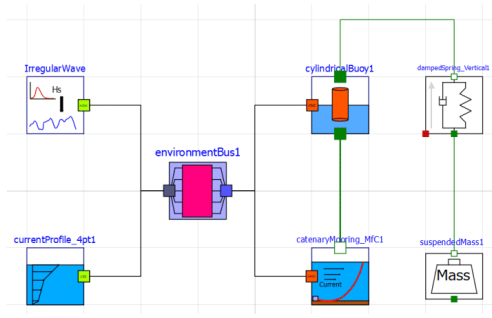

FIGURE 15. SCREENSHOT OF THE INTEGRATED COMPONENT MODEL OF THE WAVE ENERGY CONVERTER BUOY.

SYSTEM INTEGRATION

Having thus set up the library, it is very easy to build integrated system models. The drag-and-drop feature of *OMEdit* allows one to easily assemble the components in the *diagram* view.

The integrated multiphysical system model for a wave energy conversion buoy in irregular waves and current is shown in Fig. 15. Here,

1. *Modelica* model **RegularWave/ IrregularWave** determines the wave parameters, viz. $\omega_i, T_i, k_i, \varepsilon_i, \eta_{0i}$.
2. *Modelica* connector **WaveDataConnector** links this information to the *Modelica* expandable connector **EnvironmentBus**.
3. *Modelica* model **CurrentProfile** generates the specified current profile as a vectors of z_{cg} and U_{cg} values.

RESULTS

Keeping in mind the intent of the work, which is *only* to showcase the benefits of developing an *OceanEngineering* library for *OpenModelica*, the results are to be viewed from such an angle, excluding the tendency to delve into details of wave-energy conversion. Space limitations prevent the listing of all simulation parameters here and these maybe found within the respective simulation files under the *SampleSimulations* of the library. The *Orcaflex* simulations are also accessible via the download link.

Figure 18 shows the surge response of a wave energy converter buoy of diameter 1.2 m and mass 850 kg, moored with a chain of specific mass 16 kg/m, in irregular waves of significant wave height 1 m, in the presence of the earlier specified current

profile with velocity 1 m/s, and in a water depth of 50 m. Wave and current Morison loading is applied to the buoy, while only current Morison loads are considered on the mooring line.

Figure 19 shows the variation in the z-displacement of the permanent-magnet core's centre-of-gravity, about an origin fixed to the body of the buoy. This variation in displacement is an indication of the power output, and we observe that, in this case, the variation is very small for any feasible power take-off from the linear electric generator.

The component-based modeling approach followed makes it easier to analyze other design options. For example, in the Wave Energy Platform, as shown in Fig. 16, the linear electric generator coil is mounted on a support structure fixed to the pontoon, and the permanent magnetic core is formed onto the top portion of the cylindrical buoy. A guide allows the buoy to heave freely while restraining motion in other directions. Figure 17 shows the new *Modelica* component model which utilizes most of the previous components. The **CylindricalBobbingBuoy** and **BoxPlatform** are modified versions of the earlier **CylindricalBuoy**. Morison loads are applied on the mooring, pontoon as well as on the cylindrical buoy and are interconnected using flange connectors. The *boxplatform* has a length of 5 m, breadth and depth of 2 m, weighs 15,250 kg and is moored with a chain of specific mass 16 kg/m. The *bobbingbuoy* has a mass of 350 kg and diameter of 1.2 m.

Figure 18 shows the surge response of the wave energy platform under the same environmental conditions as that applied to the wave energy converter buoy earlier, while Fig. 19 shows the variation in the relative z-displacement between the deck of the pontoon and the top surface of the cylindrical buoy. We observe that in this case, the variation is large enough to possibly take off feasible amount of power from the linear electric generator. However, it is to be noted that diffraction effects and hence the hydrodynamic coupling of the multibody system is not considered in this case. The example is cited with the sole intent of showcasing the ease with which *Modelica* components maybe modified to build up similar systems governed by same physical principles.

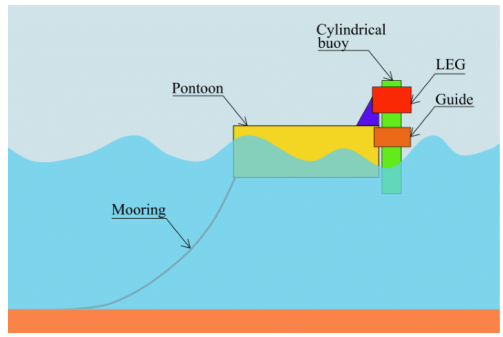

FIGURE 16. CONCEPT OF THE WAVE ENERGY PLATFORM.

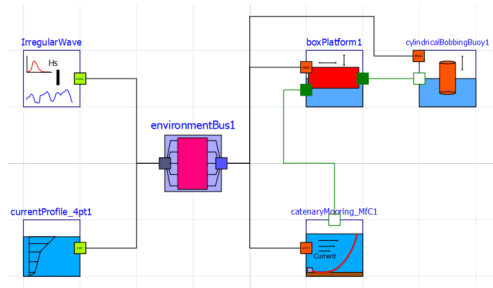

FIGURE 17. SCREENSHOT OF THE INTEGRATED COMPONENT MODEL OF THE WAVE ENERGY PLATFORM SYSTEM.

CONCLUSION

Integrated simulation of simple multiphysical systems in the domain of offshore engineering has been carried out using the free-to-use *OpenModelica* software and its *OMEdit* graphical user interface. The effectiveness of developed components and the ease of integration with already available components from the *Mechanics* library of *Modelica* has been demonstrated through the simulation of the wave energy converter buoy system, while the advantages of following a standard component-based approach has been demonstrated in the simulation of the wave energy conversion platform system.

Preliminary comparison with results from *Orcaflex* shows that the modelica simulation is satisfactory. Minor variations are seen in heave motion and in the mooring response. While the reasons for the variation in the mooring response has been reconciled, the variation in heave, though minor, is to be investigated. Also, in the present work, values have been assumed for the frequency dependent added mass and damping. To generate these values, and also to simulate the hydrodynamics of diffracting objects within *Modelica*, future work is planned towards implementing the Boundary-Integral Method for frequency domain analysis of regular geometries.

Public access to the preliminary *OceanEngineering* library has been provided and interested readers may delve into details of the code used to develop these components and improve/modify the same on their own. All the simulations including *Orcaflex* files are made available to the interested reader for constructive criticism.

Thus, it maybe concluded that the open-source *OpenModelica* software holds great potential in the domain of offshore

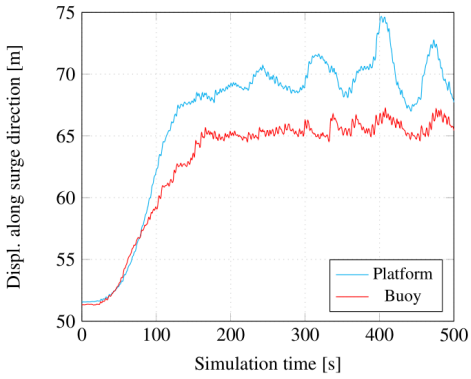

FIGURE 18. SURGE RESPONSES OF THE WAVE ENERGY CONVERTER BUOY AND PLATFORM IN IRREGULAR WAVES AND CURRENT.

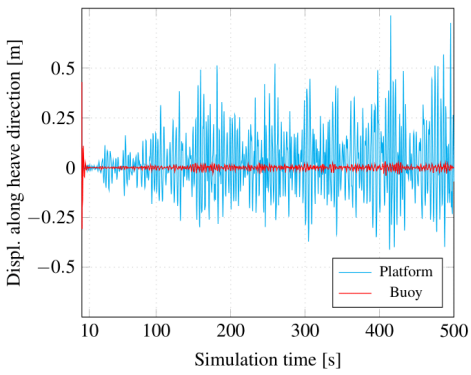

FIGURE 19. RELATIVE DISPLACEMENTS BETWEEN THE MAGNETIC CORE AND LEG COIL CENTERS.

simulations, and the development of a standard library for ocean engineering components would be benificial to academia and industry, especially when finances are constrained. Standard components from other domains can then be easily incorporated into the offshore systems to simulate for e.g., control system performance and other required analyses, thus enabling fully-integrated multiphysical system simulations.

ACKNOWLEDGEMENTS

The research in this paper has received funding from the Research Council of Norway, SFI Offshore Mechatronics, project number 90034209.

REFERENCES

[1] Fritzon, Peter. *Principles of Object-Oriented Modeling and Simulation with Modelica 3.3*. IEEE Press, New Jersey(2015).

[2] Modelica Association. *Modelica Libraries*. `www.modelica.org/`.

[3] Brommundt, Matthias, and Muskulus, Michael, and Strach, Mareike, and Strobel, Michael, and Vorpahl, Fabian. "Experiences with Object-oriented and Equation Based Modeling of a Floating Support Structure for Wind Turbines in Modelica." *Proceedings of the Winter Simulation Conference*.159:pp.1–12. Berlin, Germany, 2012. `http://dl.acm.org/citation.cfm?id=2429759.2429972`.

[4] Girilli, Stephan T., and Girilli, Annette R., and Bastien, Steven P., and Sepe Jr., Raymond B., and Spaulding, Malcom L. . "Small Buoys for Energy Harvesting: Experimental and Numerical Modeling Studies." *Proceedings of the Twenty-first(2011) International Offshore and Polar Engineering Conference*. pp.598–605. Maui, Hawaii, USA, June 19-24, 2011.

[5] Chakrabarti, Subratha Kumar. *Hydrodynamics of Offshore Structures*. Computational Mechanics Publications, and Springer-Verlag, Dorchester, Great Britain(1987).

[6] Fossen, Thor I. *Handbook of Marine Craft Hydrodynamics and Motion Control*. John Wiley & Sons, Chichester, United Kingdom(2011).

[7] Techet, Alexandra H. *Design Principles for Ocean Vehicles*. Lecture notes at the Massachusetts Institute of Technology. `https://ocw.mit.edu/courses/mechanical-engineering/2-22-design-principles-for-ocean-vehicles-13-42-spring-2005/readings/r10_froudekrylov.pdf`.

[8] SINTEF. *Handbook on Design and Operation of Flexible Pipes*. `https://sintef.no/en/latest-news/updated-handbook-on-design-and-operation-of-flexible-pipes/`.

[9] University of Victoria. *The Catenary*. `http://astrowww.phys.uvic.ca/~tatum/classmechs/class18.pdf`.

[10] Massachusetts Institute of Technology. *Mooring Dynamics-II*. `https://ocw.mit.edu/courses/mechanical-engineering/2-019-design-of-ocean-systems-spring-2011/lecture-notes/MIT2_019S11_MD2.pdf`.

4.2 Modelica component models for oceanic surface waves and depth varying current

The citation of the published article is given below:

S. Viswanathan and C. Holden. *Modelica Component Models for Oceanic Surface Waves and Depth Varying Current*. Proceedings of the American Modelica Conference 2020, Boulder, Colorado, USA, March 23-25, 2020. https://doi.org/10.3384/ecp20169

The postprint version of the paper follows.

Modelica Component Models for Oceanic Surface Waves and Depth Varying Current

Savin Viswanathan[1] Christian Holden[1]

[1]Dept. of Mechanical and Industrial Engineering, Norwegian University of Science and Technology (NTNU), NO-7491 Trondheim, Norway. {savin.viswanathan,christian.holden}@ntnu.no

Abstract

In this paper, the theory of progressive ocean-surface gravity-waves is discussed, followed by the concept of the representation of the irregular sea-state by a sea-spectrum. Fourier series decomposition of the irregular sea-surface into its constituent regular waves and the method of realizing unique time-records of the sea-surface-elevation from commonly used sea-spectra is described. A detailed description of the development of *Modelica* component-models to generate regular as well as irregular waves, and depth-varying current, with an eye on the requirements imposed by probable integrated simulation scenarios, is then presented and the results discussed.

Keywords: regular wave, irregular wave, sea-spectrum, Modelica ocean-engineering library.

1 Introduction

The advantages of developing an *OpenModelica* ocean engineering library populated with domain-specific *component-models* and *functions* to carry out the integrated simulation of multi-pyhsical ocean engineering systems was demonstrated by the authors (Viswanathan and Holden, 2019). This earlier work:

1. Gives a brief description of the simulation of systems based on the hydrodynamic response of catenary-moored non-diffracting floating objects in the presence of waves and current,

2. Demonstrates the satisfactory agreement of the *Modelica* simulation results with those obtained using a popular ocean-engineering commercial software (*Orcaflex*), and

3. Brings out the advantages of using a component-model based simulation approach.

The voluminous nature of the earlier work precluded the possibility of delving into the theoretical and implementational details of the various *Modelica* component-models of the ocean-engineering library proposed by the authors, the preliminary version of which is available for download at `github.com/Savin-Viswanathan/OELib_OMAE2019`.

The present work which deals with the development of *Modelica* component-models for simulating the kinematics and dynamics of regular and irregular waves, and depth varying current, is the first among a series of two papers which will fill in such gaps in theory and implementation.

2 Theory

The theory presented here upto Section 2.4.2 is a brief summary of that given in (Dean and Dalrymple, 2001) .

2.1 The Fundamentals

The application of the conservation of mass to a reference fluid volume yields the continuity equation:

$$\frac{1}{\rho}\left(\frac{\partial \rho}{\partial t}+u\frac{\partial \rho}{\partial x}+v\frac{\partial \rho}{\partial y}+w\frac{\partial \rho}{\partial z}\right) + \frac{\partial u}{\partial x}+\frac{\partial v}{\partial y}+\frac{\partial w}{\partial z}=0. \tag{1}$$

Here, ρ [kg/m^3] is the fluid density, t [s] is time, and u,v,w [m/s] are the fluid velocities in the x,y,z directions.

Disregarding the effects of surface tension and elasticity, the application of the translational equation of motion to a fluid particle yields the Navier-Stoke's equations:

$$\frac{\mathrm{D}u}{\mathrm{D}t}=-\frac{1}{\rho}\frac{\partial p}{\partial x}+\frac{1}{\rho}\left(\frac{\partial \tau_{xx}}{\partial x}+\frac{\partial \tau_{yx}}{\partial y}+\frac{\partial \tau_{zx}}{\partial z}\right)+X, \tag{2}$$

$$\frac{\mathrm{D}v}{\mathrm{D}t}=-\frac{1}{\rho}\frac{\partial p}{\partial y}+\frac{1}{\rho}\left(\frac{\partial \tau_{xy}}{\partial x}+\frac{\partial \tau_{yy}}{\partial y}+\frac{\partial \tau_{zy}}{\partial z}\right)+Y, \tag{3}$$

$$\frac{\mathrm{D}w}{\mathrm{D}t}=-\frac{1}{\rho}\frac{\partial p}{\partial z}+\frac{1}{\rho}\left(\frac{\partial \tau_{xz}}{\partial x}+\frac{\partial \tau_{yz}}{\partial y}+\frac{\partial \tau_{zz}}{\partial z}\right)+Z. \tag{4}$$

Here, $\frac{\mathrm{D}}{\mathrm{D}t}$ is the material derivative, p [N/m^2] is the fluid pressure, τ [N/m^2] is the shear stress where the first subscript refers to the surface perpendicular and the second subscript refers to the direction of the stress, and X,Y,Z [N] are body forces along the x, y, and z directions.

2.2 Assumptions and the Governing Equation

The following assumptions are made:

- Incompressible fluid (ρ =constant).
- Inviscid fluid ($\tau = 0$).
- Irrotational flow ($\frac{\partial w}{\partial y}=\frac{\partial v}{\partial z}$, $\frac{\partial w}{\partial x}=\frac{\partial u}{\partial z}$ and $\frac{\partial v}{\partial x}=\frac{\partial u}{\partial y}$).

- Low wave steepness, i.e., ($H \ll L$).
- Long crested waves (2D flow, in x and z directions only).
- Horizontal and time-invariant bottom boundary.

Assuming incompressible fluid and long crested waves,

$$\text{Eqn. (1)} \rightarrow \frac{\partial u}{\partial x} + \frac{\partial w}{\partial z} = 0. \tag{5}$$

Assumption of inviscid fluid gives the Euler equations:

$$\text{Eqn. (2)} \rightarrow \frac{\mathrm{D}u}{\mathrm{D}t} = -\frac{1}{\rho}\frac{\partial p}{\partial x}, \tag{6}$$

$$\text{Eqn. (4)} \rightarrow \frac{\mathrm{D}w}{\mathrm{D}t} = -\frac{1}{\rho}\frac{\partial p}{\partial z} - g. \tag{7}$$

The assumption of irrotational flow makes it possible to define a scalar velocity potential $\phi(x,y,z,t)$ [m^2/s] such that its directional derivative gives the fluid velocity in that direction. i.e.,

$$u = \frac{\partial \phi}{\partial x}, \qquad w = \frac{\partial \phi}{\partial z}. \tag{8}$$

Thus, for an incompressible, irrotational flow in the x and z directions, the integrated form of the Euler equation yields the Bernoulli equation for unsteady potential flow,

$$\frac{\partial \phi}{\partial t} + \frac{1}{2}\left\{\left(\frac{\partial \phi}{\partial x}\right)^2 + \left(\frac{\partial \phi}{\partial z}\right)^2\right\} + \frac{p}{\rho} + gz = C(t), \tag{9}$$

where $C(t)$ is the Bernoulli term and is a constant for steady flows.

With $\mathbf{u} = [u,w]^{\mathrm{T}}$, (5) may be expressed in vector form as $\nabla.\mathbf{u} = 0$. From (8), $\mathbf{u} = \nabla\phi$, so we have

$$\nabla.\nabla\phi = \nabla^2\phi = \frac{\partial^2\phi}{\partial x^2} + \frac{\partial^2\phi}{\partial z^2} = 0. \tag{10}$$

Equation (10) is the well-known Laplace equation, and consitutes the governing differential equation which is valid throughout the fluid domain. Our interest is in determining the velocity potential which satisifies the Laplace equation, which then makes it possible to determine the fluid velocities at any point in the fluid domain.

The Bernoulli equation relates the fluid velocities to the the fluid pressure, and the integration of the fluid pressure along the surface of any submerged/floating object gives the force that the fluid exerts on the object, which is, in most cases, the element of interest in wave-body interaction problems.

2.3 The Boundary Conditions

In seeking a solution for the velocity potential in (10), we make use of the following physical conditions which must be satisfied by the fluid velocity and pressure, at the domain boundaries:

1. *The Kinematic Free-Surface Boundary-Condition* (KFSBC) stemming from the fact that there cannot be any fluid flow across the interface between the liquid domain and the atmosphere at the free surface of the fluid.
2. *The Bottom Boundary-Condition* (BBC) stemming from the fact that there cannot be any fluid flow across the sea floor.
3. *The Dynamic Free-Surface Boundary-Condition* (DFSBC) stemming from the fact that 'free' surfaces such as the air-water interface cannot support pressure variations across it, and hence must be capable of responding in order to maintain the pressure continuity across the liquid and gaseous domains. This displacement of the free surface means that the position of the upper boundary is not known a priori in the water-wave problem. For small-amplitude waves, this condition is given by the requirement that the pressure on the free surface is uniform along the wave form.
4. *The Spatial and Temporal Periodicity Condition at the Lateral Surfaces* (LPBC) stemming from the fact that the solution we seek is the velocity potential associated with a wave which is periodic in both space and time.

Mathematical expressions for the kinematic boundary conditions may be derived from the equation of the form $\mathrm{F}(x,y,z,t) = 0$, describing the boundary surface. For a temporally varying surface, the total time-derivative of the surface is zero, on the surface. Hence, for a 2D wave surface-profile,

$$\frac{\mathrm{DF}}{\mathrm{D}t} = \frac{\partial \mathrm{F}}{\partial t} + u\frac{\partial \mathrm{F}}{\partial x} + w\frac{\partial \mathrm{F}}{\partial z} = 0 \text{ on } \mathrm{F}(x,z,t) = 0. \tag{11}$$

Or, rearranging and using vector notation,

$$-\frac{\partial \mathrm{F}}{\partial t} = \mathbf{u}.\nabla\mathrm{F} = \mathbf{u}.\mathbf{n}|\nabla\mathrm{F}|. \tag{12}$$

Here, $\mathbf{n} = \frac{\nabla\mathrm{F}}{|\nabla\mathrm{F}|}$ is the unit normal to the surface, and $|\nabla\mathrm{F}| = \sqrt{\left(\frac{\partial \mathrm{F}}{\partial x}\right)^2 + \left(\frac{\partial \mathrm{F}}{\partial z}\right)^2}$.

The kinematic boundary condition is thus expressed as

$$\mathbf{u}.\mathbf{n} = -\frac{\partial \mathrm{F}/\partial t}{|\nabla\mathrm{F}|} \text{ on } \mathrm{F}(x,y,z,t) = 0. \tag{13}$$

At the free surface, $F(x,z,t) = z - \eta(x,t) = 0$, where $\eta(x,t)$ is the displacement of the free surface about the horizontal plane. Equation (13) gives

$$\mathbf{u}.\mathbf{n} = \frac{\partial\eta/\partial t}{\sqrt{\left(\frac{\partial\eta}{\partial x}\right)^2 + 1}} \text{ on } z - \eta(x,t) = 0. \tag{14}$$

Taking

$$\mathbf{n} = \frac{-\frac{\partial\eta}{\partial x}\mathbf{i} + \mathbf{k}}{\sqrt{\left(\frac{\partial\eta}{\partial x}\right)^2 + 1}}, \tag{15}$$

(14) gives the KFSBC as

$$w = \frac{\partial\eta}{\partial t} + u\frac{\partial\eta}{\partial x} \text{ on } z = \eta(x,t). \tag{16}$$

Assuming a horizontal, time-invariant bottom at $z = -h$, $F(z) = z + h = 0$. Equation (13) gives $\mathbf{u}.\mathbf{n} = 0$ at $z = -h$. Here, $\mathbf{n} = \mathbf{k}$, and hence the BBC can be expressed as

$$w = 0 \text{ on } z = -h. \tag{17}$$

By specifying a uniform pressure (p_η =constant) along the wave form in the Bernoulli equation at the free surface, the DFSBC may be expressed mathematically as

$$\frac{\partial\phi}{\partial t} + \frac{1}{2}\left\{\left(\frac{\partial\phi}{\partial x}\right)^2 + \left(\frac{\partial\phi}{\partial z}\right)^2\right\} + \frac{p_\eta}{\rho} + gz = C(t) \text{ on } z = \eta(x,t). \tag{18}$$

The LPBCs may be expressed as

$$\phi(x,t) = \phi(x+L,t), \tag{19}$$
$$\phi(x,t) = \phi(x,t+T). \tag{20}$$

Here, L [m] is the wave length and T [s] is the wave period.

2.4 Solution of the Boundary Value Problem

The BVP to be solved is thus the Laplace equation (10) subject to: 1. the KFSBC in (16), 2. the DFSBC in (18), 3. the BBC in (17), and the LPBC in (19) and (20). The diagrammatic representation of the problem is shown in Figure 1.

2.4.1 Manipulation of the Free Surface Boundary Conditions

On carrying out a non-dimensional analysis of the terms in the KFSBC and the DFSBC, under the assumption of low wave steepness, i.e., $H/L \ll 1$, we notice that $u\frac{\partial\eta}{\partial x} \ll \frac{\partial\eta}{\partial t}$, $u\frac{\partial\eta}{\partial x} \ll \frac{\partial\phi}{\partial z}$ and $\left(\frac{\partial\phi}{\partial x}\right)^2, \left(\frac{\partial\phi}{\partial z}\right)^2 \ll \frac{\partial\phi}{\partial t}$.

Further, the KFSBC and DFSBC are to be evaluated at $z = \eta(x,t)$, which is a priori unknown. However, on taking a Taylor series expansion of the BCs about the mean free surface at $z = 0$, we notice that the second-order and subsequent higher-order terms can be neglected; hence, we can safely assume the validity of the BCs at the mean free surface instead of the actual free surface. Details about linearization and shifting can be found in (Techet, 2005).

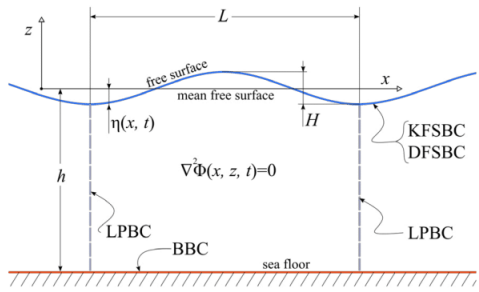

Figure 1. Boundary value problem for the velocity potential. Adapted from (Dean and Dalrymple, 2001).

Taking the pressure at the free surface as the constant atmospheric pressure, we can eliminate the Bernoulli constant and the pressure term in (9) as demonstrated in (Andersen and Frigaard, 2011). Thus, the modified BCs are:

$$\text{KFSBC:} \quad \frac{\partial\phi}{\partial z} = \frac{\partial\eta}{\partial t} \quad \text{on} \quad z = 0, \tag{21}$$

$$\text{DFSBC:} \quad \frac{\partial\phi}{\partial t} + g\eta = 0 \quad \text{on} \quad z = 0. \tag{22}$$

Differentiating (22) w.r.t. t and using (21), we can combine both the BCs to give the Combined Free-Surface Boundary-Condition (CFSBC) as:

$$\text{CFSBC:} \quad \frac{\partial^2\phi}{\partial t^2} + g\frac{\partial\phi}{\partial z} = 0 \quad \text{on} \quad z = 0. \tag{23}$$

2.4.2 Complex Exponential Form of the Velocity Potential

It is often mathematically advantageous to use the complex form of the velocity potential; see p. 4 of (Chakrabarti, 1987). Since the solution we seek is related to a progressive sinusoidal wave, we may express the velocity potential as

$$\phi = \varphi(z)e^{i(kx-\omega t)}. \tag{24}$$

The LPBCs were utilized in the formulation of the above equation, the real part of which represents the velocity potential of a sinusoidal wave progressing in the positive x-direction; see pp. 2, 12 of (Krogstad and Arntsen, 2000).

The BVP is now given by:

$$\text{Laplace eqn:} \quad \frac{\partial^2\varphi}{\partial z^2} - k^2\varphi = 0. \tag{25}$$

$$\text{CFSBC:} \quad -\omega^2\varphi + g\frac{\partial\varphi}{\partial z} = 0 \text{ on } z = 0. \tag{26}$$

$$\text{BBC:} \quad \frac{\partial\varphi}{\partial z} = 0 \text{ on } z = -h. \tag{27}$$

Assuming a solution of the form

$$\varphi(z) = \mathrm{C}_1 e^{-kz} + \mathrm{C}_2 e^{kz}, \tag{28}$$

$$\text{Eqn. (27)} \rightarrow \quad \mathrm{C}_1 k e^{-kh} - \mathrm{C}_2 k e^{kh} = 0, \tag{29}$$

$$\text{Eqn. (26)} \rightarrow \quad (gk - \omega^2)\mathrm{C}_1 - (gk + \omega^2)\mathrm{C}_2 = 0. \tag{30}$$

The above homogenous equation system has non-trivial solutions only when the determinant is zero. This gives the dispersion relation

$$\omega^2 = gk\tanh(kh). \tag{31}$$

Now, setting $\mathrm{C}_1 = \frac{1}{2}\mathrm{B}e^{kh}$ and $\mathrm{C}_2 = \frac{1}{2}\mathrm{B}e^{-kh}$,

$$\text{Eqn. (28)} \rightarrow \quad \varphi(z) = B\cosh[k(z+h)], \tag{32}$$

$$\text{Eqn. (24)} \rightarrow \quad \phi(x,z,t) = B\cosh[k(z+h)]e^{i(kx-\omega t)}, \tag{33}$$

$$\text{Eqn. (22)} \rightarrow \quad \eta = \frac{-1}{g}\frac{\partial\phi}{\partial t}\bigg|_{z=0}. \tag{34}$$

Considering that that highest value of η is the wave amplitude $A = H/2$ [m], from (33) and (34), we have

$$B = \frac{-igA}{\omega}\frac{1}{\cosh(kh)}. \tag{35}$$

The complex exponential form of the velocity potential may now be expressed as

$$\phi(x,z,t) = \frac{-igA}{\omega}\frac{\cosh k(z+h)}{\cosh(kh)}e^{i(kx-\omega t)}. \tag{36}$$

2.5 Kinematics and Dynamics of Regular Waves

Considering the real part of the velocity potential in (36),

$$\phi = \frac{gH}{2\omega}\frac{\cosh k(z+h)}{\cosh(kh)}\sin(kx-\omega t), \tag{37}$$

$$\eta = H/2\cos(kx-\omega t), \tag{38}$$

$$u = \frac{\pi H}{T}\frac{\cosh k(z+h)}{\sinh(kh)}\cos(kx-\omega t), \tag{39}$$

$$w = \frac{\pi H}{T}\frac{\sinh k(z+h)}{\sinh(kh)}\sin(kx-\omega t), \tag{40}$$

$$\dot{u} = \frac{2\pi^2 H}{T^2}\frac{\cosh k(z+h)}{\sinh(kh)}\sin(kx-\omega t), \tag{41}$$

$$\dot{w} = -\frac{2\pi^2 H}{T^2}\frac{\sinh k(z+h)}{\sinh(kh)}\cos(kx-\omega t), \tag{42}$$

$$\delta_x = -\frac{H}{2}\frac{\cosh k(z+h)}{\sinh(kh)}\sin(kx-\omega t), \tag{43}$$

$$\delta_z = \frac{H}{2}\frac{\sinh k(z+h)}{\sinh(kh)}\cos(kx-\omega t), \tag{44}$$

$$p = \rho g\frac{H}{2}\frac{\cosh k(z+h)}{\cosh(kh)}\cos(kx-\omega t). \tag{45}$$

Here, $\dot{u}$ and $\dot{w}$ [m/s^2] are the water particle accelerations, δ_x and δ_z [m] are water particle displacements from their mean position, and p [N/m^2] is the dynamic pressure. (Chakrabarti, 1987).

2.6 Kinematics and Dynamics of Irregular Waves

The process of linearization carried out in Section 2.4.1 implies the validity of the superpostion principle with regards to the quantities expressed in Section 2.5. This, in turn, justifies the representation of the irregular wave parameters as the summation of the parameters of constituent regular waves; or, in other words, as a Fourier series, as represented in Figure 2.

The way of describing the sea-state is linked to the energy content in waves. Linear theory gives the wave energy per unit area of the sea surface due to a regular wave as

$$E = \frac{1}{2}\rho g\zeta_{0i}^2. \tag{46}$$

Here, ζ_{0i} [m] is the amplitude of the regular wave under consideration; see p. 97 of (Dean and Dalrymple, 2001).

The spectrum for the irregular wave process is defined such that the area of the wave spectrum $S_\eta(\omega)$ within the frequency interval $\Delta\omega$ represents the wave energy for the same frequency interval. Hence, from a known spectrum function, we can find the amplitude ζ_{0i} [m] of the harmonic wave component which represents the wave energy for a given frequency resolution using (47); see p. 23 of (Faltinsen, 1999), and p. 122 of (Chakrabarti, 1987):

$$\zeta_{0i} = \sqrt{2S_\eta(\omega_i)\Delta\omega}. \tag{47}$$

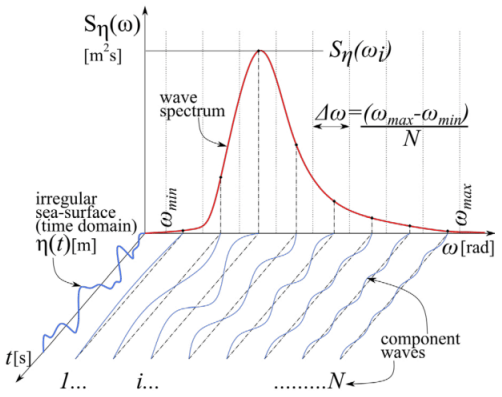

Figure 2. Concept of Fourier series representation of irregular waves and the wave spectrum. Adapted from (Faltinsen, 1999).

Once the amplitudes corresponding to each of the component regular waves is known, randomness may be introduced by the inclusion of an arbitrary phase difference ε_i [rad]. The property of the irregular wave may now be expressed as the summation of the property of the component waves of specified frequencies with random phase. For e.g., the sea surface elevation (SSE) at a given x coordinate is expressed by equation (48); see p. 123 of (Chakrabarti, 1987):

$$\eta(x,t) = \sum_{i=1}^{N} \zeta_{0i} \cos(k_i x - \omega_i t - \varepsilon_i). \qquad (48)$$

Here, N is the total number of wave components (frequency bands), ζ_0 [m] is the component wave amplitude, ω [rad/s] is the wave angular frequency, and ε [rad] is the phase. Subscript i refers to the number of the component wave under consideration. The wave number k [rad/m] is to be determined from the dispersion relation given in (31). g [m/s^2] is the acceleration of gravity and d [m] is the water depth. $S_\eta(\omega_i)$ [m^{2}s] is the energy spectral density and $\Delta\omega$ [rad/s] is the width of the frequency bands dividing the total wave spectrum.

The even distribution of component frequencies will cause the resultant wave to be periodic with a period of of $2\pi/\omega_{min}$ [s], and thus not truly irregular. Hence, the component frequency within each frequency interval is selected based on a unifrom random distribution, as advised in p. 209 of (Fossen, 2011).

3 Modelica Implementation

3.1 General Considerations

Most simulation problems envisaged would require, in one way or the other, the determination of wave/current forces acting on structures with varying degrees of restraint as illustrated in Figure 3. Since the wave forces vary both temporally and spatially, and since the location information is contained in the component-model for the body in a wave-body interaction problem, it was decided that a wave component-model that generates all the required parameters that allows for the determination of the various quantities given in the equations under Section 2.5, at any location (x, y, z) within the problem domain, at any specified simulation time t, would be the best approach.

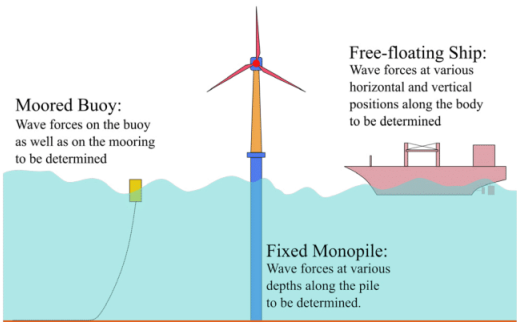

Figure 3. Expected simulation scenarios.

Once the wave parameters such as component frequencies, corresponding amplitudes and phases are determined, they would have to be made available to the body component-model for determination of wave properties at the desired location. Towards this end, an information bus holding the required data is to be specified from which the body component-model may then access this data.

Considering the above general requirements, the system model for integrated simulation may be represented by the block diagram in Figure 4. While the wave, current, and data bus are common components for any ocean engineering simulation, the other components may vary depending upon the scope of the simulation. The rest of this paper is dedicated to the implementation of the component-models for waves and current.

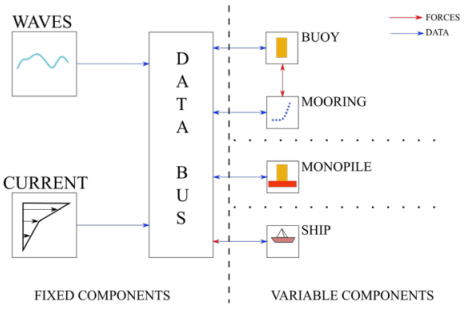

Figure 4. General block diagram for integrated simulation of an ocean engineering system.

Flow-charts provided in the following sub-sections

have been prepared with ocean engineers, most likely to be unfamiliar with *Modelica*, in mind, and some elements might appear superfluous to the *Modelica* savvy reader.

3.2 Regular-Wave Component-Model

The height of the regular wave H_r [m], time period T_r [s], water depth d [m], water density ρ_w [kg/m^3], ramp time T_{rmp} [s], delay time T_{del} [s] and the number of frequency components ${}_n\omega_i = 1$ are specified as *parameters* in the **Regular_Airy_Wave** component model. T_{sim} [s] is the required duration of simulation.

T_{rmp} is used to ramp the wave height in order to prevent impulse wave loads at the start of the simulation, while T_{del} maybe used to start the waves at a specified time into the integrated simulation.

The wave angular frequency $\omega = 2\pi/T$ [rad] and d are passed on as parameters to the function **waveNumberIterator**, which iterates for the wave number based on the dispersion relation given in (31), and returns the final value to **Regular_Airy_Wave**.

A data connector **WaveDataConnector** transmits d, ρ_w, ω, T, k, ε, ζ_{0i}, and SSE_{X0} to the data bus which is an *expandable connector* named the **EnvironmentBus**. Here, ε [rad], the phase difference is redundundant for the case of a regular wave and is set to zero, while SSE_{X0} is the sea surface elevation calculated at $x = 0$ using (38).

The algorithm for generation of regular wave parameters is depicted in the flow chart given in Figure 5, and the flow chart for the *function* **waveNumberIterator** is given in figure 6. The first value for the wave number iteration is taken to be $k_0 = \frac{2\pi}{L_0}$, where $L_0 = \frac{gT^2}{2\pi}$ [m] is the deep-water wave length as given on p. 66 of (Dean and Dalrymple, 2001).

Equations (37)–(45) can then be used to calculate the wave properties at the required position coordinates, contained in the body component-model, at any required simulation time t [s].

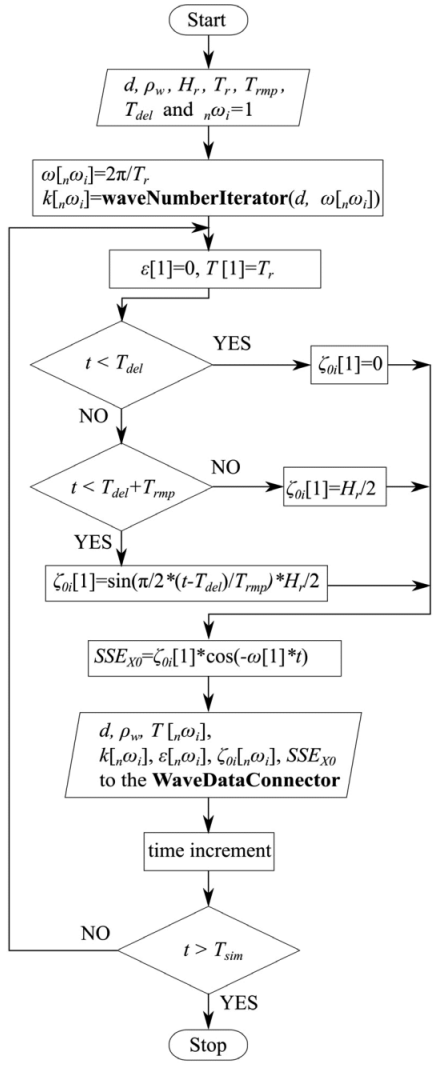

Figure 5. Flow chart for regular-wave component-model.

3.3 Irregular-Wave Component-Model

The generation of component wave parameters based on the Pierson-Moskowitz spectrum is considered for detailed description. The algorithm for the irregular-wave component-model **IRW_PM_RDFCWI** is shown in Figure 7.

The water depth d [m], significant wave height H_s [m], the ramp time T_{rmp} [s], the lower cut-off frequency ω_{min} [rad/s], the upper cut-off frequency ω_{max} [rad/s], and the number of frequency components to be considered ${}_n\omega_i$, are specified as *parameter* inputs.

The frequency resolution $\Delta\omega = (\omega_{max} - \omega_{min})/{}_n\omega_i$ [rad/s] is determined. The component frequency within each frequency interval $\Delta\omega$ is then selected based on a uniform random distribution by the *function* **frequencySelector**.

To generate a vector of random numbers, a *function* **randomNumberGenerator** based on the *Modelica.Math.Random.Generators.Xorshift64star* random number generator, with a *for* loop included, to return a vector of random numbers of specified size, corresponding to the number of frequency components ${}_n\omega_i$, is called. The **frequencySelector** function is a simple function that shifts the component frequencies randomly within the associated frequency interval based on the generated random numbers $rnd\_shft[{}_n\omega_i]$.

Once the component frequencies are identified, the corresponding spectral values are determined by calling the *function* **spectrumGenerator_PM** which calculates the

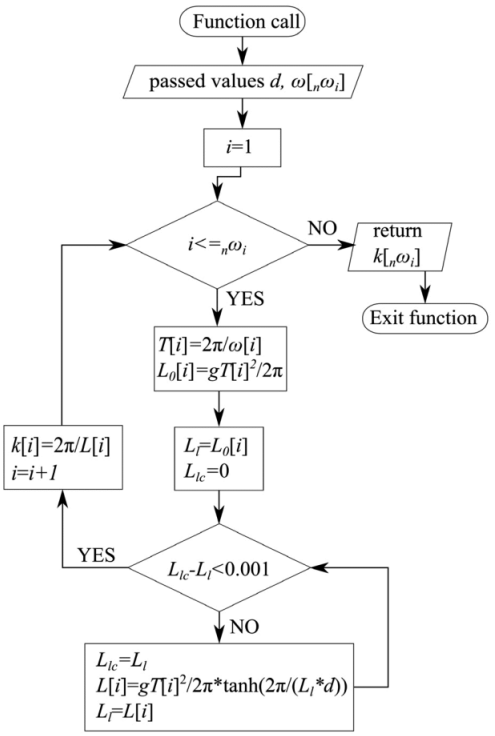

Figure 6. Flow chart for iteration of the wave number.

spectral density values based on the empirical formula

$$S_\eta(\omega_i) = \frac{5\pi^4 H_s^2}{T_p^4 \omega_i^5} \exp\left(\frac{-20\pi^4}{T_p^4 \omega_i}\right). \qquad (49)$$

Here, T_p [s] is the peak period of the spectrum, and is related to H_s through the relations $T_p = \frac{2\pi}{\omega_p}$, and $\omega_p^2 = \frac{0.161g}{H_s}$. ω_p [rad/s] is the peak angular frequency; see pp. 105–107 of (Chakrabarti, 1987).

In the future, generation of wave records based on other commonly used sea-spectra may be incorporated by defining the correspoding spectrum generating functions.

The amplitudes of the component waves ζ_{0i} are then determined using (47), and corresponding wave numbers k_i are determined using the *function* **waveNumberIterator** described in Section 3.2. The randomly distributed phases are determined by a second call to the *function* **randomNumberGenerator**. This function call returns a vector $\varepsilon[_n\omega_i]$ of uniformly distributed random numbers in (0,1] and hence, the associated phase difference is expressed as $2\pi\varepsilon$ [rad] .

Having determined all the required parameters, the sea surface elevation at $x = 0$, SSE_{X0} [m], is then calculated using the formula given in (48). The values are then linked

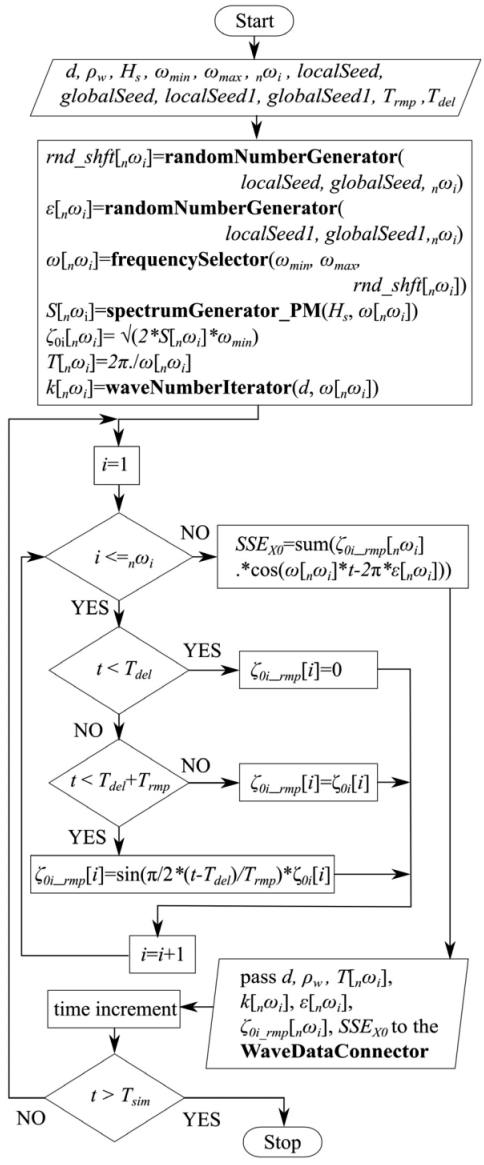

Figure 7. Flow chart for the irregular-wave component-model.

to the *expandable connector* EnvironmentBus using the **WaveDataConnector** as described in Section 3.2.

3.4 Component-Model of Depth-Varying Current

The component-model for current is a simple block which produces as its output two vectors *zcg*[*n*] and *Ucg*[*n*]. *zcg* contains the co-ordinate information and *Ucg* contains the

corresponding current velocities. The *parameters* specified are the $zcg[n]$ which is a vector containing the n depth positions where current velocities are defined, $Uf[n]$ which is a vector containing the fully developed current values, and the ramp time T_{rmp} [s]. $Ucg[n]$ holds the instantaneous value of the ramped current. A sinusoidal ramping function is used for smooth ramping. A **CurrentDataConnector** links the zcg and Ucg values to the *expandable connector* **EnvironmentBus**. The current velocity at any location may now be computed by the different body component-models by interpolation.

4 Results

All results presented below are based on outputs of the above component models. Simulation files are available for download at `github.com/Savin-Viswanathan/Modelica2020-a`.

4.1 Regular Wave

The simulation model **Check_RegularWave** under the *sample simulations* in the above link calculates the wave properties based on the parameters generated by the **Regular_Airy_Wave** component-model.

Figure 8a shows a sample sea surface elevation at $x = 0$ [m] with $T_{del} = 5$ [s], $T_{rmp} = 10$ [s], $H_r = 1$ [m], $d = 10$ [m] and $T_r = 3$ [s], for a simulation interval of 0–30 [s], while Figure 8b shows the progressive wave profile for the same wave in the spatial interval 0–30 [m] for different simulation times.

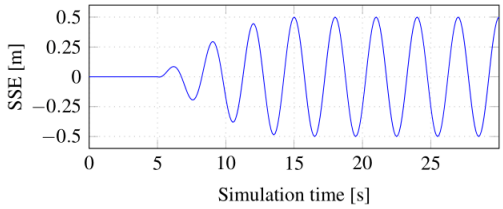

(a) Sea surface elevation at $x = 0$ for $t = [0, 30]$ s.

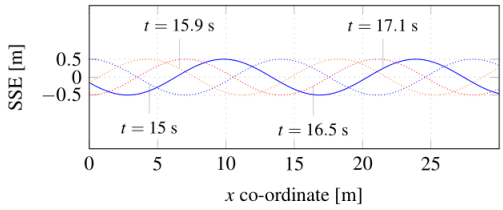

(b) Wave profile at different simulation time steps for $x = [0, 30]$ m.

Figure 8. Sea surface elevation and the progressive wave profile.

Figure 9a shows the wave profiles at $t = 0$ [s] for different T_r, and Figure 9b shows the trajectory traced by water particles with different mean positions during a complete wave cycle, at different depths, for the different wave periods, in a water depth $d = 10$ [m]. We observe that,

- For $T_r = 3$ [s], $k = 0.447414$ [m^{-1}], and $kd > \pi$. The wave is in *deep water* and the trajectories are circular. The displacements in the vertical and horizontal directions decay exponentially with depth and the particles near the bottom boundary have no horizonatal or vertical displacements.
- For $T_r = 6$ [s], $k = 0.129834$ [m^{-1}], and $\frac{\pi}{10} < kd < \pi$. The wave is in *intermediate water* and the trajectories are elliptical. The displacements in the vertical and horizontal directions decay with depth and the particles near the bottom boundary have only horizontal displacements.
- For $T_r = 22$ [s], $k = 0.029246$ [m^{-1}], and $kd < \frac{\pi}{10}$. The wave is in *shallow water* and the trajectories are elliptical. The displacements in the vertical direction decay linearly with depth, while the horizontal displacement is near constant at all depths.

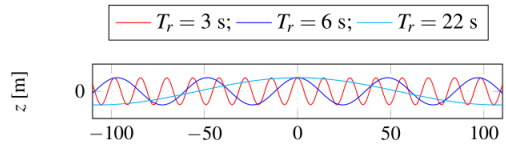

(a) Profiles of waves with different periods.

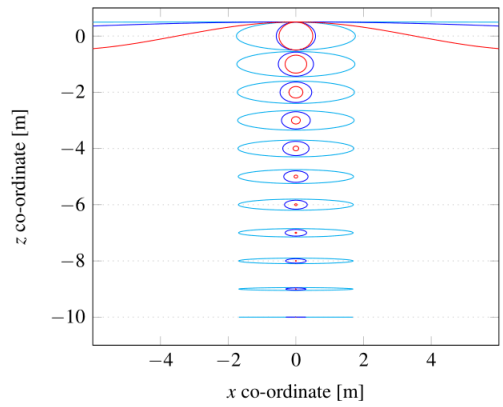

(b) Water particle trajectories of waves with different wave periods.

Figure 9. Wave profiles and water particle trajectories.

Figure 10a shows the intstantaneous wave profile for a regular progressive wave with $T_r = 6$ [s], $H_r = 1$ [m], in a water depth $d = 10$ [m], when there is a crest at $x = 0$ [m]. Figure 10b–10f shows the quiver plots for the instantaneous velocities of water-particles with different mean z co-ordinates, under different x co-ordinates.

An important consideration to keep in mind is that the linearization of the boundary conditions in the derviation of the velocity potential has the effect that the water particle kinematics derived from such a potential does not

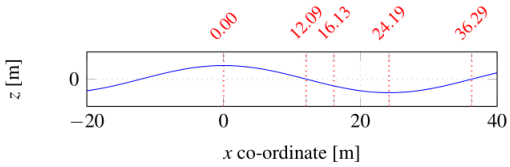

(a) Wave profile and x co-ordinates where the velocities are measured

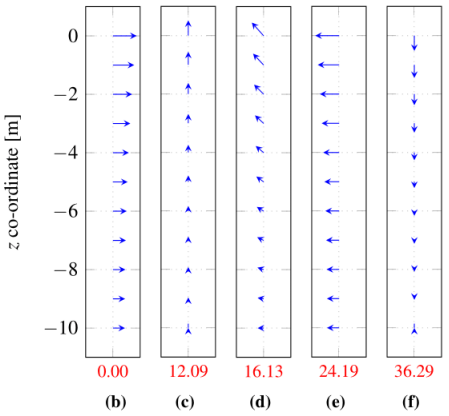

Figure 10. Wave profile (a), water-particle velocities (b)–(f).

account for the change of position of the particle within the fluid, and hence the theory cannot give a proper description for flow velocity and acceleration in the region between the still water level and the wave crest and in the void to the wave trough. Extrapolation of the values is, in general, not recommended since the wave forces will be overestimated. A better way is to apply *Wheeler stretching* or *move* the profile for velocity and acceleration to the instantaneous sea surface; see p. 221 of (SINTEF, 2014).

Figure 11 shows the pressure distribution at various x co-ordinates for the same wave as above. The dynamic pressure above $z = 0$ [m] has been calculated using a truncated Taylor series for small positive distances, as given on p. 84 of (Dean and Dalrymple, 2001).

4.2 Irregular Wave

Figure 12a depicts a Pierson-Moskowitz spectrum of $H_s = 1$ [m] generated by the **spectrumGenerator_PM** function, while Figure 12b depicts the sea surface elevation for an irregular wave record with 100 frequency components, generated from the spectrum by the **IRW_PM_RDFCWI** irregular-wave component-model with $T_{rmp} = 10$ [s], $T_{del} = 0$ [s], $\Delta\omega = \omega_{min} = 0.03141$ [rad/s], and $\omega_{max} = 3.141$ [rad/s]. Figure 12c shows an expanded view of the same wave record in a shorter time interval, for clarity.

4.3 Depth-varying Current

Figure 13 depicts the instantaneous profile for a depth varying current which is based on the output of the **CurrentProfile_4pt** component-model. The current is ramped up to full value using the parameter $T_{rmp} = 5$ [s].

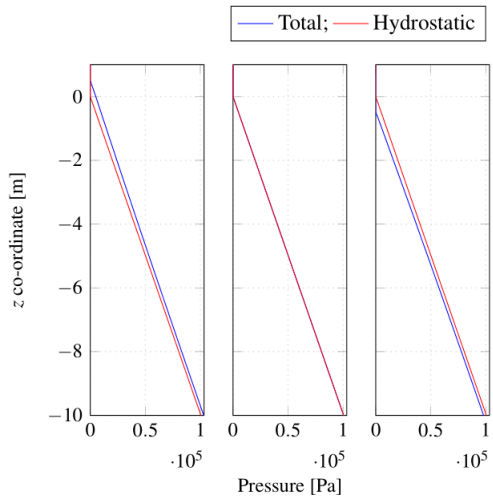

(a) $x = 0$ m **(b)** $x = 12.09$ m **(c)** $x = 24.19$ m

Figure 11. Pressures beneath the wave crest, down-crossing, and trough.

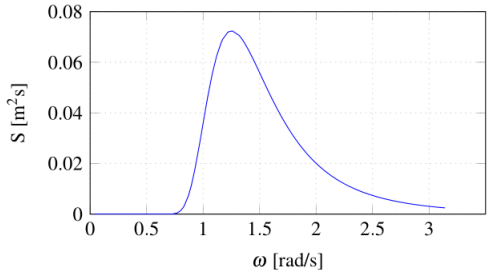

(a) Pierson-Moskowitz spectrum with $H_s = 1$ m.

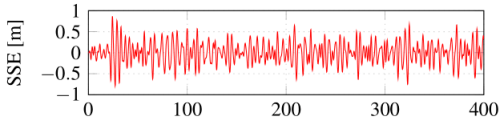

(b) SSE at $x = 0$ m for time interval [0, 400] s.

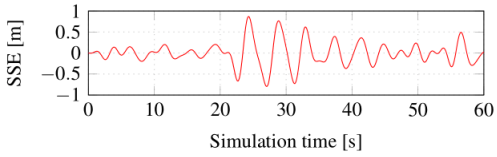

(c) SSE at $x = 0$ m for time interval [0, 60] s.

Figure 12. Irregular waves.

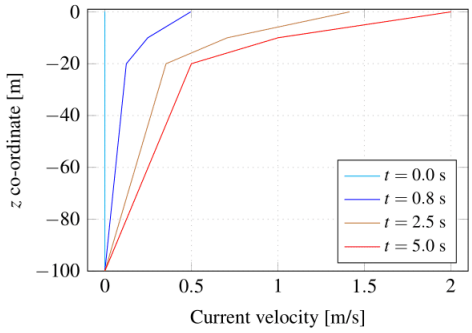

Figure 13. Current profile

5 Conclusion

General considerations to be kept in mind while formulating a framework for carrying out integrated simulation of ocean-engineering systems is presented and the algorithms for development of *Modelica* component-models for the generation of regular and irregular waves are described. The implementation of a simple component-model for generation of depth varying current is also presented.

Graphical representation of the wave kinematics and dynamics based on the output of the component-models for regular waves are then presented to show satisfactory agreement with general results discussed in (Dean and Dalrymple, 2001). A sample sea-surface-elevation based on the output of the component-model for irregular waves is presented. Since, within the assumption of linearity, the properties of the irregular wave are a linear combination of the properties of the consitutent regular waves, it is deemed that the output of the irregular wave component-model is satisfactory. Graphical representation of the output of the component-model for depth varying current is then presented.

For a better understanding of how these component models perform within an integrated simulation scenario, readers may refer to (Viswanathan and Holden, 2019). The present paper fills in for the lack of theoretical and implementational details for the wave and current component-models in the above work.

Theory and implementation of component-models for non-diffracting floating objects and for mooring forces based on the quasi-static catenary approach, used in (Viswanathan and Holden, 2019), is discussed in (Viswanathan and Holden, 2020), along with comparison of results for the same system modelled in the commonly used ocean-engineering software Orcaflex. Satisfactory agreement of surge/heave responses, and of Morison forces under various combinations of wave and current loading is demonstrated in (Viswanathan and Holden, 2020), and these maybe taken as proof for the correct representation of wave-current kinematics by the component models discussed in this work.

6 Acknowledgements

The research in this paper has received funding from the Research Council of Norway, SFI Offshore Mechatronics, project number 90034210.

References

Thomas Lykke Andersen and Peter Bak Frigaard. *Lecture Notes for the Course in Water Wave Mechanics*. Department of Civil Engineering, Aalborg University. DCE Lecture notes, No.24, 2011. URL vbn.aau.dk/en/publications/lecture-notes-for-the-course-in-water-wave-mechanics(69731932-7a17-47ea-b557-6b9e0c81050f).html.

Subratha Kumar Chakrabarti. *Hydrodynamics of Offshore Structures*. Computational Mechanics Publications, and Springer-Verlag, Dorchester, Great Britain, 1987. ISBN 0-905451-66-X.

Robert G. Dean and Robert A. Dalrymple. *Water Wave Mechanics for Engineers and Scientists*. Allied Publishers Limited, Mumbai, India, 2001. ISBN 81-7764-195-6.

Odd M. Faltinsen. *Sea Loads on Ships and Offshore Structures*. Cambridge University Press, 1999. ISBN 0-521-45870-6.

Thor I. Fossen. *Handbook of Marine Craft Hydrodynamics and Motion Control*. John Wiley & Sons, Chichester, United Kingdom, 2011. ISBN 97-8111-999-1496.

Harald E. Krogstad and Oivind A. Arntsen. *Lecture Notes on Linear Wave Theory- Part A- Regular Waves*. Norwegian University of Science and Technology, Trondheim, February 2000. URL folk.ntnu.no/oivarn/hercules_ntnu/LWTcourse/.

SINTEF. *Handbook on Design and Operation of Flexible Pipes*. 2014. URL sintef.no/en/latest-news/updated-handbook-on-design-and-operation-of-flexible-pipes/.

Alexandra H. Techet. *Free Surface Waves- Handout*. Massachusetts Institute of Technology, 2005. URL web.mit.edu/2.016/www/handouts/Free-Surface-Waves.pdf.

Savin Viswanathan and Christian Holden. Towards the development of an ocean engineering library for openmodelica. In *Proceedings of the ASME 2019 38th International Conference on Ocean, Offshore and Arctic Engineering.*, volume 7B: Ocean Engineering, OMAE2019-95054, June, 2019. URL doi.org/10.1115/OMAE2019-95054.

Savin Viswanathan and Christian Holden. Modelica component-models for non-diffracting floating objects and quasi-static catenary moorings. *Proceedings of the American Modelica Conference*, March, 2020. The referring paper and the referred paper are part of the proceedings of the same conference.

4.3 Modelica component models for non-diffracting floating objects and quasi-static catenary moorings

The citation of the published article is given below:

S. Viswanathan and C. Holden. *Modelica Component Models for Non-diffracting Floating Objects and Quasi-static Catenary Moorings*. Proceedings of the American Modelica Conference 2020, Boulder, Colorado, USA, March 23-25, 2020. https://doi.org/10.3384/ecp20169101

The postprint version of the paper follows.

Modelica Component Models for Non-diffracting Floating Objects and Quasi-static Catenary Moorings

Savin Viswanathan[1] Christian Holden[1]

[1]Dept. of Mechanical and Industrial Engineering, Norwegian University of Science and Technology (NTNU), NO-7491 Trondheim, Norway. {savin.viswanathan,christian.holden}@ntnu.no

Abstract

In this paper, the theory behind determining the hydrodynamic response of a floating object in the presence of waves is discussed, followed by a simplification for the case of wave-transparent objects. The Morison equation is introduced as a means to estimate lateral wave and current loads on slender bodies. The quasi-static catenary approach to determine mooring forces is then discussed. Development of *Modelica* component-models to simulate the hydrodynamic response of free-floating and catenary-moored non-diffracting objects, in the presence of waves and depth varying current, is then dealt with in detail, and the results dicussed.

Keywords: hydrodynamics of non-diffracting floating objects, quasi-static catenary mooring, Modelica ocean-engineering library.

1 Introduction

The advantages of developing an *OpenModelica* ocean-engineering library populated with domain-specific *component-models* and *functions* to carry out the integrated simulation of multi-pyhsical ocean engineering systems was demonstrated by the authors (Viswanathan and Holden, 2019). This earlier work:

1. Gives a brief description of the simulation of systems based on the hydrodynamic response of catenary-moored non-diffracting floating objects in the presence of waves and current,

2. Demonstrates the satisfactory agreement of the *Modelica* simulation results with those obtained using a popular ocean-engineering commercial software (*Orcaflex*), and

3. Brings out the advantages of using a component-model based simulation approach.

The voluminous nature of the earlier work precluded the possibility of delving into the theoretical and implementational details of the various *Modelica* component-models of the ocean-engineering library proposed by the authors, the preliminary version of which is available for download at `github.com/Savin-Viswanathan/OELib_OMAE2019`.

(Viswanathan and Holden, 2020) gives a detailed description of the development of *Modelica* component-models to simulate regular as well as irregular waves and depth-varying current. This present work elaborates on the theoretical and implementational details of the component-models for non-diffracting floating objects, and catenary mooring based on the quasi-static approach.

2 Theory

2.1 Hydrodynamics

Considering the steady-state interaction of a floating object with a regular wave, the loads acting on the body may be considered to be comprised of:

- The fluid pressure loads due to the *incident* wave acting on the body, which is assumed fixed at its mean position.

- The fluid pressure loads due to the *scattered/diffracted* wave from the body, which is assumed fixed at its mean position.

- The fluid pressure loads due to the *radiated* wave system set up by the body as it oscillates in its six Degrees-of-Freedom (DoF) in calm water.

An illustration of the *Diffraction-Radiation* problem is given in Figure 1.

The loads due to the incident wave are referred to as *Froude-Krylov* loads, and those due to the scattered wave are referred to as *diffraction* loads in p. 39 of (Faltinsen, 1999), and this is the convention followed in this work. Another widely used convention is to refer to the combined incident and scattered wave-problem as the *diffraction* problem as in p. 288 of (Newman, 1989).

The Froude-Krylov and diffraction loads taken together constitute the wave excitation loads and may be determined by integrating the incident and diffracted wave dynamic pressures over the mean wetted hull surface. The integration of the dynamic component of the radiation wave pressures give the associated hydrodynamic loads commonly referred to as *added-mass* and *damping*, while the integration of the hydrostatic component gives the *restoring* loads. The added-mass loads are in phase with the body acceleration and the damping loads are in phase with the body velocity.

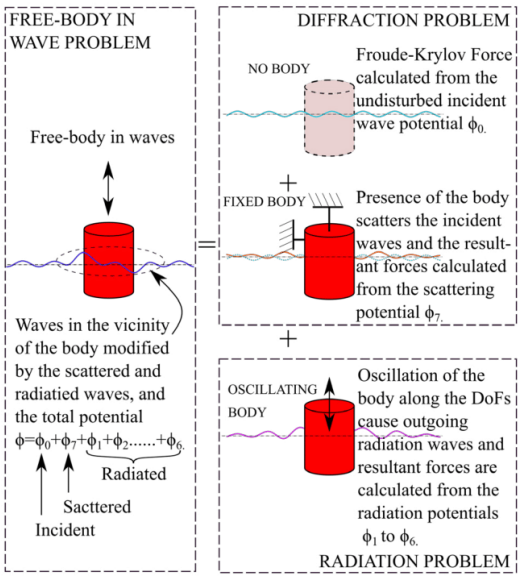

Figure 1. The diffraction-radiation problem. Adapted from (Faltinsen, 1999)

The assumption of inviscid, incompressible fluid and irrotational flow implies the existance of a velocity potential which may be determined by solving the associated linearized boundary value problem (BVP). The solution to the BVP for determining the incident wave potential is discussed in (Viswanathan and Holden, 2020). Each of the wave systems above may thus be described by its respective velocity potential, and within the assumption of linearity, the total potential ϕ [m^2/s] in the vicinity of the body is given by

$$\phi = \phi_0 + \phi_7 + \sum_{j=1}^{6} \dot{\eta}_j \varphi_j. \tag{1}$$

Here, ϕ_0 and ϕ_7 [m^2/s] are the incident and diffracted wave velocity potentials, respectively, and the summation term represents the radiation wave potential, where $\dot{\eta}_j$ [m/s] is the body velocity along the respective DoF, and φ_j [m] is the spatial component of the complex velocity-potential due to the body oscillation with unit velocity in the corresponding DoF; see (Faltinsen and Michelsen, 1974).

Numerical solutions to the diffraction-radiation problem may be sought through the Boundary Element Method or through the Harmonic Polynomial Cell method, to determine the hydrodynamic coefficients. See (Newman and Lee, 2002) and (Shao and Flatinsen, 2014).

2.1.1 Simplifications in the case of a small-volume structure

When the size of the structure is large, the diffraction forces are significant, and hence, one must solve the diffraction-radiation problem to determine the wave loads. However, when the structure is relatively small compared to the incident wave-length, depending on the relative significance of the inertia and drag forces, one may utilize the Froude-Krylov theory or the Morison equation to determine the wave loads. The Froude-Krylov theory is applicable for a relatively small structure when drag forces are small compared to the inertia forces. When the drag forces are significant, one has to use the Morison equation; see p. 168 of (Chakrabarti, 1987).

Considering the case of a vertical cylindrical buoy, drag forces are not signifcant for motions in the vertical plane, and hence the Froude-Krylov theory can be used to calculate the vertical wave-loads. However, for motion in the horziontal plane, drag forces become significant and hence, the Morison equation should be used to determine the horizontal wave-loads.

2.1.1.1 The Froude-Krylov Force

For small-volume upright cylindrical structures, the long wave approximation is applicable for $L > 5D$, where L [m] is the wavelength and D [m] is the diameter of the cylinder. Considering the translational DoFs, i.e., $i = 1,2,3$, the force on the relatively small body may then be expressed as:

$$\mathbf{F} = \mathbf{i}F_1 + \mathbf{j}F_2 + \mathbf{k}F_3 \tag{2}$$

$$\text{where } F_i = -\iint_{S_{0B}} pn_i \, \mathrm{d}s + A_{i1}a_1 + A_{i2}a_2 + A_{i3}a_3. \tag{3}$$

Here, p [N/m^2] is the undisturbed incident wave pressure, and $\mathbf{n} = (n_1, n_2, n_3)$ is the unit normal vector to the body surface, defined to be positive into the fluid. The integral is over the average wetted surface of the body. Furthermore, a_1, a_2, and a_3 [m/s^2] are the acceleration components along the x, y, z directions of the undisturbed wave field, and are to be evaluated at the geometrical mass centre of the body. A_{i1}, A_{i2}, A_{i3} [kg] are added-mass terms. **i, j, k** are unit vectors along x, y, z. We also note that the wave generation capability of the body is very small when the long-wave approximation holds true, and hence, the potential damping terms may be neglected; see pp. 60–61 of (Faltinsen, 1999).

The first term of (3) is the Froude-Krylov force, the vertical component of which is approximated as

$$F_{FK}^{z} \approx \rho g A_{wp} \eta. \tag{4}$$

Here, ρ [kg/m^3] is the water density, g [m/s^2] is the acceleration due to gravity, A_{wp} [m^2] is the water-plane area, and η [m] is the sea surface elevation (SSE) about the mean sea level. See (Techet, 2005).

The sea surface elevation η, at any x co-ordinate, may be expressed as:

$$\eta(x,t) = \sum_{i=1}^{N} \zeta_{0i} \cos(k_i x - \omega_i t - \varepsilon_i). \tag{5}$$

Here, N is the total number of wave components (frequency bands), ζ_{0i} [m] is the component wave amplitude,

ω_i [rad/s] is the wave angular frequency, and ε_i [rad] is the phase. Subscript i refers to the number of the component-wave under consideration. The wave number k_i [rad/m] is to be determined from the dispersion relation. For details, see (Viswanathan and Holden, 2020).

The SSE for a regular wave can be expressed by taking $N = 1$ in (5).

2.1.1.2 The Morison Equation Though initially formulated to calculate the horizontal wave-forces on fixed, surface-piercing vertical piles, where $D \ll L$, and the drag forces significant, the Morison equation has since been adapted to determine wave loads on oscillating slender structures. A thorough treatment of the subject can be found in Chapter 6 of (Chakrabarti, 1987).

The horizontal wave and current loads per unit length, on a cylindrical object free to move in presence of waves and current, may be determined from

$$\begin{aligned} M_F^x =& C_M^x \rho \frac{\pi}{4} D^2 \dot{u} - C_A^x \rho \frac{\pi}{4} D^2 \ddot{x} \\ &+ C_D^x \frac{1}{2} \rho D \mid u \pm U - \dot{x} \mid (u \pm U - \dot{x}). \end{aligned} \tag{6}$$

Here, M_F^x [N] is the Morison force, C_M^x [-] is the inertia coefficient, ρ [kg/m^3] is water density, D [m] is the body diameter, $\dot{u}$ [m/s^2] is the wave-induced water-particle acceleration along x, C_A^x [-] is the added-mass coefficient , $\ddot{x}$ [m/s^2] is the body acceleration along x, C_D^x [-] is the drag coefficient, u [m/s] is the wave-induced water-particle velocity along x, U [m/s] is the current velocity along x, and $\dot{x}$ [m/s] is the body velocity along x. C_M^x and C_D^x are available from numerous field and laboratory tests, e.g., (Yeung, 1981), which allows the designer to choose appropriate values; see p. 172 of (Chakrabarti, 1987). Also, $C_M^x = 1 + C_A^x$; see p. 178 of (Chakrabarti, 1987). The wave kinematics are given by (7) and (8); see pp. 48–52 of (Chakrabarti, 1987).

$$u = \frac{\pi H}{T} \frac{\cosh\left[k(z+d)\right]}{\sinh\, kd} \cos(kx - \omega t) \tag{7}$$

$$\dot{u} = \frac{2\pi^2 H}{T^2} \frac{\cosh\left[k(z+d)\right]}{\sinh\, kd} \sin(kx - \omega t). \tag{8}$$

Here, H [m] is the wave height, T [s] is the wave period, k [rad/m] is the wave number, z [m] is the vertical coordinate of the point at which the wave kinematics are to be calculated, d [m] is the water depth, x [m] is the horizontal coordinate of the point at which the wave kinematics are to be calculated, and ω [rad/s] is the angular frequency of the wave.

2.2 Catenary Mooring

When a floating object is moored by a slack mooring line, the line assumes the shape of a half catenary; see p. 9 of (Chakrabarti, 1987).

For simplicity, we consider a mooring line that acts in the x-z plane. At the point of suspension, the chain tension has a horizontal and vertical component, the magnitudes of which depend on ψ [rad], the angle made by the tangent to the caternary with the horizontal, at the point of suspension. The horizontal component of this force prevents the drifting of the floater in the direction away from the anchor position. In the absence of other external forces, the floater drifts to a position such that the suspended length of the mooring line is vertical. X [m] is the distance from the anchor point to the fairlead on the buoy, and x [m] is the distance from the touch- down-point (TDP) to the fairlead. As the buoy drifts away from the anchor, the TDP moves towards the anchor, and vice-versa, as shown in Figure 2. The total chain length is represented by l_c [m] and the suspended length of the chain is represented by l_s [m]. The length of the chain lying on the seafloor is thus $l_f = l_c - l_s$.

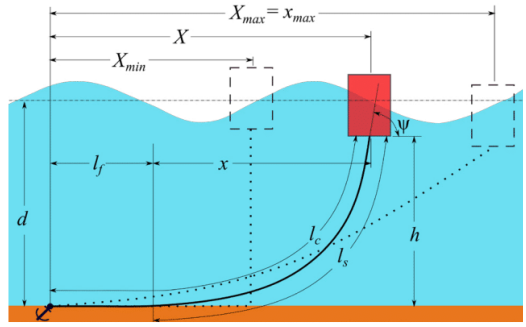

Figure 2. The mooring half-catenary.

From (Tatum, 2004) we have the following relations:

$$a = \frac{T_H}{w} \tag{9}$$

$$z = a \cosh\left(\frac{x}{a}\right) \tag{10}$$

$$l_s = a \sinh\left(\frac{x}{a}\right) \tag{11}$$

$$z = a \sec(\psi) = a + h \tag{12}$$

$$z^2 = l_s^2 + a^2. \tag{13}$$

Here, a [m] is the catenary parameter, x, z [m] are catenary co-ordinates, T_H [N] is the horizontal tension, and w [N/m] is the submerged specific weight of the catenary.

From (MIT, 2011), we have:

$$T_H = \frac{xw}{\cosh^{-1}\left(1 + \frac{wh}{T_H}\right)} \tag{14}$$

$$l_s = h\sqrt{\left(1 + \frac{2T_H}{wh}\right)}. \tag{15}$$

Considering that we are dealing with the response to linear waves of small-volume structures with small draughts and even smaller variations in draughts, and that the water depth is very large when compared to the

draught, we note that when $X = X_{min} \approx (l_c - d)$, $x \approx 0$, and when $X = X_{max} \approx \sqrt{l_c^2 - d^2}$, $x = x_{max}$.

Equation (14) can be iterated to get values of T_H for $x \in \{0, 0.1, 0.2 ..... x_{\max}\}$. We may then use the relation

$$X = l_c - l_s + x \tag{16}$$

to generate a look-up table of horizontal tension values for different horizontal positions of the floater w.r.t. the anchor position. The horizontal tensions for intermediate positions may then be determined by interpolation.

Once the instantaneous horizontal tension values are determined, we may use (10) and (12) to calculate the instantaneous suspended length of the chain, the submerged weight of which is the vertical tension at the fair lead.

The mooring line is also subject to Morison forces, both in the horizontal and vertical directions. To determine these forces, the chain is discretized into a number of segments, and the horizontal and vertical Morison loads are calculated at the mid-points of such segments, and summed up to get the loading on the entire chain. It is assumed that the catenary shape is not affected by such loads, and the sole effect of the fluid loading is a modification in the horizontal and vertical tension values for a given configuration.

The Morison loads per unit length in the normal and tangential directions to a segment, at its mid point, is calculated using equations (17) and (18). This method allows for the separate specification of C_D and C_M values, experimental values of which are scarce when the structures are inclined; see p. 205 of (Chakrabarti, 1987). This method is widely used, and is referred to as the *cross-flow* principle in p. 166 of (Orcina, 2010).

$$\begin{aligned} M_F^n =& C_M^n \rho \frac{\pi}{4} D^2 a_w^n - C_A^n \rho \frac{\pi}{4} D^2 a_l^n \\ &+ C_D^n \frac{1}{2} \rho D \mid v_w^n \pm U^n - v_l^n \mid (v_w^n \pm U^n - v_l^n). \end{aligned} \tag{17}$$

$$\begin{aligned} M_F^t =& C_M^t \rho \frac{\pi}{4} D^2 a_w^t - C_A^t \rho \frac{\pi}{4} D^2 a_l^t \\ &+ C_D^t \frac{1}{2} \rho D \mid v_w^t \pm U^t - v_l^t \mid (v_w^t \pm U^t - v_l^t). \end{aligned} \tag{18}$$

Here, superscripts n and t denote the normal and tangential directions, and subscripts w and l denote the water-particle and the mooring-segment. Further, a [m/s^2] is the acceleration, v is the velocity, U [m/s] is the magnitude of the current velocity, and the equivalent-line diameter is $D = 1.8 d_{cw}$ [m], where d_{cw} [m] is the diameter of the chain wire. See p. 303 of (Orcina, 2010).

The determination of the position of the link mid-points would require the approximation of the quasi-static catenary shape from the horizontal tension at each time step. This is effected by discretizing the mooring length l_c into a number of segments, and determining the position of each node connecting the segments using (10)–(12). Once the mid-point positions at each time step are located, the link velocity and accelerations can be expressed as time derivatives of the displacement.

The wave-induced water-particle kinematics at the link mid-point maybe calculated from (7), (8), (19), and (20); see pp. 48–52 of (Chakrabarti, 1987):

$$w = \frac{\pi H}{T} \frac{\sinh[k(z+d)]}{\sinh(kd)} \sin(kx - \omega t) \tag{19}$$

$$\dot{w} = -\frac{2\pi^2 H}{T^2} \frac{\sinh[k(z+d)]}{\sinh(kd)} \cos(kx - \omega t). \tag{20}$$

The current velocities at the required positions can be interpolated from the specified current profile. The wave-induced kinematics and the current profile are moved with the SSE. See p. 221 of (SINTEF, 2014).

Once M_F^n and M_F^t are determined for each link, they are resolved into their horizontal and vertical components, and summed up, to get the total horizontal and vertical forces acting on the mooring chain at each time step. These are then summed up with the vertical and horizontal mooring tension values to get the modified values with fluid loading as F_M^x and F_M^z [N].

2.3 The Equations of Motion

Having determined the loads acting on the cylindrical buoy, we may express the equations of motion (EoM) in the horizontal and vertical directions as:

$$M^x \ddot{x} + C^x \dot{x} + K^x x = M_F^x + F_M^x \tag{21}$$

$$M^z \ddot{z} + C^z \dot{z} + K^z z = F_{FK}^z + m_a^z \dot{w}_{cb} + F_M^z \tag{22}$$

Here M [kg] is mass, C [Ns/m] is the damping, K [N/m] is the restoring force, M_F is the Morison load on the buoy, F_M [N] is the mooring load, m_a [kg] is the added-mass, and $\dot{w}_{cb}$ [m/s^2] is the vertical wave induced water particle acceleration evaluated at the vertical centre of buoyancy of the buoy. Superscripts x and z denote the horizontal and vertical directions. In (21), the added mass load is included in the Morison force term given by (6).

3 Modelica Implementation

Flow-charts in the sub-sections that follow have been prepared with ocean engineers, most likely to be unfamiliar with *Modelica*, in mind, and some elements might appear superfluous to the *Modelica* savvy reader.

The general considerations in the implementation of *Modelica* component-models for integrated simulation of ocean engineering systems, the implementation of component-models to simulate waves and depth-varying current, and the method of linking the generated outputs to a universal data bus have been discussed in (Viswanathan and Holden, 2020).

The following data are thus available at the **EnvironmentBus**:

- $\omega[_n\omega_i]$, vector of component wave frequencies.
- $T[_n\omega_i]$, vector of component wave Time periods.
- $k[_n\omega_i]$, vector of component wave numbers.

- $\varepsilon[_n\omega_i]$, vector of component wave phases.
- $\zeta_{0i}[_n\omega_i]$, vector of component wave amplitudes.
- $zcg[n]$, vector of z co-ordinates where current velocities are provided.
- $Ucg[n]$, vector of current velocities at above z co-ordinates.

3.1 Non-diffracting Floating Cylinder Component-model

The water depth d [m], water density ρ_w [kg/m^3], density of the mooring line material ρ_c [kg/m^3], specific mass of the mooring line in air m_a [kg/m], cylinder radius r [m], height h [m], structural mass m_s [kg], ballast mass m_b [kg], vertical centre of gravity position w.r.t. the keel z_{KG} [m], added-mass coefficients C^x_{ma}, C^z_{ma} [-], drag coefficients C^x_D, C^z_D, and damping C^x, C^z [kg/s] are specified as parameters. m_{flg} is a parameter to specify if the buoy is free-floating or moored. It is set to 0 in case of a free-floating buoy, and to 1 if moored.

A composite connector **Fairlead[2]**, having two flanges of type *Modelica.Mechanics.Translational.Interfaces.Flange_a*, is specified at the centre of the bottom surface of the buoy, to transfer the horizontal and vertical mooring loads.

A data connector **ebdc** is specified to link the wave and current data from the **EnvironmentBus** to the buoy component-model.

Figure 3 shows the flow-chart for the component-model. Here, K [N/m] is the stiffness, M [kg] is the dry mass of the buoy, A_{wp} [m^2] is the water-plane area of the buoy, z_s [m] is the static draught, z_m [m] is the draught considering the mooring line length, z_{cb} [m] is the z co-ordinate of the centre of buoyancy, z_{fb} [m] is the calm-water z co-ordinate of the body CG. z_1, z_2, z_3 [m] are the instantaneous z co-ordinates of the body CG, top surface and bottom surface, respectively. z [m] is the instantaneous vertical displacement from z_{fb} and x [m] is the displacement in the horizontal direction of the body CG, both of which are to be determined from the equations of motion. v^x and v^z [m/s] are the body velocities in the x and z directions, while a^x and a^z [m/s^2] are corresponding accelerations. SSE_x [m] is the instantaneous sea surface elevation at the x co-ordinate of the body CG, a_w [m/s^2] is the vertical component of the wave-induced water-particle acceleration, calculated at the instantaneous (x, z_{cb}) position, and M^x_F [N] is the instantaneous wave-current Morison loading on the buoy. Fairlead[1].f and Fairlead[2].f [N] are the horizontal and vertical components of the mooring load, at the the fairlead. t, T_{sim} [s] are the current and total simulation times, respectively.

SSE_X is calculated using (5). The function **wave_awCalculator** returns the value of a_w calculated using (8), with consideration of the *moved* kinematic profile. The function **morisonForceCydlBuoy** returns the value of M^x_F. The EoMs along the x and z directions are then solved with the specified initial conditions to determine the body response.

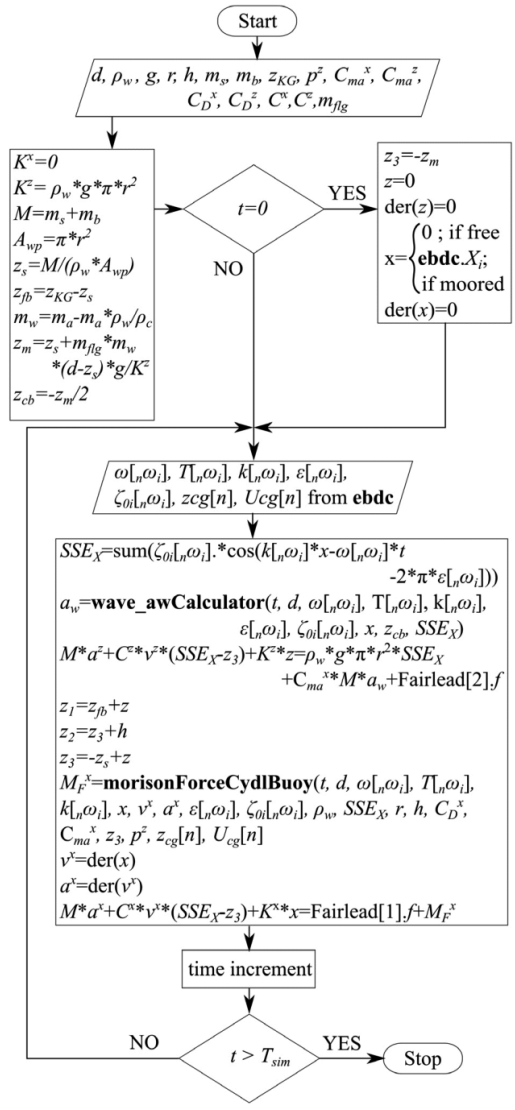

Figure 3. Flow-chart for the floating cylinder component-model.

3.2 Quasi-static Catenary Mooring Component-Model

Considering space limitations, the flow chart for the component-model **Catenary_Mooring_Mf0**, which does not take into consideration the wave and current loads on the mooring line itself, is given in Figure 4.

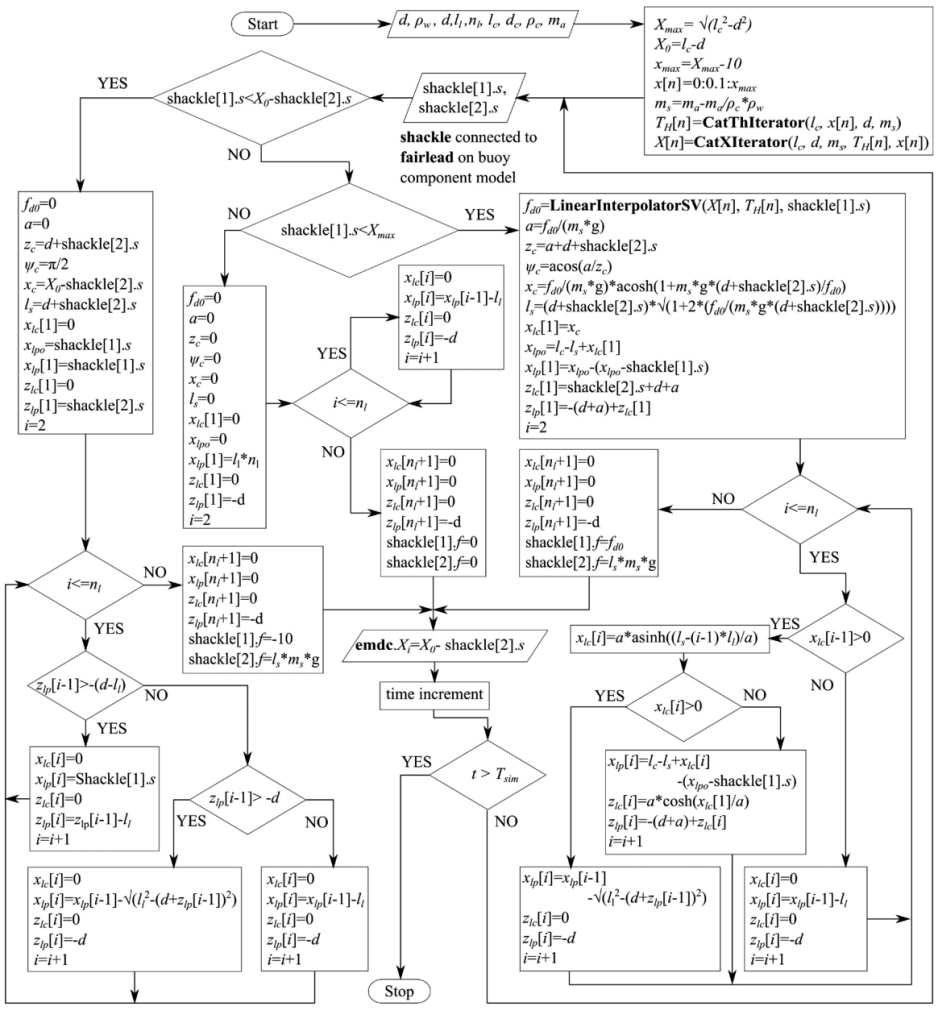

Figure 4. Flow-chart for the quasi-static catenary component-model.

A composite connector **Shackle[2]**, having two flanges of type *Modelica.Mechanics.Translational.Interfaces.Flange_b*, is specified at the top end of the catenary to transfer the horizontal and vertical mooring loads. The parameters defined are the water depth d [m], water density ρ_w [kg/m^3], the number of segments into which the mooring is discretized n_l, the length of each segment l_l [m], the density of the mooring material ρ_c [kg/m^3], and the dry specific mass of the chain m_a [kg/m]. Since the **Shackle** is connected to the **Fairlead**, the corresponding positional data are also available.

X_{max}, X_0, x_{max} [m] are calculated along with the submerged specific mass of the mooring m_s [kg/m]. The vector containing the x positions, where the horizontal mooring load is to be iterated, is defined as $x[n]$. A *function* **CatThIterator** returns the vector $T_H[n]$, containing the corresponding horizontal tension values, calculated based on (14). Another *function* **CatXIterator**, returns the vector $X[n]$ containing the X position corresponding to the x position, as defined in Figure 2.

A data connector **emdc** is specified to link the wave and current data from the **EnvironmentBus** to the mooring. In addition, the initial x co-ordinate of the top end of the mooring line X_i [m], is transmitted to the universal data bus for utilization by the buoy component-model to specify its initial condition.

f_{d0} [N] is the horizontal mooring load, for the given x

co-ordinate of the top end of the mooring line, a is the catenary parameter, z_c [m] is the z co-ordinate of the top end of the catenary, in the local co-ordinate system of the catenary, the origin of which lies at a distance of a [m] below the bottom-most point of the catenary, as described in (Tatum, 2004). ψ_c [rad] is the slope of the top-most catenary segment, x_c [m] is the x co-ordinate of the top-most point of the catenary, and l_s [m] is the suspended length of the catenary.

x_{lc} and z_{lc} are vectors holding the x and z co-ordinates of the end points of the segments, in the local co-ordinate system of the catenary. x_{lp} and z_{lp} are the vectors holding the x and z co-ordinates of the end points of the segments, in the global coordinate system. x_{lpo} is the plot correction parameter to account for the minor difference between the actual catenary shape with its top end z coordinate corresponding to the instantaneous position of the buoy keel, and the catenary shape which is back-calculated based on the horizontal tension value from the look-up table, which is in turn based on the z co-ordinate of the top end of the catenary lying at the sea-surface.

If the x co-ordinate of the shackle is less than X_{min} [m], then a small force in the positive x direction is applied to restore the buoy to a region where the mooring model is valid. The vertical mooring load is then the weight of the vertically suspended length of the mooring. For the rare cases when shackle[1].$s < X_{min}$, the plot of the mooring shows a vertically suspended-length instead of the actual shape.

When the x co-ordinate of the shackle is between X_{min} and X_{max}, the horizontal mooring load is the corresponding value interpolated from the lookup-table using a *function* **linearInterpolatorSV**, and the vertical load is based on the suspended length back-calculated from the horizontal load. The plot of the mooring line shows the catenary shape, back-calculated from the horizontal load, and corrected using x_{lpo}.

If the loads on the buoy exceed the capacity of the mooring line, then the x co-ordinate of the shackle exceeds X_{max}, the catenary is assumed to be detached from the buoy, and would lie extended on the sea-floor.

3.2.1 Current and Wave Loads on the Mooring Line

Simulation of current and wave Morision loads on the mooring line is based on the theory given in Section 2.2. The methodology is similar to the one represented by Figure 4, with additional loops for determining fluid and structure velocities and accelerations, and is easily discernible from the code. **Catenary_Mooring_MfC** considers the Morison loads due to current and mooring velocities, while **Catenary_Mooring_MfCW** considers the loads due to current, wave, and mooring line velocities and accelerations.

4 Results

The simulation files for all results discussed below are available at `github.com/Savin-Viswanathan/Modelica2020-b`. Comparison results using *Orcaflex* are also presented here.

Figure 5a shows the heave response of a cylindrical buoy of $r = 0.6$ [m], $h = 2$ [m], $m_s = 350$ [kg], $m_b = 500$ [kg], in a water depth of $d = 50$ [m], when subjected to a regular wave with $H_r = 1$ [m] and $T_r = 7$ [s], with $T_{del} = 0$ [s], and $T_{rmp} = 20$ [s]. We have assumed $C^x_{ma} = C^z_{ma} = 1$, $C^x = 0$ [kg/s], and $C^z = 3100$ [kg/s].

Figure (4) in (Viswanathan and Holden, 2019) had shown the same results for heave, and we had noticed a slight discrepancy between the *Modelica* and *Orcaflex* results. The cause was identified to be an error in the treatment of the added mass term in (4) of (Viswanathan and Holden, 2019), and has been corrected based on the theory described here in Section 2.1.1.1. Figure 5b shows the surge response.

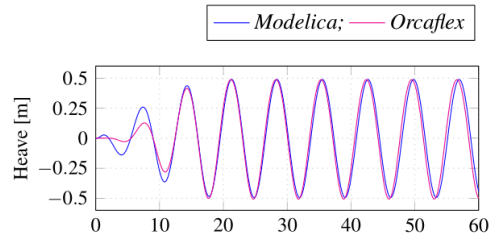

(a) Heave response.

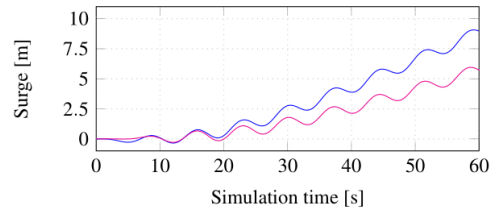

(b) Surge response.

Figure 5. Unmoored cylindrical buoy in waves.

Figure 6a shows the surge response of the above buoy, in the presence of a uniform current of 1 [m/s] in the x direction, while Figure 6b shows the same in presence of both the above wave and current.

Figure 7a shows the horizontal Morison loads on a fixed buoy with same properties as the earlier one, but with a draught of 1 [m], when subjected to a uniform current of 1 [m/s]. Figure 7b shows the surge Morison loads when only a regular wave, with the same parameters as above, acts on the fixed buoy, and Figure 7c shows the Morison loads when both the current and the wave acts on the buoy.

From Figure 7, we observe that the Morison loads are a close match, and hence, the difference between *Modelica* and *Orcaflex* values in Figures 5b, 6a, and 6b, can be attributed to the difference in the way in which the loads are ramped up during the start of simulation, as evid-

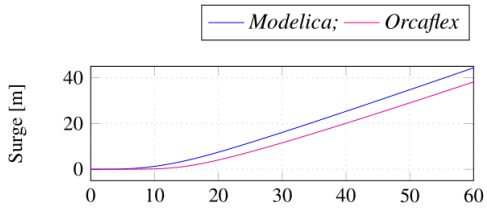

(a) Current only.

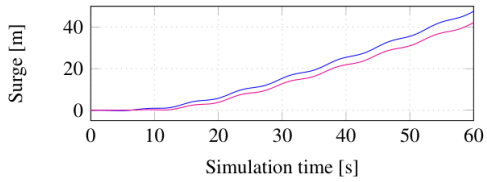

(b) Wave and current.

Figure 6. Surge response of an unmoored cylindrical buoy.

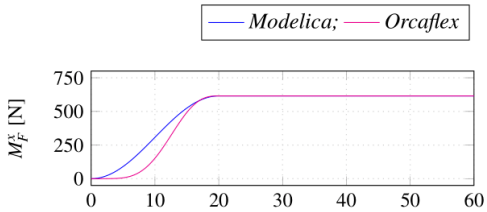

(a) Current only.

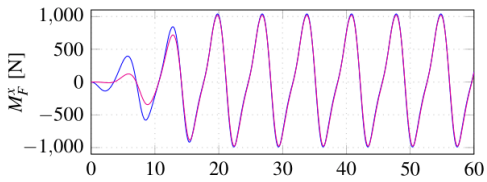

(b) Wave only.

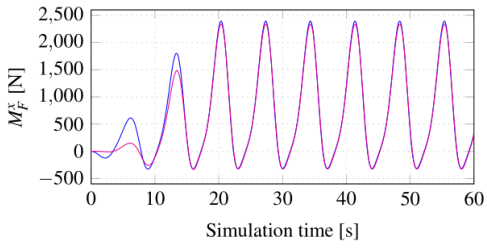

(c) Waves and current.

Figure 7. Morison loads on a fixed cylinder.

ent from Figure 7a. *Orcaflex* uses *vertical-stretching* of the water-particle kinematics, while the present *Modelica* model employs *moved* kinematic-profiles, and this could be the cause of the minute difference in peak values of the Morison loads in Figures 7b and 7c.

Orcaflex uses a lumped-mass and spring-damper model for the mooring lines, while mooring forces in the present work are based on the quasi-static catenary theory. Figure 8 shows the horizontal tension values given by *Orcaflex* and *Modelica* models for different X positions, for moorings of different specific masses. The horizontal tensions are a close fit, with *Modelica* giving slightly higher values than *Orcaflex*. e.g., for a chain with specific mass of 16 [kg/m], at $X = 70$ [m], T_H in *Modelica* is $2,336$ [N] and $2,299$ [N] in *Orcaflex*. The mooring horizontal tensions from *Orcaflex* were determined by placing the top end of the line at different X positions along the free surface manually and a small error in the values had occured in Figure 10 of (Viswanathan and Holden, 2019).

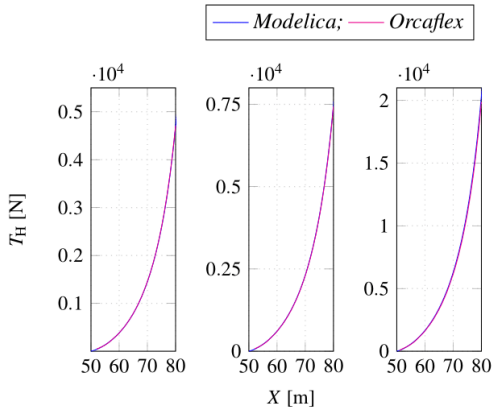

(a) $m_a = 10$ kg/m **(b)** $m_a = 16$ kg/m **(c)** $m_a = 43.5$ kg/m

Figure 8. Horizontal tensions for mooring chains with different specific masses (m_a).

Figure 9 shows the shape of a mooring line, with specific mass 10 [kg/m], in *Modelica* and *Orcaflex* when the top end is placed at X=60 [m], and at 80 [m] with z= 0 [m]. When a uniform current of 1 [m/s] is applied across the full depth of the water-column, the *Orcaflex* line, based on the lumped mass model, deflects under the influence of the current. The deflection is not expected to be large enough to cause considerable difference in the fluid loading experienced by the mooring line. However, it is evident that the static catenary model would not capture the forces that result as a consequence of the dynamics of the mooring line itself.

Figure 10 shows the surge and heave response of the above free-floating buoy, when moored with a mooring line of specific mass 10 [kg/m], under different conditions of wave and current. It was noticed that the model failed to simulate when the acceleration forces due to the fluid and the motion of the chain were considered, using the **CatenaryMooring_MfCW** component model. Hence the

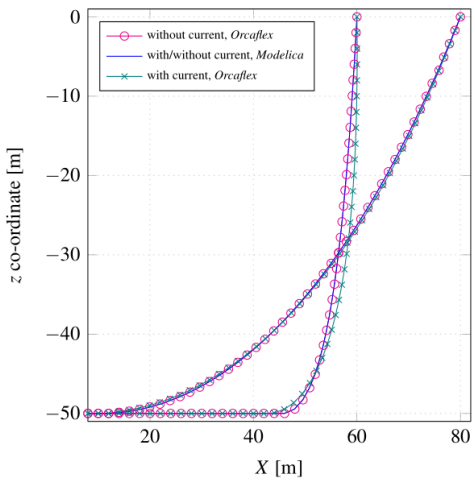

Figure 9. Shape of the mooring line.

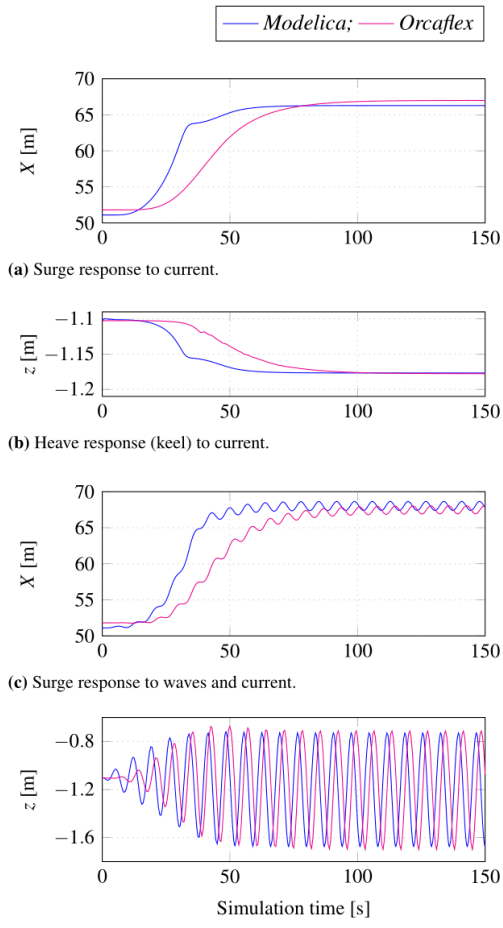

(a) Surge response to current.

(b) Heave response (keel) to current.

(c) Surge response to waves and current.

(d) Heave response (keel) to waves and current.

Figure 10. Hydrodynamic response of a moored cylindrical buoy.

results shown are with the **CatenaryMooring_MfC** component model. The combined wave-current velocity and accleration loads, and inertial loads due to the structural response of the mooring chain, are inherent in the *Orcaflex* model, while they are not accounted for by the present *Modelica* model. The phase difference in the response between the models may be because of this difference.

When the current velocity is reduced to 0.5 [m/s], **CatenaryMooring_MfCW** could be used for simulation, and the results are shown in Figure 11. However, the model is sluggish with many warnings for non-convergence. This could be due to the discontinuities in the accelerations of the segment mid-points, calculated based on the instantaneous static catenary shape. An example of the vertical component of the acceleration of the mid-point of the second segment from the top-end of the mooring, is shown in Figure 11c.

5 Conclusion

Implementation of the theory to develop *Modelica* component-models for a non-diffracting cylindrical object, and for a quasi-static mooring catenary, is described in detail. Simulations to determine the hydrodynamic response of a free-floating cylinder are carried out, and the results compared with a smilar model in *Orcaflex*. It is observed that the heave responses in both cases are in satisfactory agreement. Minor differences in the surge responses are reconciled based on the comparison of Morison forces on a fixed cylinder, under various loading scenarios, and it is concluded that these differences are a result of the differences in the ramp-up functions used in this *Modelica* model and in *Orcaflex*, and hence, do not constitute *errors* in the simulation results.

The static mooring loads, based on the catenary theory in the present *Modelica* model, and those based on the lumped-mass spring-damper system of the *Orcaflex* model, are demostrated to have satisfactory agreement. The comparison between mooring configurations under different loading scenarios points out the probability that differences in the fluid loading of the mooring line, as a result of the deviation of the mooring line from the catenary shape, might not be significant, compared with the contributions from the dynamics of the mooring line itself, which the present *Modelica* model does not capture.

The simulations of a moored floating cylinder further demostrate the satisfactory agreement between this *Modelica* model and a similar *Orcaflex* model. The simulations bring out the deficiencies caused by the assumptions of the quasi-static catenary, which is not in agreement with the actual physics of the system.

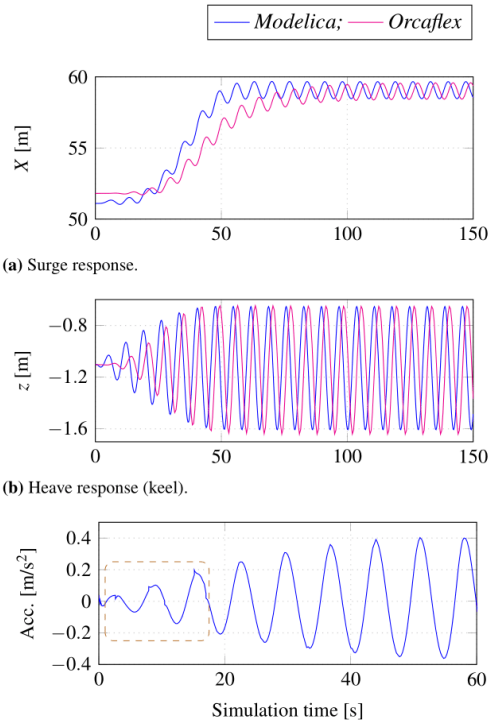

(a) Surge response.

(b) Heave response (keel).

(c) Vertical acceleration of the second chain-link from the fairlead.

Figure 11. Moored cylindrical buoy in waves and reduced current.

To overcome the deficiency of not being able to account for the mooring line dynamics, and to mitigate issues as seen in Figure 11c, a *Modelica* mooring component-model based on the lumped-mass spring-damper approach is being developed, along with a frequency-domain hyrdodynamic analysis component-model, which would enable the generation of hydrodynamic parameters for diffracting objects. The initial results appear promising and will be the topic of discussion in a future work.

6 Acknowledgements

The research in this paper has received funding from the Research Council of Norway, SFI Offshore Mechatronics, project number 90034210.

References

Subratha Kumar Chakrabarti. *Hydrodynamics of Offshore Structures*. Computational Mechanics Publications, and Springer-Verlag, Dorchester, Great Britain, 1987. ISBN 0-905451-66-X.

O.M. Faltinsen. *Sea Loads on Ships and Offshore Structures*. Cambridge University Press, 1999. ISBN 0-521-45870-6.

O.M. Faltinsen and F.C. Michelsen. Motion of large structures in waves at zero froude numbers. *Read at the International Symposium on the Dynamics of Marine Vehicles and Structures in Waves, London*, 1974.

MIT. *Lecture Notes on Mooring Dynamics-II*. Massachusetts Institute of Technology, 2011. URL ocw.mit.edu/courses/mechanical-engineering/2-019-design-of-ocean-systems-spring-2011/lecture-notes/MIT2_019S11_MD2.pdf.

J. N. Newman and C. H. Lee. Boundary-element methods in offshore structure analysis. *Journal of Offshore Mechanics and Arctic Engineering*, 124:81–89, May 2002. doi:10.1115/1.1464561.

J.N Newman. *Marine Hydrodynamics*. The MIT Press, Cambridge, Massachusetts, 1989. ISBN 0-262-14026-8.

Orcina. *Orcaflex Manual- Version 9.1a*. Orcina, 2010. URL citeseerx.ist.psu.edu/viewdoc/download?doi=10.1.1.121.721&rep=rep1&type=pdf.

Yan-Lin Shao and O.M. Flatinsen. A harmonic polynomial cell (hpc) method for 3d laplace equation with application in marine hydrodynamics. *Journal of Computational Physics*, (274):312–314, 2014.

SINTEF. *Handbook on Design and Operation of Flexible Pipes*. 2014. URL sintef.no/en/latest-news/updated-handbook-on-design-and-operation-of-flexible-pipes/.

Jeremy B. Tatum. *Lecture Notes on the Catenary*. University of Victoria, 2004. URL astrowww.phys.uvic.ca/~tatum/classmechs/class18.pdf.

A.H. Techet. *Lecture Notes on the Design Principles for Ocean Vehicles*. Massachusetts Institute of Technology, 2005. URL ocw.mit.edu/courses/mechanical-engineering/2-22-design-principles-for-ocean-vehicles-13-42-spring-2005/readings/r10_froudekrylov.pdf.

Savin Viswanathan and Christian Holden. Towards the development of an ocean engineering library for openmodelica. In *Proceedings of the ASME 2019 38th International Conference on Ocean, Offshore and Arctic Engineering.*, volume 7B: Ocean Engineering, OMAE2019-95054, June, 2019. URL doi.org/10.1115/OMAE2019-95054.

Savin Viswanathan and Christian Holden. Modelica component-models for oceanic surface-waves and depth varying current. *Proceedings of the American Modelica Conference*, March, 2020. The referring paper and the referred paper are part of the proceedings of the same conference.

Ronald W. Yeung. Added mass and damping of a vertical cylinder in finite-depth waters. *Applied Ocean Research*, 3(3): 119–133, 1981.

Chapter 5

Dynamic simulation of subsea cable structures

We had introduced the lumped mass method in Sec. 2.11.2 of the background theory. The consideration of the mooring line mass in the lumped-mass approach enables the capture of the effects of line inertia on the mooring response and thus remedies the shortcomings of the quasi-static catenary theory, discussed in Sec. 4.3. Also, in Sec. 2.10.2, we had discussed how the Morison equation may be used to compute fluid drag and inertia forces on slender marine structures.

In the articles presented in this chapter, we implement the lumped mass approach and Morison loading to (i) simulate the dynamics of a mooring line, in Sec. 5.1, and (ii) simulate the dynamics of a chain suspended subsea load , in Sec. 5.2.

In both cases, we compare the model performance to *Orcaflex* simulation results obtained for the same system, and observe satisfactory agreement.

Thus, the articles presented in this chapter have a direct cor-relation with the general project objective 1, and specific project objectives 1(a) and 1(c), as given in Sec. 2.3.

5.1 Dynamic simulation of a mooring catenary based on the lumped-mass approach– OpenModelica and Python implementations

The citation of the published article is given below:

S. Viswanathan and C. Holden. *Dynamic Simulation of a Mooring Catenary Based on the Lumped-Mass Approach: OpenModelica and Python Implementations*. Proceedings of the ASME 2020 39th International Conference on Ocean, Offshore and Arctic Engineering. Volume 6B: Ocean Engineering. Virtual, Online. August 3–7, 2020. V06BT06A042. ASME. https://doi.org/10.1115/OMAE2020-18134.

The postprint version follows.

DYNAMIC SIMULATION OF A MOORING CATENARY BASED ON THE LUMPED-MASS APPROACH – OPENMODELICA AND PYTHON IMPLEMENTATIONS

Savin Viswanathan*
Department of Mechanical and Industrial Engineering
Norwegian University of Science and Technology
(NTNU)
NO-7491, Trondheim, Norway.
Email: savin.viswanathan@ntnu.no

Christian Holden
Department of Mechanical and Industrial Engineering
Norwegian University of Science and Technology
(NTNU)
NO-7491, Trondheim, Norway.
Email: christian.holden@ntnu.no

ABSTRACT

In this paper, the theoretical background behind the formulation and solution of a *discretized* lumped-mass mathematical-model of the physically *continuous* and inelastic mooring catenary is re-visited. The drag term of the Morison equation is used to determine the fluid loads, and the sea-bed interaction is prescribed as vertical spring loads on the interacting nodes. Numerical solution to the equation of motion is sought through a finite-difference method. The initial conditions are determined using the *catenary theory*, the instantaneous boundary conditions are prescribed, and the in-elasticity of the mooring segments is specified as the constraint equation. The solution procedure is then implemented as both *Python* and *Modelica* code. Results of the *Modelica* simulation are then compared with those generated using the popular ocean-engineering software, *Orcaflex*. Finally, conclusions are drawn based on the analysis of simulation results. The codes and results are made available for download.

INTRODUCTION

The authors discuss the development of *Modelica* component-models to simulate the hydrodynamic response of a moored cylindrical buoy in [1]. The mooring forces in [1] are based on the *quasi-static* catenary and hence does not account for the inertia and deflection effects of the mooring line. The present paper is based on the work done towards implementing the lumped-mass approach to simulate the dynamics of the mooring line in order to mitigate the above deficiencies of the *quasi-static* approach.

The earliest traceable work in this direction is by Walton *et al.* [2], where a simple finite-difference based solution procedure for the system of non-linear partial differential equations governing the transient motion of a cable immersed in a fluid is discussed in detail, without considering the sea-bed interference effects. Nakajima *et al.* [3] improves upon this method by implementing the *Houbolt* finite-difference equations. The sea-bed interaction in this case is prescribed by weight-corrections to the lumped-mass nodes nearest to the sea-floor. Khan *et al.* [4] used the Lagrange's modified equation to arrive at the equation of motion for a mass-discretized mooring line where the Gauss–Jordon method is used to solve for accelerations and Runge–Kutta calculation by Gill's method is used to solve for positions and velocities, with sea-bed interactions disregarded. Ghadimi [5] presents an algorithm for the dynamic analysis of flexible marine risers where the equations of motions of a lumped-mass mathematical model of the riser is solved in time domain using the tangent stiffness incremental approach combined with the Wilson-theta numerical integration algorithm. A simple model of the sea-bed contact for catenary risers is also presented in the above work. Thomas *et al.* [6] presents a lumped-mass model of a deep-water mooring line that accounts for both friction and suction effects together with the lifting and grounding of nodes.

*Corresponding author.

The primary aim of this study being the assessment of the suitability of the lumped-mass approach for simulation in *Modelica* and subsequent implementation as a component-model, we restrict ourselves to the simplest model described in [2], coupled with modifications to account for the sea-bed interaction following the concept presented in [5].

The theory behind the finite difference solution of the non-linear equations of motion of the mass-discretized mooring catenary is discussed briefly, followed by the summary of the solution procedure as suggested in [2]. Modifications to include the effects of upward forces on the nodes in the vicinity of the sea-floor, in accordance to the outline given in [5], is incorporated into the equations of motion to simulate the vertical sea-bed reaction forces . This is followed by a description of the procedure adopted to discretize the catenary into straight cylindrical segments of specified length based on the *catenary theory*. Such a discretization is required to arrive at the nodal masses and external loads to be specified at such nodes. The initial spatial configuration of the mooring line, which is required to initiate the numerical solution, is also obtained from this step. An algorithm for the complete solution procedure is then formulated and implemented initially in *Python*, keeping in mind the ease of use and ability to obtain interim results for error checking. After successful implementation in *Python*, an *OpenModelica* code is developed.

The outputs of the simulation are then presented in a step-by-step manner to correlate with the algorithm and thus provide the reader with a better understanding of the lumped-mass approach in general. The simulation results are benchmarked with those obtained using the popular time-domain ocean-engineering software *Orcaflex*, and conclusions drawn.

Both the *Python* as well as *Modelica* codes along with *Orcaflex* simulation files are made available for download at github.com/Savin-Viswanathan/OMAE2020.

THEORY

The problem and our assumptions

Walton *et al.* [2] states the problem abstractly as: "Given the initial conditions (i.e., position and velocity at any time t_0) and boundary conditions (positions of end points at all times) of a cable immersed in fluid, determine its subsequent motions."

For the sake of simplicity, we consider a homogeneous, two-dimensional, fully submerged catenary mooring. The anchor point is assumed fixed while motions of the top end may be prescribed. The forces considered in this analysis are as illustrated in Fig. 1a and comprises of: a) damping or drag due to relative motion between the mooring line and the fluid, b) inertial reaction (added-mass) of the surrounding fluid, c) weight of the mooring, d) buoyancy, e) upward force exerted on the grounded portion of the mooring by the sea floor, and f) the tension in the mooring line.

Spatial discretization simplifies the process of the formulation of the equations of motion. Hence, the continuous shape of the catenary is approximated by the use of straight segments, and the mass of each segment is equally distributed to the end nodes of that segment. The discretized mooring line is now represented by point masses m_j [kg] connected by massless segments of length $l_{j\pm\frac{1}{2}}$ [m] as shown in Fig. 1b. In a similar line, the external forces viz. added-mass loads, drag, buoyancy, and reaction forces on grounded segments are also distributed to the end nodes.

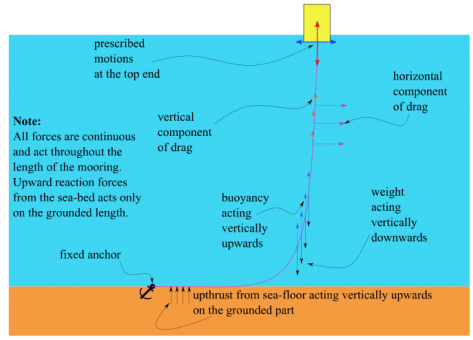

(a) Continuous catenary

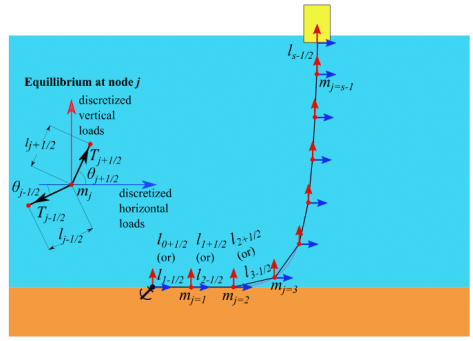

(b) Discretized catenary

FIGURE 1. DISCRETIZATION OF THE CATENARY.

Knowing the masses and external loads, the equations of motion for the system can be formulated, with the inextensibility of the mooring segments constituting the constraint equation.The initial nodal positions can be determined using catenary theory.

The initial nodal velocities and accelerations are assumed to be zero. The instantaneous boundary conditions are obtained from the fixed condition of the anchor point and prescribed motions of the top end. The motion of the top end may alternatively be determined from the equation of motions of the floater to which it is attached.

Formulation of the equations of motion

The following may be deduced from the discretized catenary shown in Fig. 1b. For details, see [2].

$$m_j = \frac{\mu}{2}[l_{j+\frac{1}{2}} + l_{j-\frac{1}{2}}] \tag{1}$$

$$e_{j+\frac{1}{2}} = \rho k l_{j+\frac{1}{2}} \sigma \tag{2}$$

$$\cos\theta_{j+\frac{1}{2}} = (x_{j+1} - x_j)/l_{j+\frac{1}{2}} \tag{3}$$

$$\sin\theta_{j+\frac{1}{2}} = (z_{j+1} - z_j)/l_{j+\frac{1}{2}} \tag{4}$$

Here m_j [kg] is the mass of node j joining segments of length $l_{j-\frac{1}{2}}$ and $l_{j+\frac{1}{2}}$ [m], where the $\mp\frac{1}{2}$ represents the preceding and succeeding segments of node j respectively. Thus, $e_{j+\frac{1}{2}}$ [kg] is the added mass of the succeeding segment and $\theta_{j+\frac{1}{2}}$ [rad] is the angle made by the succeeding segment with the horizontal. μ [kg/m] is the dry specific mass of the mooring chain, ρ [kg/m^3] is the density of the surrounding fluid, k [-] is the added-mass coefficient, and σ [m^2] is the cross-sectional area of the mooring.

The equations of motion for the j^{th} node can be expressed as

$$I_j\ddot{x}_j - K_j\ddot{z}_j = T_{j+\frac{1}{2}}\cos\theta_{j+\frac{1}{2}} - T_{j-\frac{1}{2}}\cos\theta_{j-\frac{1}{2}} + X_j \tag{5}$$

$$-K_j\ddot{x}_j + J_j\ddot{z}_j = T_{j+\frac{1}{2}}\sin\theta_{j+\frac{1}{2}} - T_{j-\frac{1}{2}}\sin\theta_{j-\frac{1}{2}} + Z_j \tag{6}$$

Here, x_j and z_j [m] are the instantaneous x and z co-ordinates of the node, $T_{j+\frac{1}{2}}$ and $T_{j-\frac{1}{2}}$ [N] are tensions in the segments succeeding and preceding node j respectively, and X_j and Z_j [N] are the horizontal and vertical components of the resultant external forces on node j.

I, J, and K are defined as

$$I_j = m_j + \frac{1}{2}(e_{j+\frac{1}{2}}\sin^2\theta_{j+\frac{1}{2}} + e_{j-\frac{1}{2}}\sin^2\theta_{j-\frac{1}{2}}) \tag{7}$$

$$J_j = m_j + \frac{1}{2}(e_{j+\frac{1}{2}}\cos^2\theta_{j+\frac{1}{2}} + e_{j-\frac{1}{2}}\cos^2\theta_{j-\frac{1}{2}}) \tag{8}$$

$$K_j = \frac{1}{2}(e_{j+\frac{1}{2}}\sin\theta_{j+\frac{1}{2}}\cos\theta_{j+\frac{1}{2}} + e_{j-\frac{1}{2}}\sin\theta_{j-\frac{1}{2}}\cos\theta_{j-\frac{1}{2}}) \tag{9}$$

X_j and Z_j are expressed as

$$X_j = -\frac{1}{2}[D_{j+\frac{1}{2}}\sin\theta_{j+\frac{1}{2}} + D_{j-\frac{1}{2}}\sin\theta_{j-\frac{1}{2}}] \tag{10}$$

$$Z_j = \frac{1}{2}[D_{j+\frac{1}{2}}\cos\theta_{j+\frac{1}{2}} + D_{j-\frac{1}{2}}\cos\theta_{j-\frac{1}{2}}] - W_j + F_j^u \tag{11}$$

Here, $D_{j+\frac{1}{2}}$ and $D_{j-\frac{1}{2}}$ [N] refers to the drag in the succeeding and preceding segments of node j respectively, while W_j [N] is the buoyancy adjusted weight at the node, and F_j^u [N] represents an upward force to account for the sea-bed reaction on the grounded nodes. These are expressed as:

$$D_{j+\frac{1}{2}} = -f^D_{j+\frac{1}{2}} q_{j+\frac{1}{2}} |q_{j+\frac{1}{2}}| \tag{12}$$

$$\text{where } f^D_{j+\frac{1}{2}} = \frac{1}{2}\rho C_D l_{j+\frac{1}{2}} D_H \tag{13}$$

$$\begin{aligned}\text{and } q_{j+\frac{1}{2}} = &-\frac{1}{2}[(\dot{x}_{j+1} - c_j) + (\dot{x}_j - c_j)]\sin\theta_{j+\frac{1}{2}} \\ &+ \frac{1}{2}[\dot{z}_{j+1} + \dot{z}_j]\cos\theta_{j+\frac{1}{2}}\end{aligned} \tag{14}$$

$$\text{also, } W_j = m_j g - \frac{1}{2}\rho g(l_{j+\frac{1}{2}} + l_{j-\frac{1}{2}})\sigma \tag{15}$$

Here, D_H [m] is the hydraulic diameter of the mooring, C_D [-] is the drag coefficient, and c_j [m/s] is the current velocity at node j.

When a node grounds/lifts-off to/from the sea-floor, neglecting friction effects, there is an instantaneous manifestation/disappearance of a vertical reaction force, equal and opposite to the forces acting vertically downwards at the node. A sudden application/removal of such upthrust forces may cause numerical instabilities and hence a ramping function of the form

$$F_j^u = \frac{W_j}{2}[1 - tanh(\beta z_j + \eta)] \tag{16}$$

is used to gradually apply/remove the loads. Here, β and η are found by imposing some conditions such as $F_j^u = W_j$ at $z_j = -d$ and $F_j^u = 0.05W_j$ at $z_j = -m_{Fu}d$, the depth at which nodal upthurst becomes 5% of nodal weight. For details see [5].

The inclusion of F_j^u which allows for the consideration of the sea-bed reaction, is a modification introduced into the equations given in [2].

The inextensibility condition of the mooring segments may be represented mathematically as

$$(x_j - x_{j-1})^2 + (z_j - z_{j-1})^2 = l^2_{j-\frac{1}{2}} \tag{17}$$

The boundary conditions are given by

$$x_0(t) = x_0(t_0) \tag{18}$$
$$z_0(t) = z_0(t_0) \tag{19}$$
$$x_s(t) = \text{prescribed} \tag{20}$$
$$z_s(t) = \text{prescribed} \tag{21}$$

And the initial conditions by

$$x_j(0) = x_j^0 \tag{22}$$
$$z_j(0) = z_j^0 \tag{23}$$

Thus, in summary, the equations governing the motion of the mooring line is given by Eqns. (5) and (6), with the constraint equation given by Eqn. 17, subject to the boundary conditions given by Eqns. (18)–(21), and with initial conditions given by Eqns. (22) and (23).

Numerical solution to the equations of motion

A detailed description of the numerical solution can be found in [2], where the following finite-difference equivalents are used

$$\dot{x}_j^{n+\frac{1}{2}} = \frac{x_j^{n+1} - x_j^n}{\Delta t}, \qquad \dot{z}_j^{n+\frac{1}{2}} = \frac{z_j^{n+1} - x_j^n}{\Delta t} \tag{24}$$
$$\ddot{x}_j^n = \frac{x_j^{n+1} - 2x_j^n + x_j^{n-1}}{(\Delta t)^2}, \qquad \ddot{z}_j^n = \frac{z_j^{n+1} - 2z_j^n + z_j^{n-1}}{(\Delta t)^2} \tag{25}$$

Here n is the current time step. $n+\frac{1}{2}$ represents the middle of the next time step.

A brief summary of the method of solution given in [2] follows.

1. Designate

$$L_j = (\Delta t)^2 I_j/(I_j J_j - K_j^2) \tag{26}$$
$$M_j = (\Delta t)^2 J_j/(I_j J_j - K_j^2) \tag{27}$$
$$N_j = (\Delta t)^2 K_j/(I_j J_j - K_j^2) \tag{28}$$

$$P_j = M_j \cos\theta_{j-\frac{1}{2}} + N_j \sin\theta_{j-\frac{1}{2}} \tag{29}$$
$$Q_j = N_j \cos\theta_{j-\frac{1}{2}} + L_j \sin\theta_{j-\frac{1}{2}} \tag{30}$$
$$R_j = M_j \cos\theta_{j+\frac{1}{2}} + N_j \sin\theta_{j+\frac{1}{2}} \tag{31}$$
$$S_j = N_j \cos\theta_{j+\frac{1}{2}} + L_j \sin\theta_{j+\frac{1}{2}} \tag{32}$$

$$U_j = M_j X_j + N_j Y_j \tag{33}$$
$$V_j = N_j X_j + L_j Y_j \tag{34}$$

$$E^n_{j-\frac{1}{2}} = (x_j^n - x_{j-1}^n)P_{j-1}^n + (y_j^n - y_{j-1}^n)Q_{j-1}^n \tag{35}$$
$$F^n_{j-\frac{1}{2}} = (x_j^n - x_{j-1}^n)(P_j^n + R_{j-1}^n) + (y_j^n - y_{j-1}^n)(Q_j^n + S_{j-1}^n) \tag{36}$$
$$G^n_{j-\frac{1}{2}} = (x_j^n - x_{j-1}^n)R_j^n + (y_j^n - y_{j-1}^n)S_j^n \tag{37}$$
$$H^n_{j-\frac{1}{2}} = (x_j^n - x_{j-1}^n)(U_j^n - U_{j-1}^n) + (y_j^n - y_{j-1}^n)(V_j^n + V_{j-1}^n) \tag{38}$$

with, $E^n_{1-\frac{1}{2}} = G^n_{s-\frac{1}{2}} = 0$; $P_0^n = Q_0^n = R_0^n = S_0^n = 0$; $P_s^n = Q_s^n = R_s^n = S_s^n = 0$; $U_0^n = 0, U_s^n = (\Delta t)^2 \ddot{x}_s^n$; $V_0^n = 0, V_s^n = (\Delta t)^2 \ddot{z}_s^n$, for all n.

2. Determine the tentative tension in the first segment using relation

$$\tilde{T}^n_{1-\frac{1}{2}} = -\frac{\left(F^n_{s-\frac{1}{2}}\beta^n_{s-\frac{1}{2}} - E^n_{s-\frac{1}{2}}\beta^n_{s-\frac{3}{2}} - \psi^n_{s-\frac{1}{2}}\right)}{F^n_{s-\frac{1}{2}}\alpha^n_{s-\frac{1}{2}} - E^n_{s-\frac{1}{2}}\alpha^n_{s-\frac{3}{2}}} \tag{39}$$

Where, for $n > 0$,

$$\psi^n_{j-\frac{1}{2}} = E^{n-1}_{j-\frac{1}{2}}T^{n-1}_{j-\frac{3}{2}} - F^{n-1}_{j-\frac{1}{2}}T^{n-1}_{j-\frac{1}{2}} + G^{n-1}_{j-\frac{1}{2}}T^{n-1}_{j+\frac{1}{2}} + H^{n-1}_{j-\frac{1}{2}} + H^n_{j-\frac{1}{2}} \tag{40}$$

while for $n = 0$,

$$\psi^n_{j-\frac{1}{2}} = H^n_{j-\frac{1}{2}} \tag{41}$$

The recursion formulae of α and β being given as

$$\alpha^n_{j+\frac{1}{2}} = \left(F^n_{j-\frac{1}{2}}\alpha^n_{j-\frac{1}{2}} - E^n_{j-\frac{1}{2}}\alpha^n_{j-\frac{3}{2}}\right)/G^n_{j-\frac{1}{2}} \tag{42}$$
$$\beta^n_{j+\frac{1}{2}} = \left(F^n_{j-\frac{1}{2}}\beta^n_{j-\frac{1}{2}} - E^n_{j-\frac{1}{2}}\beta^n_{j-\frac{3}{2}} - \psi^n_{j-\frac{1}{2}}\right)/G^n_{j-\frac{1}{2}} \tag{43}$$

with the conditions

$$\alpha^n_{1-\frac{1}{2}} = 1 \qquad \alpha^n_{1-\frac{3}{2}} = 0 \qquad \text{for all } n \tag{44}$$
$$\beta^n_{1-\frac{1}{2}} = 0 \qquad \beta^n_{1-\frac{3}{2}} = 0 \qquad \text{for all } n \tag{45}$$

3. Determine the tentative values of tensions in the remaining segments using the relation

$$\tilde{T}^n_{j+\frac{1}{2}} = \alpha^n_{j+\frac{1}{2}} \tilde{T}^n_{1-\frac{1}{2}} + \beta^n_{j+\frac{1}{2}} \tag{46}$$

4. Predict the tentative co-ordinates of the next time step based on tentative tensions calculated above using:

   For the initial time step i.e., $n = 0$,

$$\tilde{x}^{0+1}_j = x^0_j + \frac{1}{2}\left[-P^0_j \tilde{T}^0_{j-\frac{1}{2}} + R^0_j \tilde{T}^0_{j+\frac{1}{2}} + U^0_j\right] \tag{47}$$

$$\tilde{z}^{0+1}_j = z^0_j + \frac{1}{2}\left[-Q^0_j \tilde{T}^0_{j-\frac{1}{2}} + S^0_j \tilde{T}^0_{j+\frac{1}{2}} + V^0_j\right] \tag{48}$$

   for all other time steps i.e., $n > 0$,

$$\tilde{x}^{n+1}_j = 2x^n_j - x^{n-1}_j - P^n_j \tilde{T}^n_{j-\frac{1}{2}} + R^n_j \tilde{T}^n_{j+\frac{1}{2}} + U^n_j \tag{49}$$

$$\tilde{z}^{n+1}_j = 2z^n_j - z^{n-1}_j - Q^n_j \tilde{T}^n_{j-\frac{1}{2}} + S^n_j \tilde{T}^n_{j+\frac{1}{2}} + V^n_j \tag{50}$$

5. Define a function to measure the discrepancy in the distance between extrapolated positions of pairs of adjacent nodes and the original initial length of the segment between these nodes as

$$\Omega^{n+1}_{j-\frac{1}{2}} = \frac{1}{2}\left[\left(\tilde{x}^{n+1}_j - \tilde{x}^{n+1}_{j-1}\right)^2 + \left(\tilde{z}^{n+1}_j - \tilde{z}^{n+1}_{j-1}\right)^2 - l^2_{j-\frac{1}{2}}\right] \tag{51}$$

6. Calculate the correction to be added to the previously calculated tentative tension value of the first segment as

$$\delta T^n_{1-\frac{1}{2}} = -\frac{\left(\tilde{F}^{n+1}_{s-\frac{1}{2}} \lambda^n_{s-\frac{1}{2}} - \tilde{E}^{n+1}_{s-\frac{1}{2}} \lambda^n_{s-\frac{3}{2}} - \Omega^{n+1}_{s-\frac{1}{2}}\right)}{\tilde{F}^{n+1}_{s-\frac{1}{2}} \kappa^n_{s-\frac{1}{2}} - \tilde{E}^{n+1}_{s-\frac{1}{2}} \kappa^n_{s-\frac{3}{2}}} \tag{52}$$

   where,

$$\tilde{E}^{n+1}_{j-\frac{1}{2}} = (\tilde{x}^{n+1}_j - \tilde{x}^{n+1}_{j-1}) P^n_{j-1} + (\tilde{z}^{n+1}_j - \tilde{z}^{n+1}_{j-1}) Q^n_{j-1} \tag{53}$$

$$\tilde{F}^{n+1}_{j-\frac{1}{2}} = (\tilde{x}^{n+1}_j - \tilde{x}^{n+1}_{j-1})(P^n_j + R^n_{j-1}) + (\tilde{z}^{n+1}_j - \tilde{z}^{n+1}_{j-1})(Q^n_j + S^n_{j-1}) \tag{54}$$

$$\tilde{G}^{n+1}_{j-\frac{1}{2}} = (\tilde{x}^{n+1}_j - \tilde{x}^{n+1}_{j-1}) R^n_j + (\tilde{z}^{n+1}_j - \tilde{z}^{n+1}_{j-1}) S^n_j \tag{55}$$

   with $\tilde{E}^{n+1}_{1-\frac{1}{2}} = \tilde{G}^{n+1}_{s-\frac{1}{2}} = 0$ and P^n_j, Q^n_j, R^n_j, and S^n_j being the same as in *Step 1*.

   The recursion formulae for κ and λ, being

$$\kappa^n_{j+\frac{1}{2}} = \left(\tilde{F}^n_{j-\frac{1}{2}} \kappa^n_{j-\frac{1}{2}} - \tilde{E}^n_{j-\frac{1}{2}} \kappa^n_{j-\frac{3}{2}}\right) / \tilde{G}^n_{j-\frac{1}{2}} \tag{56}$$

$$\lambda^n_{j+\frac{1}{2}} = \left(\tilde{F}^n_{j-\frac{1}{2}} \lambda^n_{j-\frac{1}{2}} - \tilde{E}^n_{j-\frac{1}{2}} \beta^n_{j-\frac{3}{2}} - \psi^n_{j-\frac{1}{2}}\right) / \tilde{G}^n_{j-\frac{1}{2}} \tag{57}$$

   with conditions

$$\kappa^n_{1-\frac{1}{2}} = 1 \qquad \kappa^n_{1-\frac{3}{2}} = 0 \qquad \text{for all } n \tag{58}$$

$$\lambda^n_{1-\frac{1}{2}} = 0 \qquad \lambda^n_{1-\frac{3}{2}} = 0 \qquad \text{for all } n \tag{59}$$

7. Determine the tension corrections for the remaining segments as

$$\delta T^n_{j+\frac{1}{2}} = \kappa^n_{j+\frac{1}{2}} \delta T^n_{1-\frac{1}{2}} + \lambda^n_{j+\frac{1}{2}} \tag{60}$$

8. The corrected tension values are then given as

$$T^n_{j+\frac{1}{2}} = \tilde{T}^n_{j+\frac{1}{2}} + \delta T^n_{j+\frac{1}{2}} \tag{61}$$

9. Using the updated tensions, recalculate $\tilde{x}^{n+1}_j$ and $\tilde{z}^{n+1}_j$ and check whether $\Omega^{n+1}_{j-\frac{1}{2}}$ is within a specified tolerance limit, else repeat steps 6 to 9 until the condition is satisfied, updating the tension value for each loop traversal.
10. The values of tensions prevailing when the tolerance condition is satisfied gives $T^n_{j+\frac{1}{2}}$. The improved co-ordinates are then calculated as:

$$x^{n+1}_j = \tilde{x}^{n+1}_j + \delta x^{n+1}_j \tag{62}$$

$$z^{n+1}_j = \tilde{z}^{n+1}_j + \delta z^{n+1}_j \tag{63}$$

    Where, for $n = 0$,

$$\delta x^{n+1}_j = \frac{1}{2}[-P^0_j \delta T^0_{j-\frac{1}{2}} + R^0_j \delta T^0_{j+\frac{1}{2}}] \tag{64}$$

$$\delta z^{n+1}_j = \frac{1}{2}[-Q^0_j \delta T^0_{j-\frac{1}{2}} + S^0_j \delta T^0_{j+\frac{1}{2}}] \tag{65}$$

    and, for $n > 0$,

$$\delta x^{n+1}_j = -P^n_j \delta T^n_{j-\frac{1}{2}} + R^n_j \delta T^n_{j+\frac{1}{2}} \tag{66}$$

$$\delta z^{n+1}_j = -Q^n_j \delta T^n_{j-\frac{1}{2}} + S^n_j \delta T^n_{j+\frac{1}{2}} \tag{67}$$

Initial configuration of the catenary

The formulation of a look up table for T_H Vs. X, where T_H [N] is the horizontal tension and X is the horizontal displacement of the top end of the catenary from the anchor position, as shown in Fig. 2, is described in [1]. Here fixed frame $X-Z$ is the global co-ordinate system with its origin at the mean water level, vertically above the anchor point and translating frame $x-z$ is the catenary co-ordinate system with its origin a [m] below the lowest point of of the catenary, i.e., the touch-down-point. Here a is the catenary parameter.

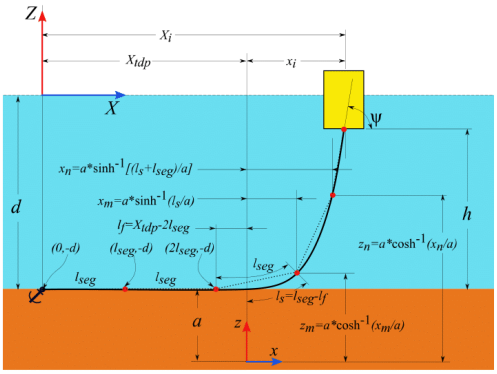

FIGURE 2. THE MOORING HALF-CATENARY.

From such a table, the horizontal tension T_H for a specified initial position X_i of the top end of the catenary can be interpolated. The initial configuration of the catenary may then be determined as follows

1. The X co-ordinate of the touch-down point may be determined from the relation

$$X_{tdp} = X_i - x_i \tag{68}$$

2. For the part of the mooring lying on the sea-floor, the X co-ordinate of the nodes is incremented by the specified fixed segment lengths, while the Z co-ordinate equals the water depth. i.e., for the 0^{th} node (anchor point), the co-ordinates are $(0*l_{seg}, -d)$, for the first node $(1*l_{seg}, -d)$, for the second node $(2*l_{seg}, -d)$ and so on for all nodes that lie between the anchor point and the touch-down point.
3. For the segment lying with its left node on the ground and the right node suspended, the length of the part of the segment on the floor l_f [m] is the difference between the X co-ordinate of the touch down point and the X co-ordinate of its left node. The suspended length l_s [m] of that segment is then obtained by subtracting the length of the floored part of the segment from the whole length of the segment. The suspended length corresponding to the second node above the sea-floor, is determined by adding the partial suspended length of the previous segment to the length of the current segment, and so on and so forth for all the remaining suspended segments.
4. The X and Z co-ordinates of a point which corresponds to a suspended length of l_s [m] may be determined from the relations

$$x = a * \sinh^{-1}\left(\frac{l_s}{a}\right) \tag{69}$$

$$a = \frac{T_H}{w} \tag{70}$$

$$X = X_{tdp} + x \tag{71}$$

$$z = a * \cosh^{-1}\left(\frac{x}{a}\right) \tag{72}$$

$$Z = -d + z - a \tag{73}$$

Here, w [N/m] is the known wet specific weight of the catenary.

5. The X and Z coordinates of all nodes that lie at equal curvilinear lengths of l_{seg} are thus determined. These nodes are then joined with straight line segments to discretize the catenary.

At regions of high curvature, the straight segments are shorter than the curvilinear lengths as shown in Fig. 2. However, this variation is infinitesimal for appropriately chosen segment lengths.

PYTHON IMPLEMENTATION

The flexibility of *Python* makes it a suitable test platform to build the code for implementing the numerical solution procedure described above. The code is accessible through the download link provided earlier. The parameters are entered in the main program **Walton_Catenary_v0.py**. The main program calls *function* **catcon_0** to determine the initial spatial configuration of the catenary. This initial configuration is passed on as arguments to the *function* **ten_0** that returns the link tensions for the initial configuration as well as parameters required for calculations in the subsequent time steps. The output of **ten_0** is passed on to the *function* **ten** and the outputs of the **ten** function is looped until the specified simulation time. The python implementation closely follows the algorithm depicted in Fig. 3b. The major difference being that both **catThIterator** and **catX-Iterator** *Modelica* function capabilities are integrated into the **catcon_0** function in *Python*. Other details are easily discernible from the python code available at the download link.

OPENMODELICA IMPLEMENTATION

In the ideal case, the implementation in *Modelica* would have been as a *model* enabling the interfacing of the mooring model with component-models for waves, current, and floating objects as described in [1]. However, it is currently not possible to implement the solution procedure as a Modelica *model* and hence it is implemented as a Modelica *function* to demonstrate the lumped-mass method of solution of the mooring catenary and obtain results for benchmarking.

Since only *models* or *blocks* can be simulated in Modelica, a *pseudo-model* that calls the *function* **mainWaltonCatenary** is coded. Here, *pseudo* refers to the fact that the *model* is not an actual dynamic model, but is only a means of running the code inside a function where *time* is specified as a variable. The flowchart of the *pseudo-model* is shown in Fig. 3a.

The water depth d [m], water density ρ_w [kg/m^3], fully developed uniform current velocity in the x-direction C^x_{max} [m/s], curvilinear lengths of the segments of the mooring used in discretization seg_l [m], number of segments n_{seg}, initial horizontal position of the top end of the mooring line in the global $X-Z$ frame X_i [m], initial vertical position of the top end of the mooring from the sea-floor h [m], the diameter of the wire of the mooring chain d_w [m], coefficient of drag of the mooring c_d [-], density of the mooring material ρ_{mat} [kg/m^3], specific dry linear mass of the mooring spm_{dry} [kg/m], percentage of water depth at which upthrust from the sea-floor becomes 5% of the weight of the node m_{Fu} [-], the coefficient of added mass of the mooring k_j [-], the fixed time interval for calculating the numerical solution dt [s], the total simulation time T_{sim} [s], the ramp time for current velocity T_{rmp}, the move time for to top end of the mooring T_{mov}, and the horizontal acceleration of the top end a_x [m/s^2], are specified as simulation parameters inside the **mainWaltonCatenary** function . x^0_j, z^0_j, are *vectors* containing initial nodal coordinates in the $X-Z$ frame, and l^0_j is the *vector* containing the initial straight segment lengths of the discretized catenary. Ten^0 and Ten^c are *vectors* containing initial and final link tensions.

Flowchart of **mainWaltonCatenary** is depicted in Fig. 3b. The *functions* **catThIterator** and **catXIterator** returns *vectors* of horizontal tensions T_H, and top end positions X, as discussed in [1]. The function **initCatShape** uses the catenary theory described earlier to determine the initial spatial configuration of the catenary. The *function* **initialTensions** makes use of the numerical solution procedure discussed earlier to calculate the initial tensions in the line segments along with values for co-ordinate positions and velocities for the next time-step as well as accelerations of the current time step. It also returns E, F, G and H values for the current time step which will be required in calculating the ψ values for the next time step by the **tensions** *function*. The values returned by the **tensions** function are looped until the specified T_{sim} is reached. Details of these *functions* are discernible from the *Modelica* code available at the download

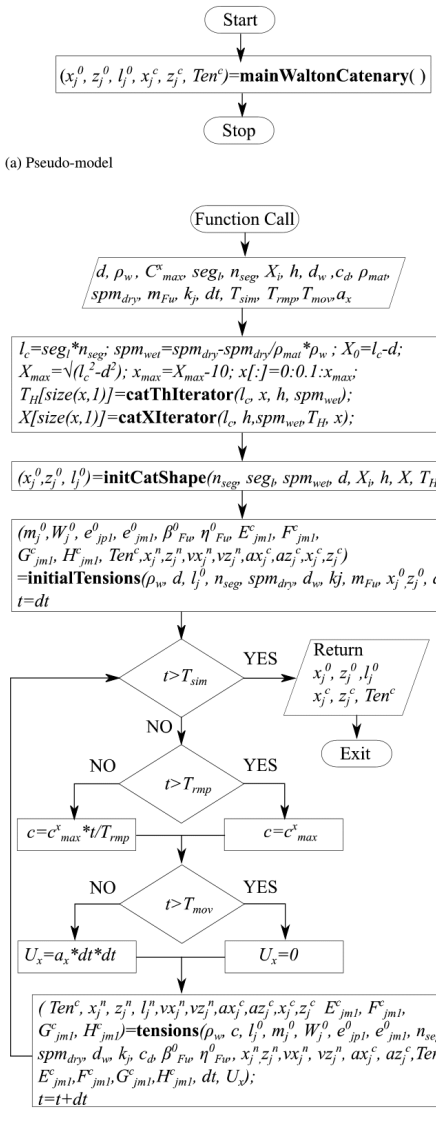

FIGURE 3. IMPLEMENTATION FLOW CHART

link.

For easy cor-relation between the flow chart, the code, and theory, m_j^0 [kg] is the discretized mass acting on node j. W_j^0 [N] is the nodal weight, e_{jm1}^0 and e_{jp1}^0 corresponds to $e_{j+\frac{1}{2}}$ and $e_{j-\frac{1}{2}}$, the added mass of the preceding and succeeding segments of node j respectively, as described in the *theory* section. β_{Fu}^0 and η_{Fu}^0 corresponds to β and η of the *theory* section. The superscript '0' indicating that such values are evaluated at the initial time step and remain unchanged for the rest of the simulation. E_{jm1}^c, F_{jm1}^c, G_{jm1}^c, and H_{jm1}^c correspond to $E_{j-\frac{1}{2}}^n$, $F_{j-\frac{1}{2}}^n$, $G_{j-\frac{1}{2}}^n$, and $H_{j-\frac{1}{2}}^n$ of the *theory* section. $Tenc^c$ corresponds to $T_{j+\frac{1}{2}}^n$ of the *theory*. ax_j^c and az_j^c correspond to $\ddot{x}_j^n$ and $\ddot{z}_j^n$ of the *theory*. Superscript c indicates that these values are for the current time step. x_j^n, z_j^n, vx_j^n, and vz_j^n correspond to x_j^{n+1} and z_j^{n+1}, $\dot{x}_j^{n+\frac{1}{2}}$, $\dot{z}_j^{n+\frac{1}{2}}$ of the *theory* respectively. The superscript n indicating that these are predicted values for the next time step.

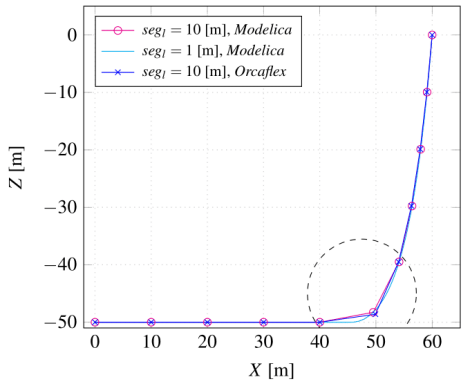

FIGURE 4. DISCRETIZATION OF THE MOORING LINE

RESULTS

We discuss the results of a mooring chain of dry specific mass 10 [kg/m] with wire diameter 22 [mm], in a water depth of 50 [m]. Where possible, we compare the results to a similar mooring line modelled in *Orcaflex*. Both *Python* and *Modelica* codes are based on the same algorithm and hence the results are similar. To avoid congestion, only *Modelica* and *Orcaflex* results are presented.

The buoyancy calculation in this work is based on the spm_{wet} calculation given in Fig. 3b. To get an approximately similar buoyancy effect, the buoyancy diameter is specified as 50 [mm] in *Orcaflex*. The drag diameters in both *Modelica* and *Orcaflex* being $D_H = 1.8d_w = 40$ [mm].

Figure 4 shows the *discretized* shape based on different segment lengths, seg_l. The configuration of a similar line modelled in *Orcaflex* is also shown. It is evident that reducing seg_l improves the shape approximation of the catenary. In regions of high curvature, the straight discretized length is smaller than the curvilinear length, as observed inside the bounding circle. Proper selection of seg_l minimizes this discrepancy and the subsequent impact on the nodal forces.

Response of the line to currents of uniform magnitude across the depth of the water-column are shown in Fig. 5a. Time history of the tensions on the top-most link is shown in Fig. 5b. $T_{rmp} = 10$ [s] in all cases.

It is observed that the *Modelica* and *Orcaflex* results for the nodal positions are in close agreement. However, the time history of the top-link tensions brings out the fluctuations in the tensions in the *Modelica* model. At this point, it is believed that this fluctuation is attributable to the simple finite difference scheme employed in the present work. At higher current velocities, the slight hump in the tension history, as observed inside the bounding circle of Fig. 5b, is deduced to be the effect of the line inertia. This deduction is based on the fact that the hump occurs immediately after $t = 10$ [s], at the end of the ramp time T_{rmp}.

By specifying values for U_s and V_s in Eqns. (33) and (34), we can specify horizontal and vertical displacements of the top end of the mooring in the *Modelica*/*Python* model. By attaching the mooring line to a *vessel* object and specifying prescribed motion for the *vessel*, we can imitate the same in *Orcaflex*. Fig. 6 compares the top link tensions as the mooring top end moves from $X = 55$ [m] to $X = 78.9$ [m] with a constant acceleration of 0.4 [m/s^2] in both *Modelica* and *Orcaflex*.

As in the earlier case, the *Modelica* and *Orcaflex* nodal positions are in good agreement, while the *Modelica* link tensions, though in general agreement with the *Orcaflex* results, exhibit fluctuations.

A wave is considered a *shallow-water* wave when $kd < \frac{\pi}{10}$, where k [m^{-1}] is the wave number and d [m] is the water depth. Shallow water waves have a constant horizontal water particle velocity across the depth of the water column. The maximum horizontal water particle velocity of a linear wave is given as $\frac{\pi H}{T}$ where H [m] is the wave height and T [s] is the wave period. For details, see pp. 79–83 of [7]. Therefore, if we specify a wave of height 7.96 [m] and period 25 [s], then the horizontal water particle velocities can be approximated as a uniform current of magnitude $\cos(0.251t)$ where t [s] is the simulation time.

Figure 7b shows the time history of the top-link tension of a mooring with $X = 70$ [m], as shown in Fig. 7a, when subject to a uniform current whose magnitude varies as $\cos(0.251t)$ in *Modelica*, while the *Orcaflex* tensions are for a mooring subjected to the above described wave. We observe fluctuation in the line tensions in *Orcaflex* also, albeit at a lower level than exhibited by *Modelica*. This further strengthens our earlier belief that the tension fluctuations are an effect of the numerical approximations.

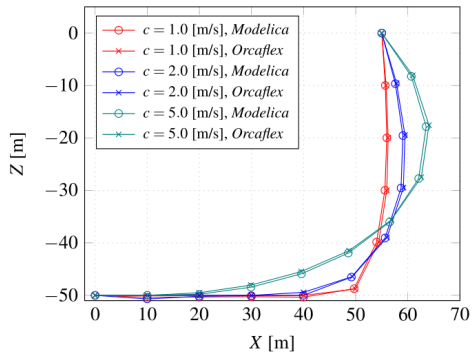

(a) Configurations.

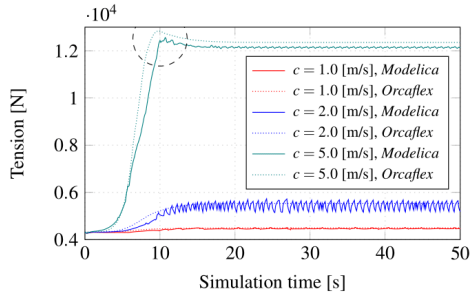

(b) Top-link Tensions.

FIGURE 5. MOORING RESPONSE TO UNIFORM CURRENT

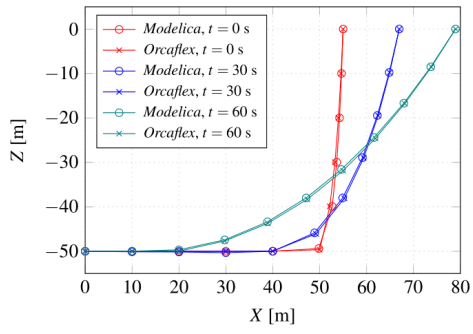

(a) Configuration.

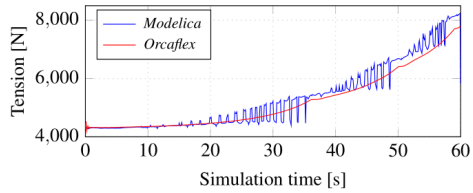

(b) Top-link Tensions.

FIGURE 6. MOORING RESPONSE TO TOP-END MOTION

Further, it is observed that the tension range is higher in the *Orcaflex* model. This is thought to be the effect of the drag induced by the vertical water particle velocities due the wave motion in *Orcaflex*, which is absent in the *Modelica* model.

Fig. 7c and 7d compares the vertical motions of nodes $j = 4$ and $j = 3$ as indicated in Fig. 7a. We observe that node $j = 3$ stays on the sea-floor in the *Orcaflex* model, while in the *Modelica* model, the specification of a gradually applied vertical load in accordance to Eqn. (16) causes the node to oscillate in response to the dynamic vertical loads.

CONCLUSION

The result comparison indicates satisfactory agreement of nodal positions between the present algorithm and *Orcaflex*. The tensions given by the present implementation, on the other hand, are observed to fluctuate considerably. Positional fluctuations are also observed to be higher in the grounded nodes of the present algorithm. Tension fluctuations were also observed in the *Orcaflex* mooring when subjected to oscillatory flow. This leads us to deduce that these tension fluctuations are the consequence of the numerical approximations employed in solving the equations of motion. There might also be possible influences from the motions of the node at the touch-down point which is higher in the present algorithm compared to the *Orcaflex* model.

It may also be noted that the present algorithm considers only the drag part of the Morison equation. If the inertia part also were to be considered, it is to be noted that since the accelerations of the next time-step cannot be approximated in the present numerical scheme, such calculations would have to be based on nodal accelerations of the previous time-step. However, if the *Houbolt* method is employed, the nodal accelerations of the next time step can also be approximated [3], thus enabling calculations based on nodal accelerations of the current time step.

Drag calculations in the present algorithm considers a common normal and tangential drag coefficient. It has been noted that calculating the fluid loads in the local axis system of the segment using appropriate normal and tangential drag coefficients and transforming it to the global co-ordinate system as discussed in [3] and [6], and referred to as the *cross-flow* principle in [8], gives better results.

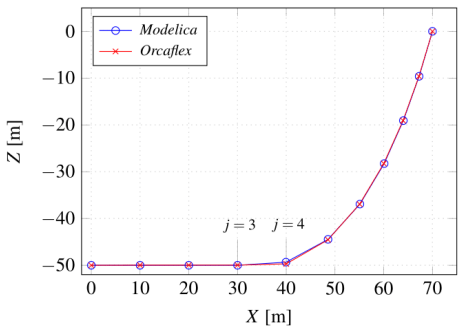

(a) Initial Configuration.

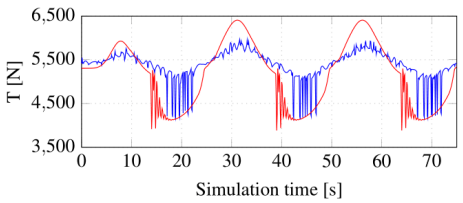

(b) Top-link Tensions.

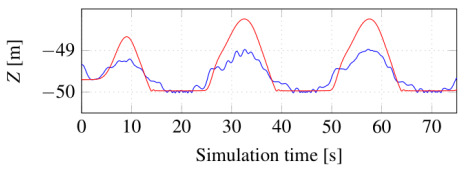

(c) Vertical motions of node $j = 4$.

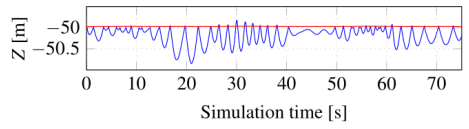

(d) Vertical motions of node $j = 3$.

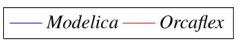

FIGURE 7. MOORING RESPONSE TO OSCILLATORY FLOW.

The main objective of this work being the assessment of the possibilities of developing a *Modelica* component-model for the mooring catenary based on the lumped mass approach, it is observed that this is presently not possible. The reasons preventing the implementation as a *Modelica* component-model, which require a considerable amount of space for demonstration, will be dealt with in a future work and solutions sought.

ACKNOWLEDGEMENT

The research in this paper has received funding from the Research Council of Norway, SFI Offshore Mechatronics, project number 90034210.

REFERENCES

[1] Viswanathan, Savin and Holden, Christian. "Towards the Development of an Ocean Engineering Library for OpenModelica." *Proceedings of the ASME 2019 38th International Conference on Ocean, Offshore and Arctic Engineering*. OMAE2019-95054. Glasgow, Scotland, June 9-14, 2019. URL doi.org/10.1115/OMAE2019-95054.

[2] Walton, Thomas S. and Polachek, Harry. "Calculation of Transient Motion of Submerged Cables.". *Mathematics of Computation*. VOL. 14 No. 69 (1960): pp. 27–46. URL doi.org/10.1090/S0025-5718-1960-0116470-5.

[3] Nakajima, Toshio, and Motora, Seizo and Fujino, Masataka . "On the Dynamic Analysis of Multi-Component Mooring Lines." *Offshore Technology Conference*. OTC-4309-MS. Houston, Texas, May 3-6, 1982. URL doi.org/10.4043/4309-MS.

[4] Khan, Najeeb Ullah and Ansari, Khyruddin Akbar. "On the Dynamics of a Multicomponent Mooring Line." *Computers & Structures*. VOL. 22 No.3 (1986): pp. 311–334. URL doi.org/10.1016/0045-7949(86)90037-4.

[5] Ghadimi, Rumbod. "A Simple and Efficient Algorithm for the Static and Dynamic Analysis of Flexible Marine Risers." *Computers & Structures*. VOL. 29 No. 4 (1988): pp. 541–555. URL doi.org/10.1016/0045-7949(88)90364-1.

[6] D.O Thomas and G.E. Hearn. "Deepwater Mooring Line Dynamics With Emphasis On Seabed Interference Effects." *Offshore Technology Conference*. 1994. OTC-7488-MS. Houston Texas, May 2–5, 1994. URL doi.org/10.4043/7488-MS.

[7] Dean, Robert G. and Dalrymple, Robert A. *Water Wave Mechanics for Engineers and Scientists*. Allied Publishers Limited, Mumbai (2001). ISBN. 81-7764-195-6.

[8] Orcina. *Orcaflex Manual- Version 9.1a*. Orcina (2010). URL citeseerx.ist.psu.edu/viewdoc/download?doi=10.1.1.121.721&rep=rep1&type=pdf.

5.2 Simulating the dynamics of a chain suspended sub-sea load using modified components from the Modelica MultiBody library

The citation of the published article is given below:

S. Viswanathan and C. Holden. *Simulating the Dynamics of a Chain Suspended Sub-sea Load Using Modified Components from the Modelica MultiBody Library.* Proceedings of Asian Modelica Conference 2020, Tokyo, Japan, October 08-09, 2020. https://doi.org/10.3384/ecp202017459.

The postprint version follows.

Simulating the Dynamics of a Chain Suspended Sub-sea Load Using Modified Components from the Modelica MultiBody Library

Savin Viswanathan[1] Christian Holden[1]

[1]Dept. of Mechanical and Industrial Engineering, Norwegian University of Science and Technology (NTNU), NO-7491 Trondheim, Norway. {savin.viswanathan,christian.holden}@ntnu.no

Abstract

In this paper, the philosophy of the lumped-mass approach is adopted in specifying *components* so as to enable the *Modelica* compiler to formulate equations governing the motion of a chain-suspended sub-sea load, subjected to waves and current. The *discretized* simulation model of the chain-suspended load is built up using the components available in the *MultiBody* library of *OpenModelica*, after making necessary modifications. The combined wave and current loads acting on the segments are determined using the Morison equation, and applied as discrete external forces on the lumped segmental masses. The component model is developed and implemented using the *OMEdit* GUI, and the simulation results are then compared with those for a similar system modelled in the popular commercial ocean-engineering time-domain simulation software, *Orcaflex*, to demonstrate satisfactory agreement. Conclusions are drawn, and the simulation files are made available for public access.

Keywords: Modelica component-model for submerged cables, dynamics of sub-sea loads, OceanEngineering library

1 Introduction

The authors discussed the benefits of developing a *Modelica* standard library for ocean-engineering applications in (Viswanathan and Holden, 2019). In the above work, the *quasi-static* approach was adopted to specify the mooring forces at any given simulation time-step. However, it was noted that this led to the omission of the inertial and deflection effects of the mooring line, as discussed in detail by the authors in (Viswanathan and Holden, 2020a). Hence, steps in the direction of developing component-models capable of simulating the dynamic behaviour of mooring chains, as accurately as possible, were adopted by the authors. The present work, which is an offshoot of such efforts, brings to the *proposed* library, basic components to simulate the dynamics of a fully submerged, suspended sub-sea load.

The earliest reference to the application of the *lumped-mass* approach to sub-sea cables is traced to Walton *et. al* (Walton and Polachek, 1960), who prescribes the lumping of masses of straight segment lengths, and associated external forces, at nodal points which connect the adjoining segments, and thus arrive at equations of motions for the *discretized* mathematical model of the physically *continuous* cable. They further suggest a fixed time-step numerical scheme to obtain the cable dynamics. Other relevant works include (Nakajima et al., 1982), and (Thomas and Hearn, 1994).

We, however, notice that such *time-step* dependent methods are inherently opposed to a fundamental philosophy behind *Modelica*, which is expressed by Dr. Michael Tiller in his words, (Tiller, 2013):

"The key point is that equations describing physical behavior cannot refer to time steps. This is because there is no timestep *in nature or the laws of physics, and so the response of a system cannot depend on it."*

The statement points to the fact that the *Modelica* user needs to specify only the differential algebraic equations governing the physics of the system, and solution methodology is best left to the *Modelica* compiler.

We, therefore, adopt the philosophy of Walton in modelling the cable/chain segments in *Modelica*, using components already available in the *Modelica.Mechanics.MultiBody* library, albeit with necessary modifications. Connecting these components enable the automatic generation of the coupled equations of motion by the *Modelica* compiler, which is then solved for obtaining the system dynamics.

The Morison equation is widely used in the ocean engineering domain to calculate fluid loads on slender structures. Numerous publications deal with the subject, and is described in detail, for e.g., in (Chakrabarti, 1987). In this work, the *Morison* equation is implemented as a *Block*, and the determined fluid drag and inertia loads are then applied as forces, along with buoyancy, at the lumped-mass points.

We, therefore, proceed by presenting a brief theoretical introduction to the *discretization* of the *continuous* cable/chain, along with the calculation of Morison loads. This is followed by a detailed description of system representation in *Modelica*. Simulation results are benchmarked using *Orcaflex*, and conclusions drawn. Both *Modelica* and *Orcaflex* simulation files are made available for public access at github.com/Savin-Viswanathan/Modelica2020Asia.

2 Theory

Figure 1a shows the forces acting on a chain suspended sub-sea load, and Figure 1b shows the discretized mathematical model for the same.

For simplicity, we consider:

- 2D motions in x and y directions only.
- Top end of the chain is fixed.
- Inelastic chain.
- Fully submerged chain and load at all times.
- End load has negligible drag area, and can be approximated as a point mass.

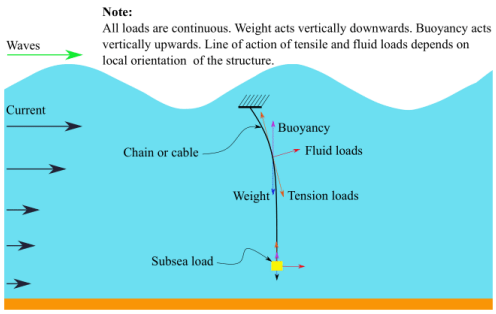

(a) Continuous physical model.

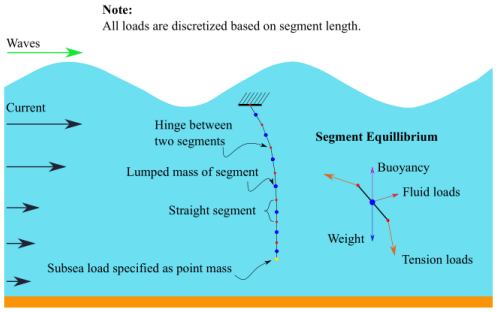

(b) Discretized mathematical model.

Figure 1. Discretization of the chain suspended sub-sea load.

The coupled equations of motion of the chain/cable segments based on the segment equillibrium may then be solved to determine the dynamic behaviour of the system.

Proper translation of the *discretized* model into a *Modelica* system-model effects the automatic generation of the coupled equations of motion governing the dynamic behaviour of the system. Details of modelling are described in detail in the next section.

Considering the j^{th} segment,

$$W_j = l_j \mu g \tag{1}$$

$$B_j = \frac{\pi D_b^2}{4} l_j \rho_w g. \tag{2}$$

Here, W_j [N] is the weight of the segment, B_j [N] is the buoyancy force experienced by the segment, l_j [m] is the length of the segment, μ [kg/m] is the specific linear mass of the chain/cable, D_b [m] is the diameter based on which buoyancy is calculated, ρ_w [kg/m^3] is the density of seawater, and g [m/s^2] is the acceleration due to gravity.

In evaluating the fluid loads, we make use of the Morison equation for combined wave and current loads on an inclined oscillating cylinder. See p. 188 of (Chakrabarti, 1987).

Experimental values for drag coefficient C_D and inertial coefficient C_M are scarce when structures are inclined. Hence, in determining these loads, we evaluate the fluid loads along the normal and tangential directions of the chain segment and then sum up their horizontal and vertical components. The advantage of this approach is that it enables the specification of separate drag (C_D) and inertia (C_M) coefficients for the normal and tangential directions. See p. 205 of (Chakrabarti, 1987). The normal and tangential components of the Morison force per unit length of the segment are thus given as

$$\begin{aligned} M_F^n =& C_M^n \rho \frac{\pi}{4} D^2 a_w^n - C_A^n \rho \frac{\pi}{4} D^2 a_l^n \\ &+ C_D^n \frac{1}{2} \rho D \mid v_w^n \pm U^n - v_l^n \mid (v_w^n \pm U^n - v_l^n). \end{aligned} \tag{3}$$

$$\begin{aligned} M_F^t =& C_M^t \rho \frac{\pi}{4} D^2 a_w^t - C_A^t \rho \frac{\pi}{4} D^2 a_l^t \\ &+ C_D^t \frac{1}{2} \rho D \mid v_w^t \pm U^t - v_l^t \mid (v_w^t \pm U^t - v_l^t). \end{aligned} \tag{4}$$

Here, superscripts n and t denote the normal and tangential directions, and subscripts w and l denote the water-particle and the mooring-segment respectively. Further, a [m/s^2] refers to acceleration, v refers to velocity, U [m/s] is the magnitude of the current velocity, and D [m] is the line drag diameter.

The current velocity, and wave induced water-particle velocities and accelerations, at the segment lumped-mass points, are to be considered in (3) and (4).

For a linear wave, the following are defined:

$$\omega^2 = gk \tanh(kd) \tag{5}$$

$$\eta = H/2 \cos(kx - \omega t), \tag{6}$$

$$u = \frac{\pi H}{T} \frac{\cosh k(z+d)}{\sinh(kd)} \cos(kx - \omega t) \tag{7}$$

$$w = \frac{\pi H}{T} \frac{\sinh k(z+d)}{\sinh(kd)} \sin(kx - \omega t) \tag{8}$$

$$\dot{u} = \frac{2\pi^2 H}{T^2} \frac{\cosh k(z+d)}{\sinh(kd)} \sin(kx - \omega t) \tag{9}$$

$$\dot{w} = -\frac{2\pi^2 H}{T^2} \frac{\sinh k(z+d)}{\sinh(kd)} \cos(kx - \omega t). \tag{10}$$

Here, ω [rad/s] is the wave frequency, η [m] is the sea surface elevation, u and w [m/s] are the horizontal and vertical components of the wave-induced water particle velocities, the overdot denotes time derivative, H [m] is the wave height, T [s] is the wave period, k [m^{-1}] is the wave number, x and z [m] are the horizontal and vertical co-ordinates of the evaluation point, d [m] is the water depth, and t [s] is the simulation time. See pp. 51–52 of (Chakrabarti, 1987).

Figure 2 gives the expression for the normal and tangential components of the wave-induced water particle velocities associated with a segment inclined at angle θ to the horizontal. Similar expressions may be obtained for the relevant current, and segment kinematics.

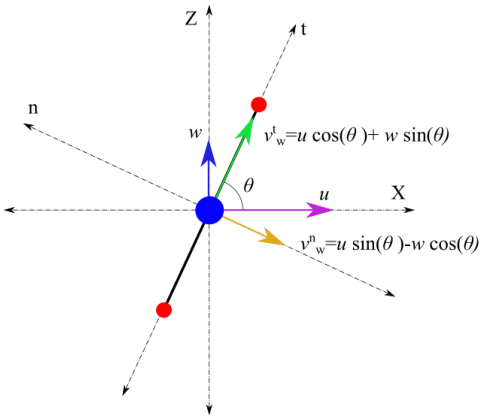

Figure 2. Normal and tangential components.

The horizontal and vertical components of the Morison loads on the segment may thus be determined as:

$$M_F^x = M_F^t \cos\theta + M_F^n \sin\theta \quad (11)$$

$$M_F^y = M_F^t \sin\theta - M_F^n \cos\theta. \quad (12)$$

The problem is implicit in the sense of the interdependency between line orientation, tension and fluid loading.

3 Building the Modelica Model

Representation of the *discretized* model in *Modelica* is realized through the use of components already available in the Multi-Body-System (MBS) library of *Modelica*, with some modifications to meet the problem requirements.

The segmental lumped mass, and the suspended load, are represented by **PointMass** components, the massless lengths of segments lying on either side of its lumped-mass are represented by **FixedTranslation** components, the point of suspension of the top end is specified by a **Fixed** component, and the hinge connection between the segments are represented by **Revolute** joint components, all of which are available in the MBS library.

In the determination of fluid loads, we require the orientation of the segment at any given simulation time step, and hence a modification is effected to the **FixedTranslation** component by specifying a *RealOutput* interface to transmit the coordinates of the flanges. Two variants of the **FixedTranslation** components are specified, the icon representations of which are shown in Figure 3.

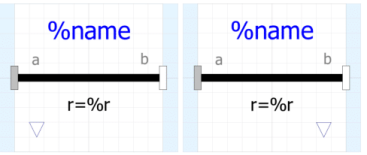

(a) UP_Seg. **(b)** LO_Seg.

Figure 3. *Icon* views of the modified *FixedTranslation* components.

UP_Seg is modified such that its *RealOutput* interface transmits the coordinates of its *flange_a*.

LO_Seg is modified such that its *RealOutput* interface transmits the coordinates of its *flange_b*.

The *diagram view* of the simplest sample system showing all used components is shown in Figure 4.

The segment model is built up by connecting the appropriate flanges of upper segment **UP_Seg**, a **PointMass**, and a lower segment **LO_Seg**. The interconnection between two segments, and of a segment with the point of suspension, can be effected through a **Revolute** joint. The point of suspension of the top end is specified by a **Fixed** component, and a **PointMass** component is used to specify the suspended load. Drag calculations are carried out by **DnB** blocks.The computed drag and buoyancy values are transformed to world forces by a **WorldForce** component, and applied as loads to the flanges of the lumped-masses. Gravity is included by the specification of the **World** component.

The environment, and cable/chain parameters, are specified inside the **DnB** block. The parameters specified are:

General: water depth d, water density ρ, ramping period for waves and current T_{rmp}.

Regular Wave: wave height H, period T.

Current: *vector* of depths at which the profile is defined z_{cg} and fully developed magnitudes of current at these depths U_f.

Cable: drag diameter D, buoyancy diameter D_b, normal and tangential added mass coefficients C_A^n and C_A^t. normal and tangential drag coefficients C_D^n and C_D^t.

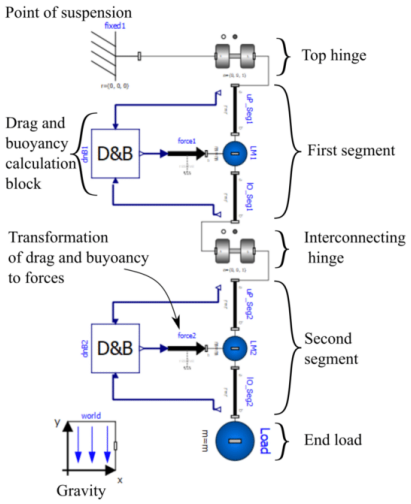

Figure 4. Modelica representation of a suspended subsea load system.

The wave number is computed by *function* **waveNumberIterator**, by iteration of the dispersion relation (5), as described in (Viswanathan and Holden, 2020b). The segment lengths, and instantaneous location of *lumped-mass* points are calculated based on the real outputs of the **UP_Seg**, and **LO_Seg**, associated with each segment.

The sea surface elevation (SSE) at the x co-ordinate of the *lumped-mass* point is calculated using (6), and the wave and current kinematic profiles are moved with the SSE as described in (SINTEF, 2014). The current velocity at the y coordinate of the *lumped-mass* point is then interpolated for using the **linearInterpolatorSV** *function*, and the wave-induced water-particle velocities and accelerations are calculated using (7)–(10).

The velocities and accelerations of the *lumped-mass* points at the current time step being provided by *Modelica*, the instantaneous drag may be determined using equations (3), (4), (11), and (12).

Drag and buoyancy forces on the end load may also be specified by using a similar **DnB** block, but has been omitted here for simplicity.

4 Results

We discuss the simulation results of a system with parameters shown in Table 1:

Figure 5 shows the diagram view of the above system in *Modelica*.

Figure 6a compares the line configurations in *Modelica* and *Orcaflex*, at $t = 100$ [s], when subject to a uniform current profile defined by $z_{cg} = \{-50,-25,-10,0\}, U_f = \{1,1,1,1\}$. Figure 6b compares the same for a current profile defined by $z_{cg} = \{-50,-25,-10,0\}, U_f = \{0,0.5,1,2\}$. In both cases, the wave height $H = 0$ [m].

Parameter	Value
Depth of suspension point below water surface	2.5 [m]
Chain length	30 [m]
Chain specific mass	10 [kg/m]
Discretization segment length	5 [m]
Chain buoyancy diameter	0.04 [m]
Chain drag diameter	0.04 [m]
Chain drag coeff. (normal)	1 [-]
Chain drag coeff. (tangential)	0.25 [-]
Chain added mass coeff. (normal)	1 [-]
Chain added mass coeff. (tangential)	0.5[-]
End load mass	100 [kg]
Ramp time for waves and current	10 [s]
Water depth	50 [m]
Water density	1025 [kg/m^3]
Current profile	*variable*
Regular wave parameters	*variable*

Table 1. System parameters

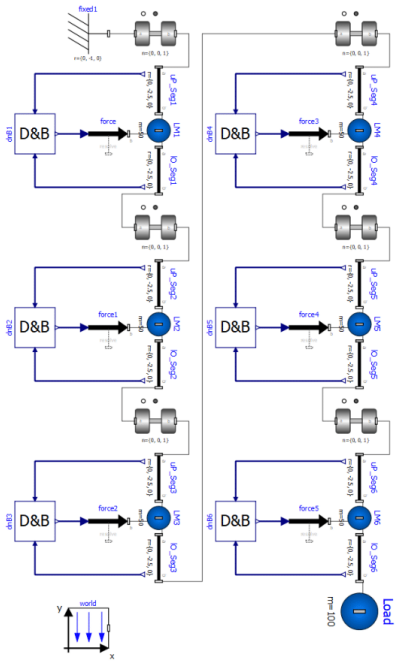

Figure 5. Diagram view of a subsea suspended load *system*.

Figure 7 compares the top end tensions for both the above cases.

Figures 8a and 8b compare the horizontal and vertical response of the suspended load to regular waves of $H = 5$ [m] and $T = 10$ [s], in both *Modelica* and *Orcaflex*, while Figure 8c compares the top end tensions. Current loading is set to zero by specifying $z_{cg} = \{-50,-25,-10,0\}, U_f = \{0,0,0,0\}$.

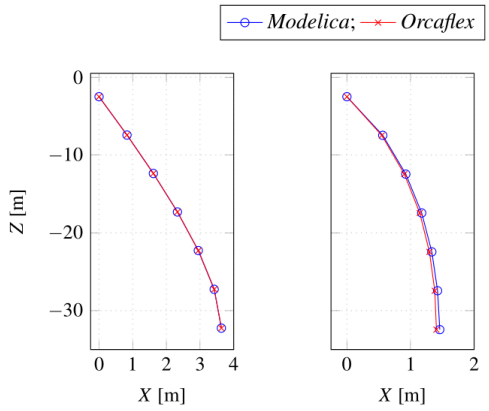

(a) Unifrom profile **(b)** Non-uniform profile

Figure 6. Line configuration for different current profiles.

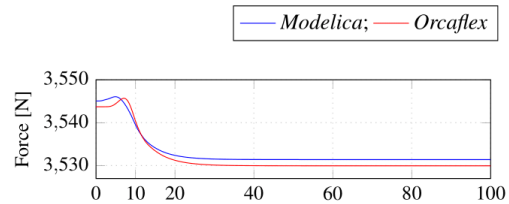

(a) Unifrom profile

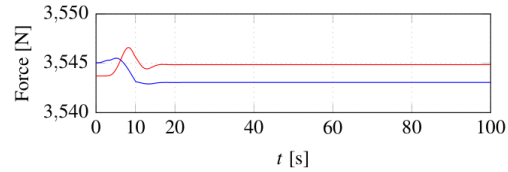

(b) Non-uniform profile

Figure 7. Line top end tensions for different current profiles.

Figure 9a and Figure 9b compares the horizontal and vertical response of the suspended load to regular waves of $H = 5$ [m] and $T = 10$ [s] in the presence of a current with profile defined by $z_{cg} = \{-50, -25, -10, 0\}, U_f = \{0, 0.5, 1, 2\}$, in both *Modelica* and *Orcaflex*, while Figure 9c compares the top end tensions.

5 Result Discussion

From the above figures, we observe a general agreement between *Modelica* and *Orcaflex* responses. To quantify the degree of agreement, we present the percentage variation between them in Table. 2.

In most cases, we observe good agreement with <5% variation. On examining the values with higher % variation, we infer that the numerical significance is quite low,

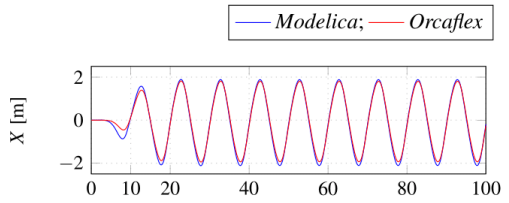

(a) Horizontal position (bottom-end)

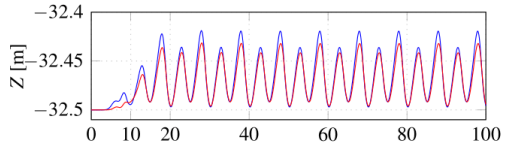

(b) Vertical position (bottom-end)

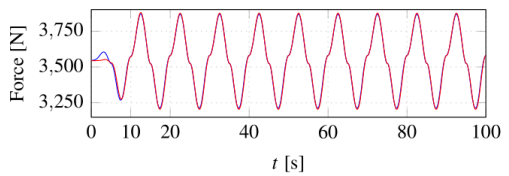

(c) Top end tension

Figure 8. Regular wave response.

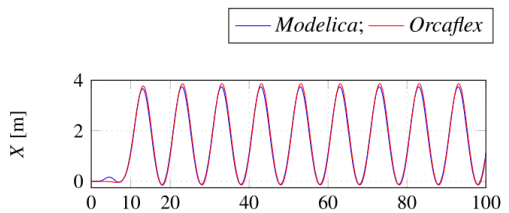

(a) Suspended load horizontal position

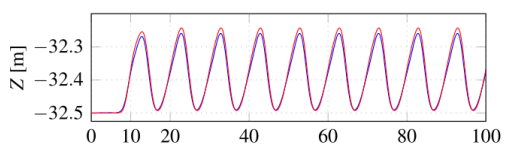

(b) Suspended load vertical position

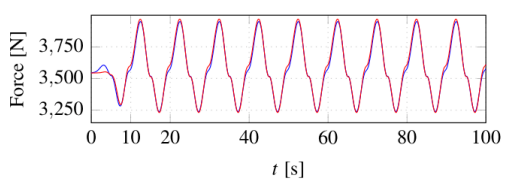

(c) Top end tension

Figure 9. Combined wave–current response.

as demonstrated below for the highest variation of 21.9%, corresponding to the vertical displacement of the suspended load, as depicted in Fig. 8b.

Numerically, the *Modelica* and *Orcaflex* responses are $-32.4193 - (-32.4970) = 0.0777$ [m], and $-32.4324 - (-32.4960) = 0.0636$ [m], indicating a difference of 0.014 [m], which is quite insignificant when we consider that this variation of 1.4 cm is for the motion of the tip of a chain that is 30 [m] long. Similar inferences can be arrived at for all other values.

These variations could be due to the fact that we use *moved* kinematic profiles, while *Orcaflex* uses *Wheeler stretching* of wave and current kinematics.

Larger variations observed during the ramp-up time $T_{rmp} = 10$ [s], in all cases, is attributed to the fact that we use a sinusoidal ramping function while *Orcaflex* uses an in-built ramping function with a different ramp curve.

The reason for the variation in initial top-end tension and tension response to currents as observed in Figure 7, though insignificant, has not yet been understood.

Variable Description	%variation
Horizontal position of end load in uniform current (Fig. 6a)	-0.07
Horizontal position of end load in profile current (Fig. 6b)	3.72
Vertical position of end load in uniform current (Fig. 6a)	0.00
Vertical position of end load in profile current (Fig. 6b)	-0.03
Top end tension in uniform current (Fig. 7a)	0.04
Top end tension in profile current (Fig. 7b)	-0.05
Horizontal response in waves (Fig. 8a)	6.47
Vertical response in waves (Fig. 8b)	21.9
Top end tension response in waves (Fig. 8c)	-2.34
Horizontal response in waves and current (Fig. 9a)	-3.62
Vertical response in waves and current (Fig. 9b)	-7.31
Top end tension response in waves and current (Fig. 9c)	-11.11

Table 2. Variation between *Modelica* and *Orcaflex* results.

6 Conclusion

The work presented in this paper introduces a novel method for specifying fluid loads on a mass discretized subsea cable using components already available in the *Modelica MultiBody* library, with minor modifications.

Based on the agreement between *Modelica* and *Orcaflex* simulation results, it is concluded that the model exhibits satisfactory representation of structural and fluid inertia effects, and accurate modelling of the drag loads on a cable structure.

The only traceable reference to an attempt to use *Modelica* in a similar scenario, by other researchers, is in the modelling of the station keeping system of an offshore wind turbine in (Leimeister and Thomas, 2017), where limitations included the inability to account for:

- Relative accelerations in wave load calculation.
- Current loads on submerged structures.

These limitations have been successfully mitigated in the present model.

It may also be noted that the authors are relatively new to *Modelica*, and the results presented here are for a work in progress. The code presented along with this work may show instances of under-utilization of advantages offered by *Modelica*, for e.g., the use of the *array* concept in implementing the lumped mass philosophy. The main focus of the present stage of the authors' research is to build a general framework for simulation of ocean engineering systems in *Modelica*. Code refinement is planned for the next stage of the project.

Extension of the modelling philosophy presented in this work is expected to open the window towards the development of *Modelica* component models for catenary as well as taut moorings. Inclusion of linear and torsional spring elements is expected to enable *Modelica* representation of flexible structures with elasticity and bending stiffness viz. risers, elastic moorings, and umbilicals, in the future.

The further development of this work, coupled with the development of component models for waves and currents as described in (Viswanathan and Holden, 2020b), and for non-diffracting floating objects as described in (Viswanathan and Holden, 2020a), followed by the development of component models for diffracting objects in the future, would thus enable the integrated simulation of multiphysical ocean-engineering systems, in their entirety, using *Modelica*.

Presently, the authors are developing an *open-source* code for determining the hydrodynamic coefficients which appear in the equation-of-motion of diffracting floating-objects. The initial results look promising, and the subject will be dealt with in a future publication.

7 Acknowledgements

The research in this paper has received funding from the Research Council of Norway, SFI Offshore Mechatronics, project number 90034210.

References

Subratha Kumar Chakrabarti. *Hydrodynamics of Offshore Structures*. Computational Mechanics Publications, and Springer-Verlag, Dorchester, Great Britain, 1987. ISBN 0-905451-66-X.

Mareike Leimeister and Philipp Thomas. The onewind modelica library for floating offshore wind turbine simulations with flexible structures. In *Proceeding of the 12th International Modelica Conference*, pages 633–642, 05 2017. doi:10.3384/ecp17132633.

Toshio Nakajima, Seizo Motora, and Masataka Fujino. On the dynamic analysis of multi-component mooring lines. In *Proceedings of the Offshore Technology Conference*, 1982. doi:10.4043/4309-ms.

SINTEF. *Handbook on Design and Operation of Flexible Pipes*. 2014. URL sintef.no/en/latest-news/updated-handbook-on-design-and-operation-of-flexible-pipes/.

D.O Thomas and G.E. Hearn. Deepwater mooring line dynamics with emphasis on seabed interference effects. In *Proceedings of the Offshore Technology Conference*, volume OTC-7488-MS, May 1994. doi:10.4043/7488-MS.

Michael Tiller. Response to questions on determining variable values of previous time steps in modelica. In *Stackoverflow*, 2013. URL https://stackoverflow.com/questions/16558587/how-to-determine-value-from-previous-time-step-during-simulation-in-modelica.

Savin Viswanathan and Christian Holden. Towards the development of an ocean engineering library for openmodelica. In *Proceedings of the ASME 2019 38th International Conference on Ocean, Offshore and Arctic Engineering*, volume 7B:Ocean Engineering. OMAE, November 2019. doi:10.1115/OMAE2019-95054.

Savin Viswanathan and Christian Holden. Modelica component-models for non-diffracting floating objects and quasi-static catenary moorings. In *Proceedings of the American Modelica Conference*, 2020a. The conference has been postponed due to the prevailing COVID-19 situation. A link to the referred publication will be provided along with the download files for the referring publication, as and when such a link becomes available.

Savin Viswanathan and Christian Holden. Modelica component-models for oceanic surface-waves and depth varying current. In *Proceedings of the American Modelica Conference*, 2020b. The conference has been postponed due to the prevailing COVID-19 situation. A link to the referred publication will be provided along with the download files for the referring publication, as and when such a link becomes available.

Thomas S. Walton and Harry Polachek. Calculation of transient motion of submerged cables. *Mathematics of Computation*, 14(69):27–46, 1960. doi:10.1090/S0025-5718-1960-0116470-5.

Chapter 6

Hydrodynamics of diffracting objects

We discussed the wave-body interaction problem in Sec 2.3. In Sec. 2.4, we discussed the diffraction-radiation problem, and the frequency dependence of added-mass and radiation damping. In Sec. 2.9.1, we discussed how the effect of the presence of objects within a flow domain may be approximated by a judicious distribution of sources and dipoles. Further in Sec 2.9.3, we discussed how we can use Green's second identity to express the velocity potential in a flow domain as the effects of distribution of *singularities* on the domain boundary. We had further seen in Sec. 2.9.3.1 how the velocity potential due to an object placed in an infinite flow domain could be expressed as the result of *source* distributions on the body alone. In Sec. 2.9.4, we discussed the Hess and Smith *panel method* of transforming the boundary integral equations into a set of linear algebraic equations.

In the article presented in this chapter, we extend the *panel method* to the case of an object in an infinite fluid domain with uniform incident flow, and to an object in a semi-infinite fluid domain bounded by a free-surface, in the presence of either a uniform incident flow or surface waves.

Thus, the work presented in this chapter has a direct correlation with general project objective 1 and specific project objective 1(b), as discussed in Sec. 3.2.

6.1 An open-source Python-based boundary-element method code for the three-dimensional, zero-froude, infinite-depth, water-wave diffraction-radiation problem.

The citation for the *submitted* article is given below:

S. Viswanathan, C. Holden, O. Egeland, M. Greco. *An open-source Python-based boundary-element method code for the three-dimensional zero-Froude, infinite-depth, water-wave diffraction-radiation problem.* Journal of Modeling, Identification and Control, xx(x):xx–xx,xxx. doi:xx.xxxx/mic.xxxx.x.x

The preprint version of the article follows.

Chapter 7

Co-simulation of offshore systems

We introduced the riser-tensioner system in Sec. 2.12. In the article presented in Sec. 7.1, we formulate a co-simulation methodology to carry out dynamic analysis of top-tensioned risers. The simplified platform and the riser is modelled in *OrcaFlex*, a popular ocean-engineering software package, and the hydro-pneumatic riser-tensioner system is modeled in the *Modelica* based *SimulationX* software.

In the article presented in Sec. 7.2, we benchmark the simulation results using field measurements associated with a *planned* disconnect event, and demonstrate the possibilities that the methodology opens up.

Thus, the articles presented in this chapter have a direct correlation with general objective 2, and specific objective 2(b), as discussed in Sec. 3.2.

7.1 Co-simulation of the hydro-pneumatic riser-tensioner system I – Methodology synthesis

The citation for the *submitted* article is given below:

S. Viswanathan, C. Holden, O. Egeland, R. Sten. *Co-simulation of the hydro-pneumatic riser-tensioner system I – Methodology synthesis.* Journal of Offshore Mechanics and Arctic Engineering, xx(x):xx–xx,xxx. doi:xx.xxxx

The preprint version of the article follows.

This paper is awaiting publication and is not included in NTNU Open

7.2 Co-simulation of the hydro-pneumatic riser-tensioner system II – Field verification and advanced simulations

The citation for the *submitted* article is given below:

S. Viswanathan, C. Holden, O. Egeland, R. Sten. *Co-simulation of the hydro-pneumatic riser-tensioner system II – Field verification and advanced simulations.* Journal of Offshore Mechanics and Arctic Engineering, xx(x):xx–xx,xxx. doi:xx.xxxx

The preprint version of the article follows.

Chapter 8

Conclusion

This chapter gives a bird's eye-view of the work presented in this thesis. Specific discussions and conclusions are available inside the articles in Ch. 4–7. A generalized discussion and conclusion follows.

8.1 Discussion

The main limitation when it comes to using *Modelica*-based multiphysics software for dynamic analysis of ocean-engineering systems, is the lack of component models to simulate aspects that are inherent to offshore systems viz. hydrodynamic loads on larger structures like offshore platforms, mooring and other station keeping loads, hydrodynamic loads on slender structures like risers etc.

Similarly, when it comes to using *finite element*-based analysis tools for the analysis of multiphysical ocean-engineering systems, the lack of component models to accurately capture the multiphysics of the system is the major limitation.

Two approaches may be adopted to overcome this limitation:

- Develop *Modelica* component models for simulating hydrodynamics, moorings, and other salient aspects of ocean-engineering systems, build the system model using these components in conjunction with the numerous component models from other domains already available in the *Modelica* standard library, and carry out multiphysical simulations of the system using this *integrated* approach.
- Formulate a methodology for data exchange between the *finite element*-based ocean-engineering software and the *Modelica*-based multiphysics software, and carry out multiphysical simulations of the system using this *co-simulation* approach. Here, the fluid-structure interaction is modeled in the ocean-engineering software, and the electro-mechanical part of the system is modeled in the *Modelica*-based software, with load/motion coupling between the two systems.

Both of the above approaches have their inherent advantages and disadvantages:

- The main advantage of the *integrated* approach is that once the wave-structure interaction models are developed, the *Modelica* compiler can then translate the whole *model* for efficient simulation with standard numerical integration methods, which is the forte of *Modelica*. The other advantage is that the user is liberated from the task of building component models for modeling the rest of the system, since most of it, if not all, are already available in the *Modelica* standard library. The disadvantage is that the user needs to develop component models for fluid-structure interaction, and depending on the aspect to be captured, the user would require specialized knowledge and time to develop such component-models.
- The main advantage of the *co-simulation* approach is that the user is liberated from the task of developing component models for fluid-structure interaction. Modern ocean-engineering analysis software have capabilities for modelling advanced fluid-structure interaction effects, and the user can readily take advantage these capabilities without the need for having an in-depth understanding of the underlying theory. The other advantage is that the user gets access to the whole palette of ready-made results from both the ocean-engineering software and the multiphysics software. The major disadvantage of this approach is that not all ocean-engineering software support interfacing. Further, there might be limitations in the access to simulation variables during the runtime. One may also note that most, if not all, ocean engineering software are *commercial*, and hence have a *black-box* nature, and are also costly.

The approach to be adopted depends on the nature of the problem to be tackled and the background of the person tackling the problem. Academia tends to be interested in open-source approaches since it affords the possibility for wider research access without cost implications. The industry, on the other hand, is more concerned about development time and market acceptability of the analysis tools, which, at present, seems to be in favour of the *commercial* simulation environments for both multiphysics and ocean-engineering analysis tools.

In this work, we cater to both sections. For academia, we develop component-models using the free-to-use *OpenModelica* modeling and simulation environment, and its GUI, *OMEdit*. For the industry, we develop a co-simulation methodology for top-tensioned drilling riser analysis by interfacing the riser to the platform, both modelled in *OrcaFlex*, through a hydro-pneumatic riser tensioner system, modeled in *SimulationX*. Both *OrcaFlex*, and *SimulationX* being commercial, industry-accepted analysis software.

In developing component-models for ocean engineering systems, one needs a fair understanding of the theory behind fluid-structure interaction problems. Also, the interdependence between the fluid loads and the structure response necessitates a parallel development of all associated ocean-engineering component models. A condensed form of the requisite theory is given in Ch. 2.

From Sec. 2.4, we note that simulating the hydrodynamic response of a floating

object requires the determination of frequency-dependent hydrodynamic parameters. In Sec. 2.10, we note that the frequency dependence may be ignored for relatively smaller objects, and the fluid loading may be determined using the Froude-Kryloff and Morison equations, as described in detail in Sec. 4.3. Analytical expressions for parameters of small amplitude (Airy) waves can be determined by solving the linearized BVP formulated in Sec. 2.8, and solved in Sec. 4.2. Using the relations given in [21], one may approximate the mooring loads based on the quasi-static catenary theory, as described in detail in Sec. 4.3. Further, Sec. 4.2 also describes the simulation of irregular waves and depth varying current.

Thus, one of the simplest configurations that encompasses the salient features of a multiphysical ocean-engineering system would be a catenary-moored non-diffracting floating object, in waves and current, with a simplified multiphysical component.

Sec. 4.1 models such a simplified system, and illustrates the advantages of using a *Modelica* based approach for the simulation of ocean-engineering systems. Though more emphasis is placed on the ocean-engineering aspects of the system in the article, it is to be noted that the *spring* component inside the WEC buoy can be replaced by any electro-mechanical system which can easily be modeled using the already available component models in the *Modelica* standard library. The hydrodynamic response determined in the *Modelica* simulation is in satisfactory agreement with *OrcaFlex* results, and is an indication of the effectiveness of the approach.

The limitations of using the quasi-static catenary theory to determine mooring loads are discussed in Sec. 4.3. Sec. 5.1 describes the implementation of the lumped-mass approach in the dynamic simulation of subsea cable structures, to remedy the limitations of the quasi-static approach. In hindsight, I realized my foolishness in trying to specify a time stepping method for *Modelica*. For reasons discussed in Sec. 5.2, it is best to leave the solution procedure to the *Modelica* compiler. Nevertheless, it was our observations during the development of the article discussed in Sec. 5.1, that led to the work presented in Sec. 5.2.

In Sec. 5.2, we discuss the dynamic simulation of a chain-suspended subsea load, and we note the excellent agreement of the results with the results obtained using *OrcaFlex*. The *Modelica* model discussed in Sec. 5.2 can easily be extended to the case of a mooring line, where blocks similar to the *DnB* blocks can be used to specify sea-bed interaction forces, with the vertical reaction on the grounded nodes being modeled in a way as discussed in Sec. 5.1. The initial configuration of the catenary, which is the starting point for the dynamic simulation, can be specified using the quasi-static approach discussed in Sec. 4.3 and Sec. 5.1. Effects of sea-bed friction may also be specified in a similar fashion. Inclusion of linear and torsional spring elements in specifying the *segments* will enable the extension of the model to determine the dynamics of slender structures with elasticity and bending stiffness, like the riser pipe.

Building component models to simulate the hydrodynamic response of larger diffracting objects is not so straightforward since one needs to determine the frequency-

dependent hydrodynamic parameters, as discussed in Sec. 2.3 and 2.4. Also to be noted is that the linearized diffraction radiation problem is solved based on the mean position of the sea-surface and the wetted body-surface. Hence, large changes in the position of the mean wetted body-surface necessitates recalculation of the frequency dependent parameters.

Though the theory behind the solution to the diffraction-radiation problem is many decades old, and well developed at present, it is dispersed throughout literature, with details of computer implementation hidden behind the veil of costly commercial software. This is a hindrance to our view of developing open-source tools for academia, and hence in Sec. 6.1, we consolidate the theory behind the panel method and describe the development of *OMHyD*, a basic 3D boundary element method (BEM) code in *Python*. This is with a view to facilitate the development of an interface in the future between *Modelica* and *OMHyD*, to facilitate recalculation of frequency dependent parameters, as required, during the course of the dynamic simulation, and to develop BEM codes for determining the hydrodynamic response of porous structures, like aquaculture enclosures, on which extensive research is being undertaken at present at many academic institutions across the world.

To cater to the industry requirement of developing multiphysical analysis tools which may be put to use without much of a delay, we present a co-simulation methodology for the analysis of top tensioned drilling risers by interfacing *OrcaFlex* and *SimulationX* models using an interface file coded in *Python*, in Sec. 7.1, and demonstrate the capabilities of the methodology. In Sec. 7.2, we extend the methodology to the full scale riser tensioner system and benchmark model performance with field measurements to demonstrate satisfactory agreement. We further demonstrate the advantages of adopting the methodology by carrying out the analysis of an entire disconnect sequence, starting from the *connected* condition and ending with the *soft hang-off* of the riser.

8.2 Conclusion

Thus, with reference to the two main objectives of the project, as discussed in Sec. 3.2, and the discussion in Sec. 8.1 we conclude:

I. The research carried out as part of the PhD has, in principle, partly met the objective of developing component-models to constitute a *Standard Library* for carrying out multiphysical simulation of ocean engineering systems using *Modelica* simulation environments. However, it has prepared the ground for future research that would enable the realization of the objective in full.

II. The research carried out as part of the PhD has, in principle, met the objective of developing a *co-simulation methodology* to simulate the fully coupled response of a drilling riser in recoil by interfacing the platform and riser model in *OrcaFlex*, with the hydro-pneumatic riser-tensioner model in *SimulationX*.

With reference to the specific objectives of the project, as discussed in Sec. 3.2, we conclude:

i. The research carried out as part of the PhD has fully met project objective 1(a) of the project. The articles discussed in Ch. 4 correlates to objective 1(a).

ii. The research carried out as part of the PhD has partly met objective 1(b) of the project. The 3D BEM code, *OMHyD*, which has been developed during the course of this research, is presently capable of determining the frequency dependent hydrodynamic parameters for cuboidal objects. It may be developed further to accommodate objects of arbitrary shapes. The article presented in Ch. 6 correlates to objective 1(b).

iii. The research carried out as part of the PhD has partly met objective 1(c) of the project. The article presented in Sec. 5.2 demonstrates how the dynamics of a chain-suspended subsea load may be simulated using *Modelica*. This concept may be extended to moorings and risers in the future. The articles presented in Ch. 5 correlates to objective 1(c).

iv. The research carried out as part of the PhD has not met objective 2(a) of the project. However, using the co-simulation model presented in Sec. 7.2, one can easily study the influence of the riser tensioner system on the fatigue in the riser stack and formulate a control strategy to minimize it.

v. The research carried out as part of the PhD has met objective 2(b) of the project. The articles presented in Sec. 7.2 correlates to objective 2(b).

8.3 Contributions of the present work

A summary of the specific contributions of the present work follows.

1. *Modelica* component-model for two-dimensional, regular, small-amplitude (Airy) waves.
2. *Modelica* component-model for two-dimensional, irregular waves, based on the Fourier series representation of the irregular sea-surface, and the Pierson-Moskowitz sea-spectrum.
3. *Modelica* component-model for unidirectional depth-varying current with linear interpolation.
4. *Modelica* component-models for catenary moorings based on the quasi-static theory.
5. *Modelica* component-models for the heave-surge response of non-diffracting floating objects based on the Froude-Kryloff formulation and the Morison equation.
6. The open-source *Modelica* library for ocean-engineering applications containing the above component-models along with three publications in peer-reviewed international conference proceedings, detailing the development of the above component-

models and the ocean-engineering library, with public links to the *Modelica* code and simulation files.

7. The open-source *OMHyD* 3-D BEM code for the determination of frequency dependent hydrodynamic parameters of diffracting cuboidal objects, along with one submitted paper to a peer-reviewed international journal, detailing the development of the BEM code, with public links to *OMHyD*, and associated analysis files.
8. Open-source implementations of the lumped-mass approach in simulation of catenary mooring forces in *Modelica* and *Python*, along with one publication in a peer-reviewed international conference proceedings, detailing the development of the code, with public links to the code and simulation files.
9. *Modelica* component-model to simulate the dynamics of a chain-suspended subsea load using components available in the MultiBody library of *OpenModelica*, along with one publication in a peer-reviewed international conference proceedings, detailing the development of the component-model, with public links to the code and simulation files.
10. A *co-simulation* methodology for analysis of top-tensioned drilling risers using commercial analysis tools, along with a submitted paper to a peer-reviewed international journal, detailing the development of the methodology, with public links to the code and simulation files.
11. Benchmarking of the above *co-simulation* model performance with field data, along with a submitted paper to a peer-reviewed international journal, detailing the benchmarking procedure, and demonstrating the possibilities that such a methodology opens up.

8.4 Outlook for further research

The present work opens up numerous avenues for research. The *open-source* philosophy facilitates research access, without cost-implications, to most of the fronts offered by the current research.

The most prominent avenue for potential research is in improving the component models for the hydrodynamics of non-diffracting floating objects through inclusion of more simple geometries, and the reformulation of the component models to accommodate response in all six DoFs.

Another area for potential research is in developing component-models for moorings and risers based on the lumped-mass approach. The ground work has been done in Sec. 5.1 and Sec. 5.2, and this can be easily extended to the case of moorings and risers.

Another direction to consider would be the simulation of the hydrodynamic response of diffracting objects. Two routes may be considered:

a Obtain the hydrodynamic parameters from commercial frequency domain hydrodynamic analysis software, and use these parameters to carry out dynamic analysis in *Modelica*, by specifying component models that accept these parameters as inputs.

b Develop *OMHyD* further, to enable handling of arbitrary shapes, removal of irregular frequency effects, handling of finite water-depth cases, consideration of porous body surfaces, etc.

A parallel approach which facilitates for the use of externally sourced hydrodynamic parameters, until in-house capabilities are well developed, seems to be the best route to take.

One may likewise develop component models for the dynamic positioning thrusters, active heave compensation systems, shipboard cranes, etc. The list is practically limitless.

Fig. 8.1 gives a glimpse of the possibilities that further research in this direction opens up.

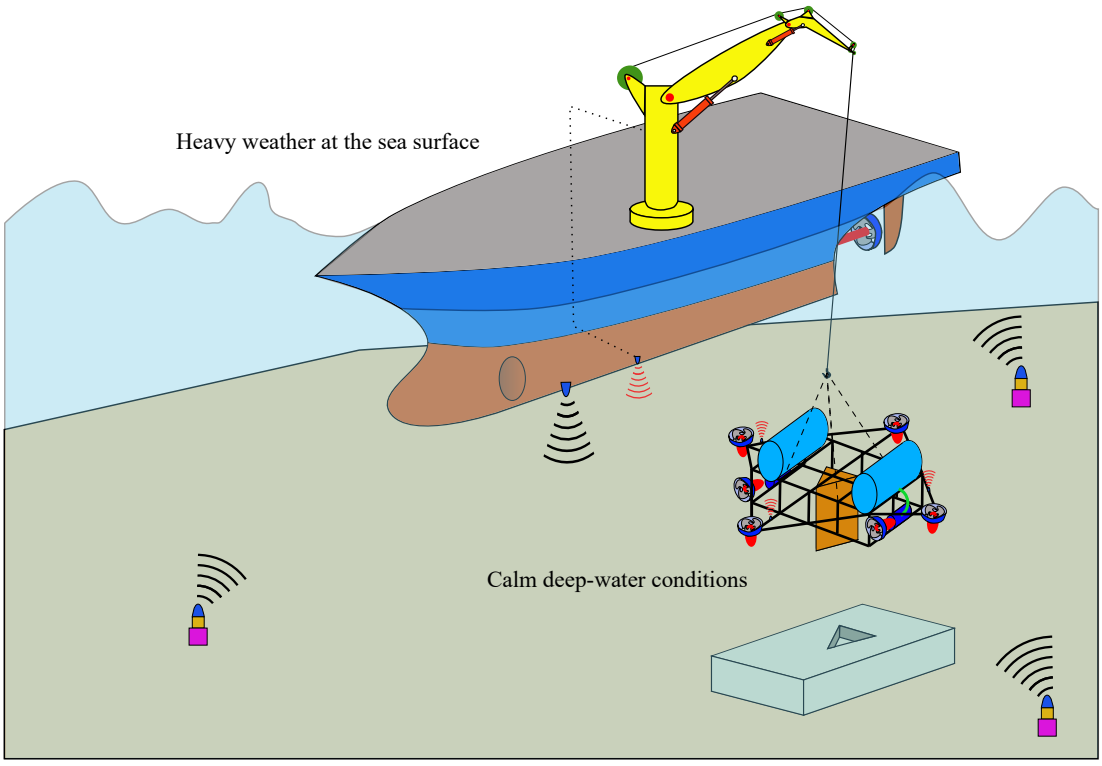

Figure 8.1: Subsea installation in heavy weather

Here, we consider a scenario where a subsea installation is in progress in heavy weather. In present times, if the weather conditions turn bad, the installation is suspended till the weather clears. However, with the development of AI and underwater

drone technology, we may be able to carry on with subsea installation since the effects of bad weather are not usually present at greater depths. However, this would require the interfacing of the crane with the positioning system so as to maintain sufficient slack in the crane wire during the final phases of the installation, where the underwater drone positions the load precisely for docking with the template, while the ship drifts from the optimal position due to heavy weather.

Before venturing out to carry out such procedures, it is imperative to ascertain that the infrastructure is capable of handling such situations. Detailed multiphysical simulations appear to be the only way of estimating system performance in such scenarios.

Now, imagine that the installation was being carried out in a world, far away from our own, to make the place ready for habitation by the first set of humans to arrive.

Multiphysical simulations are the only way for evaluation of the best course of action, especially in pioneering engineering endeavours, and we are left without a choice, but to develop such capabilities.

The author has been offered a post-doctoral researcher position, subsequent to the successful defense of this thesis, for conducting further research in this direction.

References

[1] *Lecture notes on Water Waves*. Massachusetts Institute of Technology. URL https://ocw.mit.edu/courses/mechanical-engineering/2-017j-design-of-electromechanical-robotic-systems-fall-2009/course-text/MIT2_017JF09_ch06.pdf.

[2] Y. Bai and Q. Bai. *Subsea pipelines and risers*. Elsevier, 2005. URL https://www.elsevier.com/books/subsea-pipelines-and-risers/bai/978-0-08-044566-3.

[3] R. K. Bansal. *Fluid mechanics and hydraulic machines*. Laxmi Publications (P) Ltd., 2000.

[4] S. K. Chakrabarti. *Hydrodynamics of Offshore Structures*. Computational Mechanics Publications, and Springer-Verlag, Dorchester, Great Britain, 1987. ISBN 0-905451-66-X.

[5] S. K. Chakrabarti. *Handbook of Offshore Engineering*. Elsevier Ltd, 84 Theobalds Road, London WC1X8RR, UK, 2005.

[6] R. G. Dean and R. A. Dalrymple. *Water Wave Mechanics for Engineers and Scientists*. Allied Publishers Limited, Mumbai, India, 2001. ISBN 81-7764-195-6.

[7] M. W. Dingemans. *Water Wave Propagation Over Uneven Bottoms*. PhD thesis, TUDelft, Netherlands, November 1994.

[8] O. M. Faltinsen. Lecture notes on source-sink methods and wave-induced loads.

[9] O. M. Faltinsen. *Sea Loads on Ships and Offshore Structures*. Cambridge University Press, 1999. ISBN 0-521-45870-6.

[10] O. M. Faltinsen and F. C. Michelsen. Motions of large structures in waves at zero Froude number. Technical report, 1975. URL https://www.studocu.com/no/document/norges-teknisk-naturvitenskaplige-universitet/akademisk-skriving/essay/motions-of-large-structures-in-waves-at-zero-froude-number/6109623/view.

[11] T. I. Fossen. *Handbook of Marine Craft Hydrodynamics and Motion Control*. Wiley, 2011.

[12] Fritzon, Peter. *Principles of Object-Oriented Modeling and Simulation with Modelica 3.3*. IEEE Press, New Jersey(2015).

[13] D. S. Henningson and M. Berggen. *Lecture notes on Fluid Dynamics: Theory and Computation*. KTH Royal Institute of Technology, August 2005. URL https://www.mech.kth.se/~henning/CFD/CFD_main.pdf.

[14] J. L. Hess and A. Smith. Calculation of non-lifting potential flow about arbitrary three-dimensional bodies. Technical report, Douglas Aircraft Co., Long Beach CA, 1962. URL https://apps.dtic.mil/dtic/tr/fulltext/u2/282255.pdf.

[15] F. John. On the motion of floating bodies. i. *Communications on Pure and Applied Mathematics*, 2(1):13–57, 1949. doi: https://doi.org/10.1002/cpa.3160020102.

[16] J. Katz and A. Plotkin. *Low-Speed Aerodynamics*. 2001. doi: 10.1017/cbo9780511810329.

[17] Kimberly Amadeo. *Oil Price Forecast 2018-2050: How High Oil Prices Will Rise in 2018*. The Balance. URL https://www.thebalance.com/oil-price-forecast-3306219.

[18] S. H. Lamb. *Hydrodynamics*. Cambridge University Press, 1879. URL https://www.cambridge.org/no/academic/subjects/mathematics/fluid-dynamics-and-solid-mechanics/hydrodynamics-6th-edition?format=PB&isbn=9780521458689.

[19] J. N. Newman. *Marine Hydrodynamics*. MIT Press, 1977. URL https://mitpress.mit.edu/books/marine-hydrodynamics-40th-anniversary-edition.

[20] Orcaflex. Example f03 pid controlled active winch. URL https://www.orcina.com/resources/examples/?key=f.

[21] J. B. Tatum. *Lecture Notes on the Catenary*. University of Victoria, 2004. URL astrowww.phys.uvic.ca/~tatum/classmechs/class18.pdf.

[22] Tavyis Dunnahoe. *Deepwater exploration seeks value over volume in new oil price environment*. Oil and Gas Journal, January 5, 2017. URL https://www.ogj.com/articles/print/volume-115/issue-5/special-report-offshore-petroleum-operations/deepwater-explorations-seek-value-over-volume-in-new-oil-price-environment.

[23] J. V. Wehausen. The motion of floating bodies. *Annual review of fluid mechanics*, 3(1):237–268, 1971. URL https://www.annualreviews.org/doi/pdf/10.1146/annurev.fl.03.010171.001321.

[24] J.-H. Westhuis. *The Numerical Simulation of Nonlinear Waves in a Hydrodynamic Model Test Basin*. PhD thesis, University of Twente, Netherlands, May 2001.

Appendices

Appendix A

Call for application

NTNU
Norwegian University of Science and Technology

TRONDHEIM | GJØVIK | ÅLESUND

NTNU - knowledge for a better world

The Norwegian University of Science and Technology (NTNU) creates knowledge for a better world and solutions that can change everyday life.

Faculty of Engineering

Department of Mechanical and Industrial Engineering

PhD 3 Positions in Offshore Mechatronics (IV-89/17, IV-90/17, IV-91/17)

PhD - 3 Positions in Offshore Mechatronics (IV-89/17, IV-90/17, IV-91/17)

Faculty of Engineering Science (http://www.ntnu.edu/iv) at the Norwegian University of Science and Technology (NTNU) has vacancy for three PhD positions at Department of Mechanical and Industrial Engineering (http://www.ntnu.edu/mtp).

Do you wish to create the future in offshore operations?

Three PhD positions are available at Department of Mechanical and Industrial Engineering at the Norwegian University of Science and Technology (NTNU), Trondheim, Norway. The positions are full-time positions for 3 years to reach the PhD degree at NTNU. It may be possible to have a 4-year position with 25% duty work. Applicants should have an MSc in mechanical engineering, mechatronics, marine technology, control theory, cybernetics, physics and mathematics, or similar.

The positions are funded by SFI Offshore Mechatronics (sfi.mechatronics.no), which is a program for research-based innovation (SFI) and a joint collaboration between NTNU, the University of Agder, the Norwegian Government, and industrial partners. The research in close contact with the industrial partners, which provides an exciting combination of long-term academic research and industrial innovation. The PhD candidates employed under this program will be part of a coordinated research group of 15-20 members with extensive laboratory facilities

Information about the department
The Department of Mechanical and Industrial Engineering (MTP) has broad interdisciplinary expertise in the fields of logistics, machine design, product development, materials science, risk and reliability of complex systems. The research at the department focuses on development, optimization and improvement of industrial processes and production systems. One of our goals is to secure the Norwegian industry and administration with access to knowledge and expertise on an international level. The PHD candidates will be affiliated to the Production Systems Group.

Position 1: WP4.1 Integrated simulation of multi-physical systems in offshore operations (IV-89/17)

Background: Modern offshore operations involve many diverse physical systems that must all work harmoniously to achieve the desired objectives in a safe and economical manner. Simulation is an invaluable tool in planning, coordinating and developing new operations. These simulations may involve FEM models, CFD models, signal-based simulators, and component-oriented simulators. Such simulators can be run in combination in some cases, while in other cases the simulators must be integrated. Design methods and guidelines for how to combine different types of simulators for different simulation tasks pose and interesting academic challenge and would be of great use to the industry.

Objectives: The PhD candidate will investigate simulator design for systems that are described by FEM, CFD, signal-oriented modules and component-oriented modules. Design rules for simulator implementation will be developed. In particular, the candidate will investigate when different simulators can be run in combination, and when simulators must be integrated in a Modelica or Simulink implementation. The study will include the use of the Modelica framework to define component-oriented model libraries, and will in this context introduce results and techniques from the automotive and aerospace industries to the offshore sector.

Contact: Associate Professor Christian Holden, christian.holden@ntnu.no

Mark your application with **ref.no. IV-89/17**

Position 2: WP4.2 Component-based simulation systems for drilling automation and crane systems (IV-90/17)

Background: Drilling and crane systems are an essential part of many offshore operations, operations which are made complicated by inclement weather and complex dynamics. To safely plan and perform these operations and control the expensive and complex

equipment, simulations are a necessity. Component-based simulation systems will aid in this. These simulations are based on libraries of models of physical system components and lead to very efficient implementation of modular simulation systems. The simulator performance will depend on proper interfacing between the library modules. In particular, the selection of input and output variables is important.

Objectives: In this project, the PhD candidate will develop a library of component models in Modelica for simulation in Dymola and Simulink. Design rules for interconnection of library modules will be developed for use in simulator development. The use of multiple CPUs and GPUs for fast and real-time simulation will be studied. This library will be used to build an implementation of simulators for case studies in drilling automation and crane systems.

Contact: Associate Professor Christian Holden, christian.holden@ntnu.no

Mark your application with **ref.no. IV-90/17**

Position 3: WP4.4 Modeling and simulation of cable and pulley systems in offshore cranes (IV-91/17)

Background: Cable and pulley systems are critical components in offshore cranes. It is important to have mathematical models that can be used in simulation and analysis to investigate challenges in design, operation and maintenance due to distributed mass, flexibility and stick-slip friction effects.

Objectives: This PhD project will develop dynamic models of offshore cranes with focus on cables and pulley systems in interaction with crane models including mechanism dynamics in finite-element models. Component-oriented modeling and the use of real-time simulation in a digital twin solution will be investigated.

Contact: Professor Terje Rølvåg, terje.rolvag@ntnu.no

Mark your application with **ref.no. IV-91/17**

Qualifications

The regulations for PhD programmes at NTNU state that a Master degree or equivalent with at least 5 years of studies and an average grade of A or B within a scale of A-E for passing grades (A best) for the two last years of the MSc is required, and C or higher of the BSc. Candidates from universities outside Norway must send a Diploma Supplement or a similar document describing in detail the study and grade system and the rights for further studies associated with the obtained degree: http://ec.europa.eu/education/tools/diploma-supplement_en.htm

The positions require spoken and written fluency in English.

Applicants who are finalizing their MSc during the spring of 2017 are also encouraged to apply.

Conditions:

PhD Candidates are remunerated in code 1017, and are normally remunerated at wage level 50, gross NOK 430 200 before tax. There will be a 2 % deduction to the Norwegian Public Service Pension Fund from gross wage.
Engagement as a PhD Candidate is done in accordance with “Regulation concerning terms and conditions of employment for the posts of post-doctoral research fellow, research fellow, research assistant and resident”, given by the Ministry of Education and Research of 19.07.2010. The goal of the positions is to obtain a PhD degree. Applicants will engage in an organized PhD training program, and appointment requires approval of the applicants plan for a PhD study within three months from the date of commencement.
See https://innsida.ntnu.no/doktorgrad for more information.

The engagement is to be made in accordance with the regulations in force concerning State Employees and Civil Servants. The positions adhere to the Norwegian Government's policy of balanced ethnicity, age and gender. Women are encouraged to apply. According to the new Freedom of Information Act, information concerning the applicant may be made public even if the applicant has requested not to be included in the list of applicants.

The application:

Applications must contain information of educational background and work experience, reference person(s), CV, possible publications and other scientific works, certified copies of transcripts and reference letters. In addition a project description of 1-2 pages including a short presentation of the motivation for a PhD study, how the applicant sees his/her background suitable, the applicant’s view of research challenges within the area of the PhD position and how the competence of the applicant can contribute to solve these challenges.

Applications and attachments have to be submitted electronically through www.jobbnorge.no. Applications submitted elsewhere will not be considered.

Please state clearly in the application each IV-number of the position(s) you apply for

Start-up date may be discussed, but tentatively August 2017.

Application deadline for all 3 positions: 31 March 2017

According to the new Freedom of Information Act, information concerning the applicant may be made public even if the applicant has requested not to be included in the list of applicants.

Jobbnorge ID: 135599, Deadline: 31.03.2017, Internal ID: IV-89/17, IV-90/17, IV-91/17

Appendix B

Project description

NTNU

Norwegian University of Science and Technology
Faculty of Engineering

Date
05.02.2019
dd.mm.yyyy

Our reference
2018/8635/RUNA

Dated
14.10.2018
dd.mm.yyyy

Your reference

Savin Viswanathan
Department of Mechanical and Industrial Engineering

Ph.d.- Approved Project Description - Savin Viswanathan

The description of your research project has been approved by the Doctoral Degree Committee in their meeting on January 30th 2019.

Yours sincerely,

Runa Nilssen
Senior Executive Officer

In accordance with delegated authority, this document is approved electronically and therefore requires no handwritten signature

Copy to:
Department of Mechanical and Industrial Engineering
Associate Professor Christian Holden

Address
7491
NO-
Norway

Org.no. 974 767 880
Email:
postmottak@iv.ntnu.no
http://www.ntnu.no

Location
Høgskoleringen 6,
Geologibygget, 2. etg.

Phone
+47 73 59 45 01
Fax
+47

Our contact person
Runa Nilssen
Phone: +47 73 59 37 02

Project Description

Integrated Simulation of Multiphysical Systems in Offshore Operations

Project No. 90034209

Submitted towards the partial fullfilment of the requirements for the award of the Doctor of Philosophy Degree by the Norwegian University of Science & Technology, Trondheim, Norway. The research work is performed as part of work package 4.1 of the SFI Offshore Mechatronics project.

NTNU
Norwegian University of Science and Technology

sfi Centre for Research-based Innovation
The Research Council of Norway

.....
Savin Viswanathan[1]
Ph.D Candidate

.....
Assoc.Prof. **Christian Holden**[1]
Principal Supervisor

.....
Prof. **Olav Egeland**[1]
Co-Supervisor

.....
Sr.Er. **Ronny Sten**[2]
Co-Supervisor

[1]Deptartment of Mechanical & Industrial Engineering, NTNU, Trondheim.
[2]National Oilwell Varco.

Contents

1 Motivation for Research

With the current outlook in oil and gas industry pointing to brent crude oil prices of around USD 60 per barrel in 2019 [1], rising to around USD 109 per barrel in 2040, when the cheap reserves of oil are expected to run out [2], the main focus of offshore field development would be to lower capex and opex costs. The pre-2014 trend of overdesign is being stripped away from offshore projects and the industry is now witnessing a trend where operators are making deepwater projects more competitive to be economically feasible at crude oil prices around USD 50 per barrel [3].

The large degree of conservatism incorporated into conventional analysis methods result in a smaller operability envelope, thus driving up offshore project costs. Hence, better methods of analysis that aid in maximizing the operability envelope with minimal increase in risk is the need of the hour [4].

To an industry reeling under financial woes, the blow delivered by another Deepwater Horizon incident would be back-breaking [5]. However, for its very survival, the industry must exploit the operable weather window to its maximum limit, and this requires operator confidence based on sound scientific methods. Under the prevailing requirement to maximize operability, there is an increased possibility of drift-offs of the dynamically positioned (DP) vessel under harsher environmental conditions necessitating more frequent and quicker Emergency Disconnect Sequences (EDS) [6]. The nature of such a disconnect would exclude the possibility of lowering the riser tension and/or re-circulating out the drilling mud before disconnection.

In an EDS, the blind shear rams of the Blow Out Preventer (BOP) will cut through the drill string and the Lower Marine Riser Package (LMRP) will be disconnected from the BOP. The sudden release of the riser tension will cause the riser to recoil [7]. The drilling mud with higher density than the sea water would gush out of the opening and make the riser behave much like a suspended hose with water being discharged through its lower end with high velocity. This behaviour becomes all the more critical with the increased riser tension and mud pressure build up in deeper waters [8].

The timing of the EDS is critical. Two aspects are of primary importance:

1. *Excessive Loads on the Riser and Well Head* – The riser must be disconnected before the riser loads and/or the well head loads exceed safety limits.

2. *Riser Recoil Behaviour* – As the riser recoils, the following incidents can occur [9]:

   (a) The motions of the lower end with the LMRP attached renders it probable to hit the BOP, with the potential to cause heavy sub-sea structural damage, given the weight of the LMRP package.

(b) As the heave compensator goes into anti-recoil mode to lift the LMRP clear of the BOP, the riser accelerates upwards and the loss of mudweight enhances this acceleration and there are chances of the tensioner cylinder hitting end-stroke and getting damaged (or) causing damage to the drill floor.

(c) The elastic energy in the riser, which is a function of the tension at the lower end, will lead to generation of a stress wave that travels up to the platform, and this may cause compression in the riser, and may lead to buckling near the top end.

(d) A pressure wave is also set up in the mud column due to sudden discharge from the breached end. However, this is not considered a dominating effect.

For the first aspect, safe EDS is initiated using *watch circles*. Watch circles are set thresholds in terms of horizontal offset between the platform and the well head, which define when the EDS must be initiated, and the riser disconnected. Usually there are two watch circles, *yellow* and *red*. The yellow is the limit for initiating the EDS sequence, and the red is the latest Point of Disconnect (PoD) [10].

Various approaches exist for the determination of the watch circles. The simplest one defines watch circles as fixed percentage of water-depth, without considering the effects of the environment. An improved method calculates the independent vessel drift-off based on metocean data, to predict the trajectory of the vessel drift, and uses this as in input to a Finite Element-based riser model to determine the latest PoD and thus arrive at the threshold circles. However, this method does not consider the coupling between the riser and the platform. The latest method uses a fully coupled model of the vessel and the riser system to better predict the drift-off trajectory, considering environmental loads on the vessel as well as the riser, and the effects of the interaction of both systems, to arrive at the PoD, and subsequently determine the watch circles with the highest accuracy [11].

The fully coupled approach has helped to avoid potential over-conservatism in the calculation of watch circles based on allowable maximum tension in the riser/bending loads on the BOP.

For the second aspect, there are two factors that have a profound impact on the recoil behaviour:

1. The response of the riser tensioner (heave compensator) system.

2. The outflow of drilling mud through the breached end.

Majority of the conventional riser analysis methods apply the tensioner force as a constant vertical point load at the top of the riser. This is obviously an oversimplification, with the implication that decisions based on conclusions drawn from such a procedure would be overtly conservative. In order to improve the accuracy of the analysis, an integrated analysis of the riser and the heave compensator system is required.

As far as mud flow modelling is concerned, it has been found that the Herschel-Bulkley mud flow model agrees well with experimental data for flow velocities, and the results can be incorporated into the riser model during analysis [12].

2 Current Technology and Methods

Modern riser management systems allow one to monitor riser stresses and displacements in real-time. Real-time simulations based on actual weather conditions along with vessel response characteristics are used to determine operability envelopes and fix threshold circles [13].

Conventional practice is to apply the riser tensioner force as a constant point load on the top of the riser during this analysis. A few leading companies in the domain have developed in-house capabilities to model the response of the riser taking into consideration the behaviour of the riser tensioner system and the characteristics of the Anti Recoil Valve (ARV) [14].

- 2H Offshore uses their proprietary software 2HRECOIL along with ANSYS to model the hyrdo-pneumatic riser tensioner system and uses the data to improve riser recoil analysis [15].

- Wood Group has developed and markets their DeepRiser software, which has an optional recoil module which incorporates the dynamic behaviour of the hydro-pneumatics of the riser tensioner into the simulation model [16].

- Castor Drilling Services use Orcaflex, SimulationX and Python to carry out recoil analysis [17].

In his PhD thesis [18], Ronny Sten determines the stroke length of the heave compensator under various wave and current conditions by using the marine riser analysis program RIFLEX. He then uses these displacements to introduce forced motions to the hydro-pneumatic system modelled in SimulationX, and develops a spring-damper model to introduce dynamic tension variations to the riser in the subsequent RIFLEX analysis.

The limitation of the above model is the lack of direct time-domain communication between the riser analysis (FE program) and the hydro-pneumatic tensioner analysis (multi-physics) program. Considerable time is consumed in the manual transfer of information from riser analysis software to multiphysics software and feedback to the riser analysis software for realistic simulation. To improve the accuracy of real-time riser analysis, this gap is to be bridged by developing effective interfacing between the riser analysis program and the program used to model the hydro-pneumatic heave compensator system.

Another interesting aspect is the developments in the field of multiphysical modelling using the *Modelica* language. The *Modelica* language and its simulation environments like OpenModelica, Dymola, SimulationX, etc., has been in extensive use for the acausal modelling of multiphysical systems [19]. Standard libraries for domains ranging from waste water management to aerospace are already extensive and freely available [20]. Libraries for specific applications in ocean engineering have not yet been developed. The Fraunhofer Institute for Wind Energy and Energy System Technology has implemented and carried out initial trials of the *OnWind* Modelica Library for Offshore Wind Turbines and has developed components for modelling of wind, waves, buoyancy and mooring lines. The library is not yet fully developed and the main shortcomings are:

- The inability to model the variation in buoyancy as members are immersed into and emerge from passing waves.
- The inability to model the wave loads considering relative acceleration. At present the wave load calculation takes into consideration the relative velocities only.
- The inability to model current loads.

Efforts are underway to address these shortcomings [21, 22].

Mud-shedding modelling has an evident impact on riser recoil behaviour simulation. The two-parameter Bingham-Plastic or Power-Law rheological models are being replaced by three-parameter models such as the Herschel-Bulkley and Robertson-Stiff models. Maglione and Klessidis demonstrated that the Herschel-Bulkley model exhibits the best fit of the raw experimental data compared to Casson and Robertson-Stiff Models [12].

Traditionally, fully developed flow is widely used for pressure drop prediction or flow-rate calculation in the drilling industry. However, developing flows and unsteady flows are typical in riser disconnect events, and current models take this effect into consideration. It has also been found that widely used laminar flow assumptions over-estimate flow velocity due to underestimated friction forces and exclusion of the effects of vapour cavities, and this leads to inaccurate top tension and riser-recoil control [12].

3 Opportunities for Research

The following potential areas of research were identified after evaluation of the current scenario:

1. To tap the full potential of riser management systems, and to maximize operability envelopes without compromising on safety, accurate and reliable real-time updating of threshold circles, considering the effects of a potential EDS, including riser recoil behaviour, in addition to induced riser and wellhead stresses, is extremely desirable.
2. Though a few companies are offering solutions for fully coupled multiphysical analysis, there is a clear lack of published literature on such analyses. Also, gudielines on the implementation of such models are lacking. Research into the effectiveness and benchmarking of such models is therefore highly desirable.

There is a clear lack of literature on a feasible and quick interface between the finite element-based riser analysis software and multiphysics-based simulation tools for the hydro-pneumatic heave compensator and riser-tensioner. Techniques for fully coupled models incorporating the hydrodynamic response of the vessel and riser system are already available and well developed. The weak link is the incorporation of tension variation due to the heave-compensator/riser-tensioner system behaviour into the riser analysis. Also, the short time available for riser-recoil management makes it all the more important to model the heave-compensator/riser-tensioner system as accurately as possible, considering the effects of details like temperature variation on the pressure drops, since these factors have a considerable impact on the response of the tensioner cylinders, and hence has a direct bearing on the closure curves of the ARV. Though a few leading offshore firms cite the incorporation of these conditions in their recoil analyses, there is a near to total vacuum situation on the availability of information on the methodology adopted in effecting this linkage. This points to a phase where the techniques are under the development and monitoring stage. Thus, it may safely be assumed that efforts in enabling and optimizing such an interface will not result in a re-invention of the wheel.

As of now, riser tensioners are passive systems. The development of an interface as outlined above would pave the way to test the effectiveness of active control of the heave compensator/riser tensioner system to limit undesirable effects such as riser fatigue.

3. Another promising opportunity is the exploration of the possibilities of developing *Modelica* libraries for offshore engineering applications. Components for modelling waves, buoyancy and mooring lines are already being developed for use in commercial versions, but needs to be optimized, and simulation outputs need to be verified with actual response characteristics. There is a total lack of published literature in this direction. There is also a lack of initiative in developing ocean engineering component libraries for use in the free-to-use *OpenModelica* enviroment. The development of such a library would indeed be benificial to academics and the industry, especially when finances are constrained.

4. The *FlexBody* library of *Modelica* enables one to build complete mechanical models combining flexible structures and rigid bodies. FEA tools like Nastran, Genesis and Abaqus has methods of model reduction known as Component Mode Synthesis (or) Craig-Bampton Reduction, which transforms detailed FEM models with 100,000s of nodes to more efficient representations, to be used in dynamics. The reduced models can be read into Dymola to represent the flexible component which can be used as part of a *Modelica* system model. This approach enables the dynamics of the flexible structure to be incorporated into the behaviour of the complete system [23]. Investigations into the adaptation of this method to represent the riser dynamics during disconnect could yield fascinating results.

5. The modelling of mud-shedding is another area with research potential. Standard *Modelica* libraries have components to model Newtonian fluid flow, whereas drilling mud is non-Newtonian. Rita Streblow *et. al* [24] presents results for a method to model non-Newtonian fluid flow in *Modelica* without loss of simulation time, and this approach can possibly be used to describe mud-shedding and account for its effects during riser recoil in an exclusive *Modelica*-based riser dynamic analysis package.

4 Scope

Considering the above potential areas for research, the scope of this research work has been limited to :

1. Development of component models and domain-specific functions to populate an ocean engineering library for use in the free-to-use *OpenModelica* environment. The components to be developed would be limited to models and functions to simulate:

   (a) Irregular seas from a Pierson-Moskowitz spectrum of specifiable significant wave height.

   (b) The hydrodynamics of a wave-transparent floating object of specifiable dimensions, the heave being calculated by using the Froude-Krylov formulation, and the surge forces being calculated using the Morison force (uncoupled heave-surge).

   (c) The non-linear response of a catenary mooring system of specifiable length and specific weight.

(d) The hydrodynamics of a large (diffracting) regular shaped floating object of specifiable dimensions, the forces being calculated by solving the diffraction-radiation problem using panel methods.

(e) The hydrodynamics of a semi-submersible platform with rectangular pontoons and cylindrical columns, of specifiable dimensions.

(f) The response of a dynamic-positioning system.

(g) The time-domain response of a riser system by using/modifying the already availabe components in the FlexBody library of *Modelica*. The scope being limited to simulation of the kinematics by considering the riser to be composed of rigid bodies connected together through joints (or other simplifications as deemed necessary as the work proceeds). The model would exclude formulations to determine stresses and strains, the main intent being the determination of angles at the upper and lower flex joints, so as to determine the point of disconnect for recoil analyses of the simplified *OpenModelica* model.

2. Benchmarking of simulation results of above ocean engineering components with results obtained from commercial hydrodyanmics software ANSYS and mooring/riser analysis software ORCAFLEX.

3. Multiphysical modelling of the riser-tensioner/heave-compensator system using components already available in exisiting *OpenModelica* libraries, and benchmarking with results obtained from multiphysical models built using the commerical software SIMULATION X.

4. Development of a fully coupled multiphysical model using commercial software ANSYS-AQWA to specify the semi-submersible hydrodynamic response, ORCAFLEX to model the riser system response, and SIMULATION X to model the heave-compensator/riser-tensioner. In particular, the influence of the closure curve of the Anti-Recoil Valve of the riser-tensioner system on the fatigue performance of the riser will be investigated, with the aim to optimize the closure curve for improving the fatigue life of the riser.

5. Benchmarking the performance of the *OpenModelica* multiphysical model with the model developed using commercial software.

6. Comparison of the simulation model with field data, if efforts to source such data through the industrial partner is successful. The extent and nature of such comparison will depend on the available data, and hence, specific comments cannot be made at this stage.

The following items would be out of the scope of this project:

1. Determination and real-time updation of threshold circles for the DP system.

2. Study of effects of mud-shedding models on riser response.

3. Higher-order wave forces on component models developed in *OpenModelica*.

5 Objectives

Operating within the scope mentioned above, the main objectives of the proposed project are as listed below:

1. Develop components to constitute a Standard Library for Ocean Engineering in the open source *OpenModelica* environment. This is to be achieved through the performance of three sub-tasks viz:

   (a) Modelling of a simple wave energy conversion system involving the implementation of Modelica components to simulate irregular waves, heave and surge response of a cylindrical floating object, and the response of a catenary mooring system.

   (b) Simulate the response of a simple geometry semi-submersible by the implementation of a Modelica component that solves the diffraction-radiation problem, to determine the hydrodynamic response of large floating bodies.

(c) Simulating the response of a flexible slender structure like the marine riser in the *Modelica* environment.

2. Develop a multiphysics model using industry accepted commercial software (ANSYS, SIMULATION X and ORCAFLEX) to simulate the fully coupled response of a drilling riser in recoil, effectively capturing the influences from the platform, the riser hydrodynamics, and the response of the hydro-mechanical riser-tensioner system to:

   (a) Formulate a method to improve fatigue performance of the riser by controlling the response of the anti-recoil valve of the heave compensator system.

   (b) Compare the performance of the multiphysics model with real world operational data (not necessarily recoil only) sourced through industrial partners.

6 Research Methodology

Objective 1: Literature review and relevant course work $\longrightarrow$ Component model to simulate irregular waves $\longrightarrow$ Component model to simulate the hydrodynamic response of a cylindrical floating object $\longrightarrow$ Component model to simulate the response of a catenary mooring system $\longrightarrow$ Integration of the component models to simulate the behaviour of the wave energy conversion system $\longrightarrow$ Component model to simulate the hydrodynamic response of a simple geometry semi-submersible platform $\longrightarrow$ Model to simulate the respone of the heave compensator system $\longrightarrow$ Component model to simulate the response of the dynamic positioning system $\longrightarrow$ Component model to simulate the behaviour of a marine riser $\longrightarrow$ Integration of component models to simulate the fully coupled response of the platform-riser tensioner-riser system exclusively in *Modelica*.

Objective 2: Literature review and relevant course work $\longrightarrow$ Surface modelling of the semisubmersible platform in ANSYS design modeller $\longrightarrow$ Hydrodynamic analysis in ANSYS Aqwa $\longrightarrow$ Modelling of the heave compensator system in SIMULATION X $\longrightarrow$ Modelling of the riser system in ORCAFLEX $\longrightarrow$ Integrated simulation of the models in SIMULATION X and ORCAFLEX $\longrightarrow$ Research on the control of the heave compensator system to improve riser fatigue performance $\longrightarrow$ Comparison of simulation results with operational data sourced through the industry partner.

7 Expected Outcome of Research

The following outcomes are envisaged:

1. A free-to-use and open-to-public *OpenModelica* standard library for the ocean engineering domain containing models and functions to simulate:

   (a) Irregular waves from a Pierson-Moskowitz spectrum of specified significant wave height.

   (b) Hydrodynamic response of a cylindrical/rectangular buoy.

   (c) Response of a catenary mooring system.

   (d) Hydrodynamic response of large (diffracting) floating objects.

   The following academic literature would be an offshoot of the research work performed in connection with the above:

   (a) Conference/journal paper(s) outlining the development of *OpenModelica* component models for the ocean engineering domain to showcase the benefits of using *OpenModelica* to model simple offshore systems.

   (b) Conference/journal paper(s) detailing the development of *OpenModelica* component models.

   (c) Conference/journal paper(s) detailing the benchmarking of the performance of the component models developed above with results obtained from commercial software.

The above listed research outputs would enable low-cost (or no-cost) modelling of multiphysical systems in the domain of offshore engineering by bridging the gap that exsists at present, i.e., the lack of component models to simulate hydrodynamics, mooring etc. Engineers in industry as well as in academia will then be able to use these components to model, for example, performance of wave energy converters, hydrodynamic response of research data buoys, etc., where the return on investment is not high enough to facilitate the use of costly commercial software to carry out analysis. This would also form the basis for inclusion of ocean engineering components other than the ones mentioned above by researchers in the future.

2. Academic literature describing the outcome of first-time efforts to model the hydrodynamic response of an offshore semisubmersible platform exclusively in *Modelica*, with the potential to act as a seed towards the development of free-to-use software, fully compatible with *Modelica* components from other engineering domains, which could form the basis for low-cost fully integrated myltiphysical modelling of offshore systems. The realization of such a system would play a huge role in lowering design costs, thus making offshore projects more viable financially, and safer to operate.

3. Academic literature describing the outcome of first-time efforts to model the response of slender structures like a marine riser, exclusively in *Modelica*, with the potential to act as a seed towards the delvelopment of free-to-use riser analysis software for use in academic/research projects dealing with activities like offshore mining, snake-type wave energy converters, etc., where low return on investments limit the use of costly commercial software during the design evaluation stage.

4. Academic literature on the process of fully coupled multiphysical simulation and analysis of the drilling riser using commercial software.

   At present, there is a lack of literature dealing with fully coupled multiphysical co-simulation and interpretation of results of such analyses. Most of the offshore operators still rely on models that simulate the effect of the heave-compensator/riser-tensioner action as a spring load on the riser. Presentation of results of fully coupled multidomain analyses which bring out the advantages of employing such simulation methods would indeed be beneficial with regards to economics and safety.

   It is expected that the outcome from the performance of this part of the project will help in enhancing operator confidence through the presentation of more accurate anlysis results obtained through realistic simulations of the drilling riser response, thereby enabling the operator to maximize the utilization of the operational weather window in a safe manner. This is in turn expected to bring down the operational cost and thus contribute towards the enhancement of the financial viability of offshore oil and gas projects.

5. Academic literature on methods to improve the fatigue performance of a drilling riser through control of the riser-tensioner system.

6. Academic literature on the comparison of results of fully coupled multiphysical simulation of offshore riser systems to field data (depending on the type of data sourced through the industry partner).

8 Ethics

Major ethical issues are not envisaged with the performance of the project.

While it may be argued that pushing the drilling operations to the limit of the operational weather window might pose risk, it may be countered with the fact that the performance of research in this direction contributes to the improvement of existing analysis methods, and thereby reduces the uncertainity associated with offshore operations.

Another potential issue is with the publication of data sourced through the industrial partner. To ward off such an incident, it has been agreed that such instances will be discussed during review meetings and written permission from the industrial partner will be obtained before publication of any such data.

9 Course Work

IFEL8000 Introduction to Research Methodology, Theory of Science and Ethics.

MR8208 Dynamic Analysis of Slender Marine Structures.

MR8303 Kinematics & Dynamics of Ocean Surface Waves.

MR8300 Hydrodynamic Aspects of Marine Structures -I.

10 Work Plan


2018
2019
2020
Spring
Autumn
Spring
Autumn
Spring
Autumn
1 2 3 4 5 6 7 8 9 10 11 12 13 14 15 16 17 18 19 20 21 22 23 24 25 26 27 28 29 30 31 32 33 34 35 36
Course Work
IFEL8000
MR8208
MR8303
MR8300
Literature Review
Objective 1
Objective 2
Research Work
Objective 1(a)
Objective 1(b)
Objective 1(c)
Objective 2(a)
Objective 2(b)
Thesis Writing
Thesis Writing

References

[1] U.S Energy Information Administration. *Short-term Energy Outlook.* January 9, 2018; https://www.eia.gov/outlooks/steo/report/prices.php.

[2] Kimberly Amadeo. *Oil Price Forecast 2018-2050: How High Oil Prices Will Rise in 2018.* The Balance, https://www.thebalance.com/oil-price-forecast-3306219.

[3] Tavyis Dunnahoe. *Deepwater exploration seeks value over volume in new oil price environment.* Oil and Gas Journal, January 5, 2017, http://www.ogj.com/articles/print/volume-115/issue-5/special-report-offshore-petroleum-operations/deepwater-explorations-seek-value-over-volume-in-new-oil-price-environment.

[4] Conon Quigley, Dara Williams. *A Revised Methodology for the Calculation of MODU Watch Circles.* Proceeding of the ASME 2015 34th International Conference on Ocean, Offshore and Arctic Engineering, OMAE2015, May 31-June 5, 2015, St. John's, Newfoundland, Canada.

[5] British Petroleum. *Deepwater Horizon Accident Investigation Report.* https://www.bp.com/content/dam/bp/pdf/sustainability/issue-reports/Deepwater_Horizon_Accident_Investigation_Report.pdf.

[6] Dr. Xiao Bing Shi *et. al*. *Case Study of DP Vessels Performing SIMOPS.* Dynamic Positioning Conference, November 15-16, 2005. https://dynamic-positioning.com/proceedings/dp2005/operations_shi.pdf.

[7] Arlid Grnevik. *Simulation of Dirilling Riser Disconnection- Recoil Analysis.* Master Thesis, NTNU. https://core.ac.uk/download/pdf/52099847.pdf .

[8] Ryan Koska. *Mudshedding Modelling for Accurate Drilling Riser Recoil Analysis.* 2H Offshore. https://2hoffshore.com/blog/mud-shedding-modelling-accurate-drilling-riser-recoil-analysis/.

[9] Guttorm Grytor *et. al. Marine Drilling Riser Disconnect and Recoil Analysis.* 2011 AADE National Technical Conference & Exhibition, Houston, Texas, April 12-14, 2011.

[10] Donogh Lang. *Latest Advancements in Drilling Riser Analysis Technology.* InnoOil Issue 58, October 26, 2017, http://www.innovoil.co.uk/single-post/2017/10/26/Latest-advancements-in-drilling-riser-analysis-technology.

[11] Lew Weingarth. *Refining the DP Watch Circle.* Dynamic Positioning Conference, October 17-18, 2006. https://dynamic-positioning.com/proceedings/dp2006/op_procedures_weingarth.pdf.

[12] Song Cheng Li *et. al. Effect of Mud Shedding on Riser Anti-Recoil Control at Emergency Disconnect.* Proceedings of the ASME 2012 Conference on Ocean Offshore and Arctic Engineering OMAE 2012, Rio de Janeiro, Brazil, July 1-6, 2012.

[13] Kongsberg. *Riser Management System.* https://www.km.kongsberg.com/ks/web/nokbg0240.nsf/AllWeb/98FC23B43375AF3EC1256F560049A936?OpenDocument.

[14] Dara Williams. *Analysis of Drilling Risers in Harsh and Deepwater Environments.* https://www.offshore-mag.com/articles/print/volume-70/issue-4/drilling-__completion/analysis-of-drilling-risers-in-harsh-and-deepwater-environments.html.

[15] Songcheng Li *et. al*. *Tension Loss of Hyrdo-Pneumatic Riser Tensioners.* Proceeding of the ASME 2013 32nd International Conference on Ocean, Offshore and Arctic Engineering, June 9-14, 2013, Nantes, France.

[16] Wood Group. *Deep Riser- Intgrated engineering application to optimize and streamline the design and analysis of dirlling riser and top-tensioned production riser systems.* https://www.woodgroup.com/what-we-do/view-by-products-and-services/digital-solutions/riser.

[17] Castor Drilling Solutions. *System Simulations.* http://www.cds.as/service/system-simulations/.

[18] Ronny Sten. *Dynamic Simulation of a Deepwater Drilling Riser With Heave Compensating System.* PhD Thesis, NTNU, 2012.

[19] Peter Fritzon. *Principles of Object-Oriented Modeling and Simulation with Modelica 3.3.* IEEE-WILEY, 2015.

[20] Modelica and the Modelica Association. *Modelica Libraries.* https://www.modelica.org/.

[21] M. Strobel *et. al. The OnWind Modelica Library for Offshore Wind Turbines- Implementation and First Results.* The Fraunhofer Institute for Wind Energy and Energy System Technology.

[22] Brommundt, Matthias, and Muskulus, Michael, and Strach, Mareike, and Strobel, Michael, and Vorpahl, Fabian. *Experiences with Object-oriented and Equation Based Modeling of a Floating Support Structure for Wind Turbines in Modelica.* Proceedings of the Winter Simulation Conference.159:pp.1–12. Berlin, Germany, 2012. URL: http://dl.acm.org/citation.cfm?id=2429759.2429972.

[23] Claytex. http://www.claytex.com/products/dymola/model-libraries/flexbody-library/#14990261471766-0e78cb7a-cb82.

[24] Rita Streblow *et. al. Simulation of Non-Newtonian Fluids using Modelica.* RWTH Aachen University-E.ON Energy Research Center.

ISBN 978-82-326-6112-1 (printed ver.)
ISBN 978-82-326-6218-0 (electronic ver.)
ISSN 1503-8181 (printed ver.)
ISSN 2703-8084 (online ver.)

NTNU

Norwegian University of
Science and Technology